A design study of a 1 MW stall regulated rotor

Fuglsang, P.; Aagaard Madsen, Helge

Publication date:
1995

Document Version
Publisher's PDF, also known as Version of record

A Design Study of a 1 MW Stall Regulated Rotor

Risø-R-799(EN)

Peter L. Fuglsang, Helge Aa. Madsen

Risø National Laboratory, Roskilde, Denmark
May 1995

Abstract

The main objective of the present work has been to design a 1 MW stall regulated rotor and investigate the potential improvements by using special tailored airfoils. The target rotor should have an improved cost performance compared to existing rotors. Cost performance is the annual production of energy seen relative to the material consumption. A newly developed numerical optimization tool and an aeroelastic code have been used in the study.

Design parameters have been the blade chord, twist, tip pitch angle, angular velocity and airfoil characteristics. The objective function for the optimization has been the annual production of energy in the Danish roughness class 1. Constraints have been put on mean and extreme blade root flapwise moments, rated power, tip speed and blade geometry.

By performing aeroelastic calculations on the optimized designs with different levels of constraints on the mean blade root flapwise moments, an almost linear correlation between the mean blade root flapwise moment and the equivalent fatigue loads appears. The optimum ratio of rated power to swept area appears to be around 400 W/m^2 having the mean flapwise blade root moment constrained to 80%.

The maximum annual production of energy has been obtained for the airfoil section maximum lift coefficient, C_{Lmax}, being high over the entire blade independent on constrained loads. The direct improvement from the use of special tailored airfoils has been found to be around 4% on the annual energy production and 1.5% on the material consumption. When the entire rotor geometry is included as optimization design variables, the choice of C_{Lmax} becomes less important since the design space is flat in the neighbourhood of the optimum. Therefore other qualities like roughness insensitivity can be given more attention in the design process at the expense of a specific C_{Lmax}.

The results indicate a potential improvement of the cost performance of about 11% of which 5.5% can be achieved with the use of traditional airfoils. Whereas the proposed methodology have been very beneficial to constrain the fatigue loads, the extreme loads have not yet been entirely included.

The work presented has been funded by the Danish Ministry of Energy in the contracts:

ENS-1364/91-0001
ENS-1364/94-0001
ENS-1363/95-0001

The report has passed an internal review at The Test Station for Wind Turbines performed by:

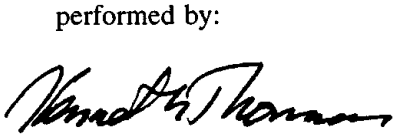

Kenneth Thomsen

Flemming Rasmussen

ISBN 87-550-2057-7
ISSN 0106-2840

Grafisk Service, Risø, 1995

Contents

1 Introduction

In recent years, one of the development trends in the Danish wind turbine industry has been towards larger wind turbines. Both the swept area and the generator rated power have been increased remarkably. Prototypes having a rated power of up to 1500 kW and a rotor diameter of about 60 m are expected to be erected in the near future. This evolution has lead to increased focus on the aerodynamic design of rotors, since an improvement of the cost efficiency will lead to improved competitiveness compared to other energy sources, both renewable and conventional. The rotor aerodynamic design has until now been based on a long period of innovation, but modern rotor design should contain both the development of special tailored airfoils and numerical optimization of the entire rotor geometry.

At Risø, research in aerodynamic optimization of rotors has been performed since 1989, where an optimization method was developed in connection with a CEC founded research project, Hoadley et al. [1]. The aim of this first optimization approach was to improve the annual production of energy by optimizing the blade airfoil characteristics for maximum rotor power coefficient, C_p, at a single design wind speed. The output was optimum airfoil characteristics, that were used for the development of new airfoils. In 1993 this optimization method was used for the design of a 20 kW rotor for retrofit of old Kuriant turbines [2]. This rotor was equipped with special tailored airfoils developed at Risø and measurements have recently shown a reliable stall of the power curve [3]. During the optimization process it was realized, that optimizing for the maximum value of C_p would cause a relatively large thrust force on the rotor. Therefore the aerodynamic optimum was deviated by reducing the rotor solidity and increasing the swept area. This lowered maximum C_p a few percent, whereas the thrust force on the rotor was remarkably reduced.

In 1994 Risø began the work with a multi pointed optimization method, initially developed in a master thesis project at Aalborg University [5]. This method is based on a general numerical optimization algorithm. With this method it is possible to optimize the entire rotor geometry directly for an improvement in the annual production including both design point and off design performance. Additionally, constraints can be put on loads, so that the optimization goal is not necessarily the aerodynamic optimum. The method has been found useful for parameter investigations as well as for actual design studies. Using the multi pointed optimization method, initial investigations have shown a potential improvement of the annual production by performing a number of optimizations of different parts of the rotor blades [6]. The entire blade geometry including the airfoil characteristics have been optimized with fixed swept area. Here, an improvement in the annual production of about 10% appears. However, this investigation implied no airfoil drag. When the drag is included, the improvement reduces to about 5%. It is likely, that the development of new airfoils will result in further improvements with regard to qualities like roughness insensitivity and low drag, but it appears, that a substantial improvement in the cost effectiveness can not be obtained alone by developing special tailored airfoils.

The limited potential improvement of the annual production from optimizing the blades with the rotor radius kept constant and the involvement of a considerable thrust force from finding the aerodynamic optimum led us to perform a parameter

investigation of the ratio of rated power to swept area. The annual production is very sensitive to variation of this parameter and eventually this could be a way to increase the cost effectiveness. However, also the loads on the blades and the entire wind turbine are strongly sensitive to this parameter and therefore a detailed analysis is required.

The aim of this report is to design a 1 MW stall regulated rotor. This rotor should have an optimized blade geometry, optimum airfoil characteristics and an optimum ratio of rated power to swept area. This ratio is found by an extensive parameter investigation. The aim of the parameter investigation is however not only to clarify the variation of the annual production, but a possible trade off between this and the fatigue loads.

A number of optimizations will be carried out at different ratios of the rated power to swept area between 200 and 600 W/m^2. At each of these ratios, a family of rotors will be optimized by applying different degrees of constraints on the mean blade root flapwise moment at normal condition and the extreme blade root flapwise moment occurs at rotor stand still. Aeroelastic calculations will be performed on some of these families to do comparisons on the variation of life time equivalent blade and rotor fatigue loads. By assuming that the fatigue loads will determine the overall wind turbine weight, the material consumption will be calculated for comparison on a relative basis between different rotors.

To limit the number of parameters in the investigation, the optimization will mainly concern the rotor chord and twist distributions, tip pitch angle and angular velocity, though some optimizations will also include the blade section airfoil characteristics. The aim will be the annual production of energy in Danish roughness class 1. Besides the constraints on loads in the parameter investigations, constraints will be added to the generator rated power on 1 MW and the rotor tip speed will be bounded to 60 m/s.

The report follows the following outline:

Chapter 2 contains a brief description of the calculation foundation concerning the optimization method, the fatigue load calculations and the material consumption evaluation.

Chapter 3 is the parameter investigation of the ratio of rated power to swept area. Conclusions will be drawn on the variation of the annual production, mean loads at normal operation, the extreme loads at rotor stand still, equivalent fatigue loads and the material consumption. An optimum ratio of rated power to swept area will be found and the influence from roughness class will be commented on.

Chapter 4 involves the finding of optimum airfoil characteristics for a rotor having an optimum ratio of rated power to swept area. The sensitivity on the performance from different choices of airfoil characteristics will be investigated and the variation of the optimum airfoil characteristics with both extreme and fatigue loads, tip pitch angle, tip chord and minimum drag will be found resulting in a recommendation for the choice of suitable airfoil characteristics.

Chapter 5 contains a comparison between an optimum rotor, based on Chapter 3 and 4 and the LM 24.0 blade [23].

Chapter 6 summarizes the drawn conclusions.

2 Calculation foundation

This Chapter contains a brief description of the theory used in the report. References will be given for further information. The optimization code, "Rotor" is explained in Section 2.1. Section 2.2 briefly describes the calculation of the life time equivalent fatigue loads. Section 2.3 explains the calculation of the material consumption.

2.1 The optimization method

The optimization method is based on a general optimization algorithm. This optimization algorithm uses calculation models according to the flow chart in Figure 2.1.

The optimization algorithm is basically a search direction method. It allows multiple inequality constraints. The optimization process consist of a number of iterations. Each iteration is subdivided into two sub problems. First, the search direction, **S**, is found using "The Method of Feasible Directions" and "The Conjugate Gradient Method". Next, the step length, α, is found with "The Golden Section Method" and quadratic refinement [7].

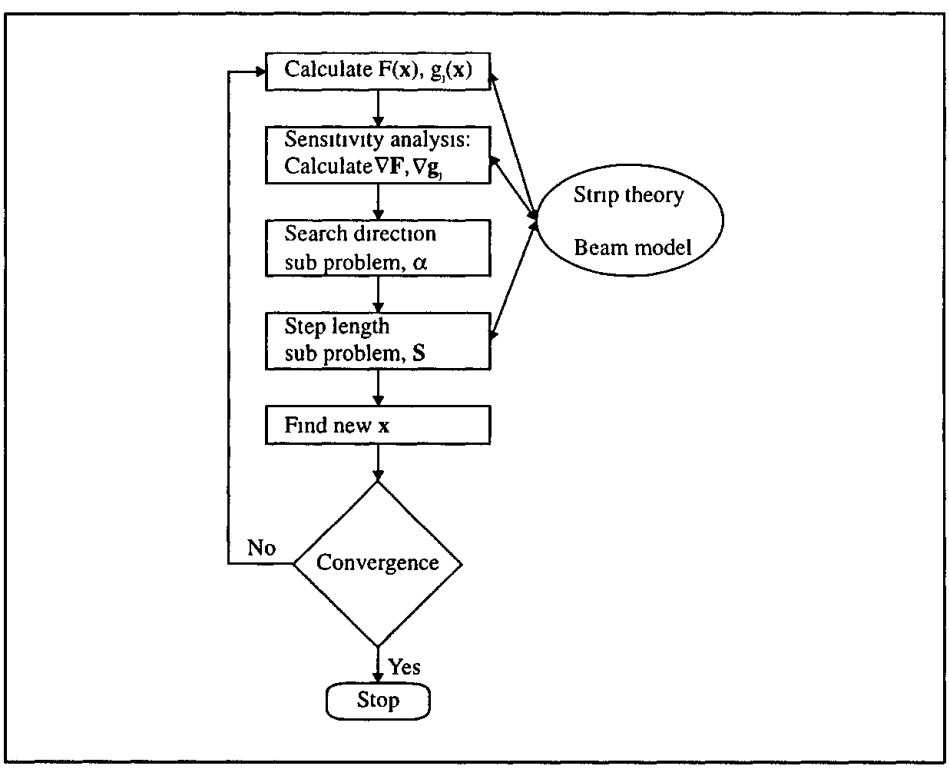

Figure 2.1 Flowchart of the overall iteration loop for the Method of Feasible Directions.

Since optimization calculations are time consuming, the calculation models used are rather simple. Momentum strip theory, with at tip loss correction, is used to calculate the mean blade loads. A linear elastic beam model represents the blade stiffness and the blade mass. Extreme loads at rotor stand still are calculated after

a code [8]. Here, a wind speed of 70 m/s is assumed and the airfoil characteristics corresponds to the angles of attack at rotor stand still. At the present time aeroelastic calculations aiming for determining the fatigue loading are not implemented. The included calculation models have been found sufficiently accurate for the optimization having in mind the uncertainties involved from stall hysteresis, 3D rotational flow effects and dynamic inflow. In addition the calculation models are primarily used for relative comparison between different rotor designs.

Much effort has gone into linking the calculation models with the optimization algorithm, since this is essential for a rational use of the theory. This has resulted in a comprehensive computer code, "Rotor" [5].

2.1.1 Formulation of the optimization problem

The purpose of an optimization is basically to minimize the objective function, F. F is characterized by n design variables. These are organized in the design vector, **x**. The design variables form a vector space, bounded by the constraints which can be both equality and inequality constraints. The form of a general optimization problem with multiple inequality constraints is [7]:

Minimize:

$$F(\boldsymbol{x}) = F(x_1, x_2, \ldots, x_n) \tag{1}$$

subject to the inequality constraints

$$g_j(\boldsymbol{x}) \leq 0; \quad j = [1;m]. \tag{2}$$

Even though F is always minimized, and the inequality constraints are on the form "less than or equal", every optimization problem can be formulated in this general way.

The sensitivity of the objective function and the constraints, on the design variables, are found using a numerical forward difference approximation by perturbation of each of the design variables. This means that the objective function and the constraints have to be calculated n+1 times for each sensitivity analysis. Furthermore, the calculation of the step length requires a number of calculations.

2.1.2 Objective function

The objective function is chosen directly as the negative annual production of energy, E_{prod}, and is calculated as a sum of m contributions of the electric power, $P_{el,i}$, at the wind speed, V_i, weighted by the Weibull distribution, $P(V_{10} \leq V)$, based on 10 minute wind speed mean values, V_{10}:

$$E_{prod} = 8.761 \frac{kWh\ s}{J\ year} \sum_{i=1}^{m} P_{el,i}(V) \left[P\left(V_{10} \leq \frac{1}{2}(V_i + V_{i+1})\right) - P\left(V_{10} \leq \frac{1}{2}(V_i - V_{i-1})\right)\right] \tag{3}$$

where

$$P(V_{10} \leq V) = 1 - \exp\left(-\left[\frac{V}{A}\right]^k\right) \tag{4}$$

A is the Weibull scale parameter, k is the Weibull shape parameter.

It is an advantage that the objective function contains information about both the maximum efficiency and the off design performance, compared to single design point optimization, where the power coefficient at some design wind speed is often used. However, the objective function can easily be changed e.g. to a performance parameter including both annual production and loads. This is planned to be implemented in the near future.

2.1.3 Design variables

The design variables are the parameters describing the rotor geometry which can be changed by the optimization algorithm. A large number of design variables gives larger flexibility, and thereby a better chance of improving the objective function. However, it also makes the optimization problem more difficult to survey and increases the calculation time.

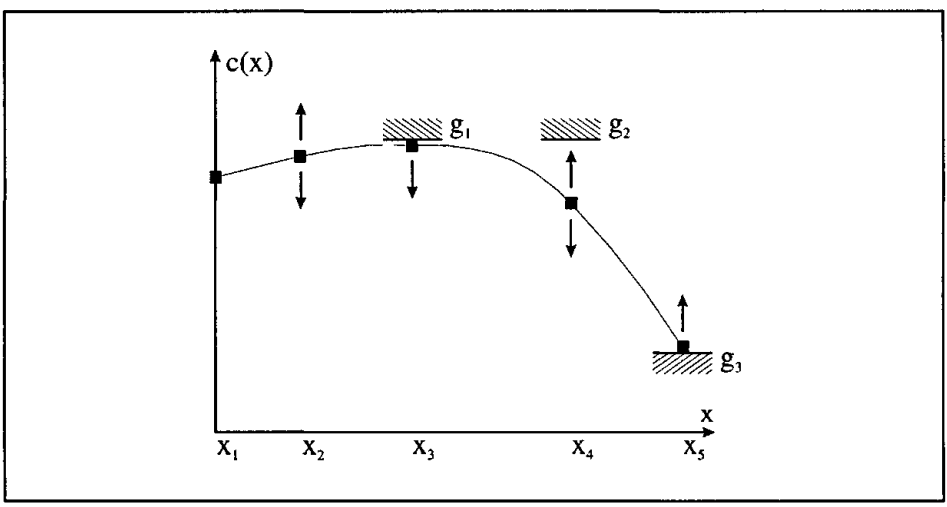

Figure 2.2 Distributions are described by discrete design variables. Here 5, $[x_1..x_5]$ are interpolated by cubic splines, $[g_1..g_3]$ are constraints.

The following design variables are at the present time possible:

1) The rotor diameter

2) The blade tip pitch angle

3) The spanwise blade chord distribution.

4) The spanwise blade twist distribution.

5) The spanwise blade thickness relative to chord distribution.

6) The spanwise blade shell thickness distribution

7) The rotational speed

8) The airfoil characteristics in the blade sections, treated directly as the relation between the angle of attack, α, and the C_L and C_D coefficients.

In order to limit the number of design variables and to ensure smooth curves, chord, twist and relative thickness are represented by either cubic splines or Bezier curves typically using between 4 and 8 equally distributed points. An example with 5 points is shown in Figure 2.2.

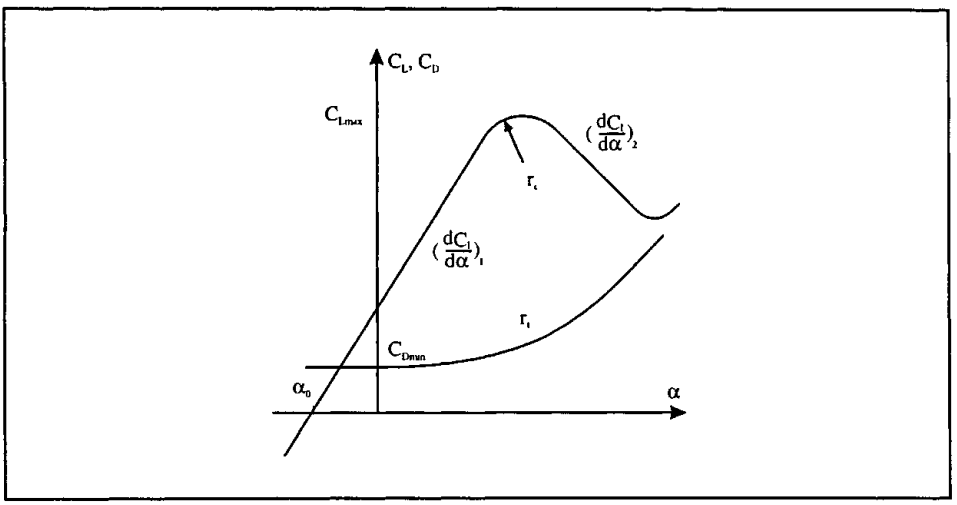

Figure 2.3 Simplified parametric description of the airfoil $C_L(\alpha)$ and $C_D(\alpha)$ coefficients.

$C_L(\alpha)$ and $C_D(\alpha)$ are described by simplified curves with a limited number of design variables as shown in Figure 2.3:

1) Slope of lift curve before stall, $\left(\frac{dC_L}{d\alpha}\right)_1$

2) Slope of lift curve after stall, $\left(\frac{dC_L}{d\alpha}\right)_2$

3) Radius of curvature for lift curve at stall, r_c

4) Angle of attack at zero lift, α_0

5) Maximum lift coefficient, C_{Lmax}

6) Minimum drag coefficient, C_{Dmin}

7) Rate of transition from minimum drag, r_t

To ensure a smooth variation, each of these parameters are represented by cubic splines along the blade span. Furthermore, C_{Lmax} and the transition, r_t from C_{Dmin} are linked based on a number of airfoils taken from [9]. At large angles of attack greater than 25 deg, corrected values for NACA 632xx from [10] have been used. The parametric representation has been found to represent leading edge separation as well as trailing edge separation well.

2.1.4 Constraints

The constraints bound the optimization problem into a feasible region in the design space, making a realistic result possible. At present, a comprehensive range of different aspects is being covered:

1) The maximum generator rated power.

2) Extreme loads on blade and rotor at rotor stand still

3) Mean loads on blade and rotor at normal operation

4) The deterministic fatigue load on the blade root originating from gravity

5) The loading of the blade structure, controlled by bounding the maximum stress in the blade shell.

5) The manufacturing costs, controlled by bounding the total mass of the individual wind turbine components

6) The tip noise, partially controlled by bounding the tip speed.

Fatigue loads on the wind turbine structure are not includes as constraints in the present optimization formulation. However, these loads can be calculated afterwards for the optimized designs.

2.2 Lifetime equivalent fatigue load calculation

The life time equivalent fatigue loads are calculated using the following procedure. Time simulations of the wind turbine dynamics are performed by using the time domain aeroelastic computer code, "Flex4" [11]. These time series form the basis for Rainflow counting [12]. Finally Rainflow counting at different windspeeds are combined into a life time spectrum represented by equivalent fatigue loads referenced to a number of cycles [13].

2.2.1 The aeroelastic code, "Flex4"

The aeroelastic code, "Flex4", developed by Stig Øye, is described in detail in [11]. It is formulated in the time domain and can use a total number of 20 degrees of freedom (DOF) for a three bladed wind turbine: Each blade bending is found from a mode shape formulation with 2 flapwise and 2 edgewise mode shapes (total 12 DOF). Additional DOF's are tower bending (2 DOF), rotation of tower top (tilt), tower torsion (yaw), main shaft bending (2 DOF), shaft torsion and shaft rotation.

The equations of motions are formulated with the deflections of each DOF as generalized coordinates. No small angle assumptions are made. The equations are solved for accelerations and integrated over small time steps using a Runge-Kutta-Nyström method.

The aerodynamic loads on the blades are calculated with the blade element momentum method [4]. The mean wind field over the rotor plane includes wind shear, yaw error, tower shadow and a vertical slope of the wind vector. The

turbulent part of the wind is included in the model as time series of simulated turbulence. The turbulence is a full field three-dimensional three-component field. Each component is generated using the Veers method [15].

To prevent aerodynamic instability in stall from the negative slope of the lift curves in post stall, a dynamic stall simulation model is included. The applied method is based on corrections to the static airfoil lift data to be able to represent stall hysteresis, resulting in a positive contribution to the total damping in post stall [16].

2.2.2 Rainflow counting

Having calculated time series of load variations, Rainflow counting is used to count the number, n_i, of load ranges, M_i, where i represents the load range index. The different load ranges are collected in the Rainflow vector, $M_i(n_i)$. The global maximum load range defines the upper bound of this vector and it is divided into a number of equidistant boxes. The counting method is described in detail in [12].

The fatigue damage accumulation, D_{tot}, is found by use of the Palmgren-Miner damage hypothesis, assuming linear damage accumulation:

$$D_{tot} = \sum_i n_i M_i^m \tag{5}$$

where m is the S-n curve exponent.

2.2.3 Life time spectrum

The life time spectrum, $L_j^m(N_j)$, is based upon the Rainflow counting, $M_i(n_i)$, at different load conditions. Here j corresponds to the different global load cases. These are weighted with a probability distribution, p(U), of different load condition events, U. Typically a number of different wind speed intervals, eventually combined with start up sequences etc.

The number of cycles at each global load range can then be found from:

$$N_i = \sum_u n_i p(u) \tag{6}$$

The number of cycles as a function of the load range is then the total life time spectrum. By using eq. (5) on the life time spectrum, this can be described by a single parameter, the equivalent load range, R_{eq}, characterised by the S-n curve exponent, m, and a reference number of cycles, N_{eq}:

$$R_{eq} = \left[\frac{\sum_i L_j^m(N_j)}{N_{eq}} \right]^{\frac{1}{m}} \tag{7}$$

This equivalent load then gives the same damage as the life time spectrum. By choosing the same N_{eq} and m, fatigue from different rotors can be compared as life time equivalent fatigue loads.

2.3 Material consumption calculation

The total material consumption is calculated as a weighted sum of contributions from the different wind turbine components [14]. Each contribution is described by the material consumption, split into a fixed part and a variable part which depends on loads. By choosing a reference rotor having a total material consumption of 100%, the relative percentage difference in the total cost between this and the actual rotor is being calculated by assuming that the stresses in each component are equal. This means that the calculation of cost is based on existing technology without any considerations on optimization of individual components.

The relative cost of the different components and their cost functions are shown in Table 2.1. The material factor, mf, is an expression for a the component weight. mf is then calculated so that the stress is equal to the same quantity in the reference rotor.

Table 2.1 Relative cost and material consumption for the different wind turbine components. mf is the material factor [14].

Component system	Relative cost (%)	Material consumption, mc (%)
Blades	24.5	0.2 + 0.8 mf
Hub	3.2	mf
Main shaft	3.3	0.3 + 0.7 mf
Main gear	14.3	mf
Generator	6.4	mf
Machine foundation	4.5	0.4 + 0.6 mf
Yaw system	4.0	mf
Controller	9.5	1
Tower	17.6	0.4 + 0.6 mf
Brake system	4.7	mf
Cover, finish	5.0	1
Assembly	3.0	1
Total	100%	

Except for the blade, it is assumed that each material factor can be described as a function of life time equivalent fatigue loads, R_{eq}, and the maximum torque, T_{shaft}:

$$mf = f(R_{eq,flap}, R_{eq,edge}, R_{eq,thrust}, R_{eq,tilt}, R_{eq,yaw}, T_{shaft}) \quad (8)$$

All equivalent fatigue loads are calculated at 10^7 cycles. The blade root flapwise moment, $R_{eq\ flap}$, and edgewise moment, $R_{eq\ edge}$, are both assumed to have a S-n curve exponent of, m = 10, corresponding to fibreglass whereas the rotor thrust force, $R_{eq\ thrust}$, the rotor tilt moment, $R_{eq\ tilt}$, and the rotor yaw moment, $R_{eq\ yaw}$, have an exponent of, m = 4, as an average representing welded steel.

Having found the material factors, the material consumption, mc, is calculated from:

$$mc = c + (1 - c) \cdot mf \tag{9}$$

where c is the load independent part of the material consumption, whereas (1-c) is the load dependent part.

Finally, the material consumptions from the individual components are weighted by their relative cost, and the total material consumption is calculated.

The following contains a brief description of the individual component material factors:

blades

The distributed blade weight is found along the blade span by modelling the blade as an elastic beam. The hub section is represented by a tube, whereas the airfoil sections are represented by an I-beam, as shown in Figure 2.4.

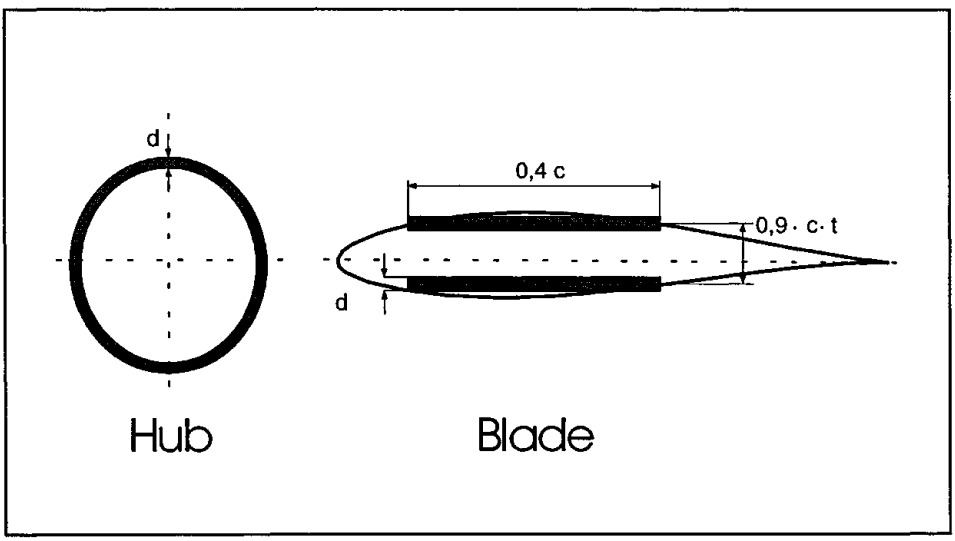

Figure 2.4 The blade is modelled as an elastic beam where the hub is a tube and the airfoil section is an I-beam.

The blade weight is the dominating parameter for the edgewise blade root bending moment. In return the fatigue loads are determined partially from the blade weight. Since the fatigue loads and the blade mass are mutually dependent it would be necessary to perform iterations to solve for the material consumption. Instead, the mean moment distribution perpendicular to the local blade chord is calculated at the windspeed corresponding to peak power where the entire blade is stalled. This mean load is not directly an impression of the fatigue load, but is expected to have some correlation to the fatigue load.

Having found the load distribution, the tube/ beam thickness is then calculated, so that the stress distribution corresponds to a calculated stress distribution from the LM 17.0 blade [5]. This ensures similarity with an existing blade.

main shaft
The shaft weight is assumed to be determined from the resulting bending moment from yaw, tilt and gravity from the rotor. The shaft weight will be proportional to the applied moment.

main gear, brake system and generator
The main gear, brake system and generator weights are determined from the main shaft torque resulting from the blade inplane loads.

machine foundation
The machine foundation weight is determined from the resulting bending moment from yaw and tilt.

yaw system
The machine yaw system weight is determined from the yaw moment.

tower
The tower weight is the plate thickness that is linearly dependent on the tower height. It is determined from the resulting bending moment distribution resulting from rotor tilt, thrust and the rotor shaft torque. Furthermore the torsion from yaw, is applied (Figure 2.5). The total length of the moment vector, M(h), is found by summation of the individual moment vectors.

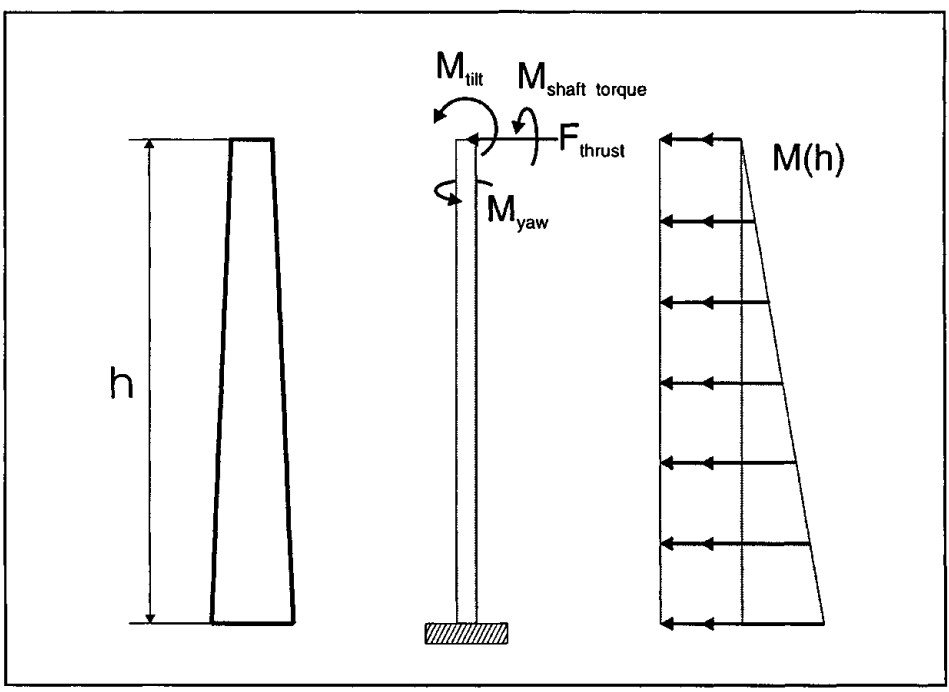

Figure 2.5 The modeling of the tower as an elastic beam.

3 Ratio of rated power to swept area

The purpose of this Chapter is to find an optimum ratio of rated power to swept area by performing a parameter investigation leading to maximization of the ratio between annual energy yield and the cost of the entire wind turbine. First, a tendency for the ratio of rated power to swept area for Danish wind turbines is revealed. Next the extent of the parameter investigation is determined. Analysis of the variation of the annual production, mean loads, extreme loads and fatigue loads with different constraints is being carried out. Finally a material consumption is calculated and this is seen relative to the annual production to find a cost performance optimum. The dependency on the cost effective optimum from roughness class is briefly discussed.

A number of optimizations will be performed. The objective of the optimization will be the annual energy yield in the Danish roughness class 1 according to the code, DS 472 [17]. Design variables will be the chord distribution represented by an 8 point cubic spline, the twist distribution represented by a 5 point cubic spline (twist at tip will be set to zero), angular velocity and tip pitch angle. Constraints will be applied to the generator rated power on 1 MW and to the tip speed on 60 m/s. For simplicity, the airfoil coefficients are not included as optimization variables but chosen to be the NACA 634xx series. This will give the opportunity to investigate variations from the overall rotor geometry without the airfoil characteristics. These will instead be treated in Chapter 4. Optimum airfoil characteristics could have an influence on the optimum ratio of rated power to swept area. However, the use of existing airfoils will prevent unrealistic airfoil characteristics to be decisive for judgement of the results.

Representative parts of the optimization results will be shown as an Appendix, for a more extensive study, while summarising figures will be shown within the text.

3.1 Background

The ratio of rated power to swept area, the specific power, is a key parameter in the design process. A high value of the specific power means a high rotor loading pr. area. Lowering the specific power will decrease the rotor loading pr. area but will increase both the annual production as well as the total blade and rotor loads. It is likely that both the annual production and the loads depend nonlinear on the actual specific power. Therefore, an optimum specific power should be found where there is the best possible trade off between the annual production of energy and the manufacturing costs.

In Figure 3.1 the rated power is shown as a function of the specific power for Danish wind turbines between 150 kW and 600 kW [24]. A tendency towards higher specific powers for higher rated powers is revealed. This can partially be explained by the increase in the mean wind speed with tower height, since this should increase with the generator rated power. However, for rated powers about 500 kW the specific power lies within 400 W/m^2 and 530 W/m^2.

The increase in the specific power is somewhat in conflict with the basis for recent developments of special tailored airfoils, where the aim has been to develop tip airfoils having a lower C_{Lmax}, so that the swept area can be increased

to the same rated power resulting in a lower specific power. The reason for this discrepancy might be, that the tailored tip airfoils have only been used in a few cases by the Danish industry. For some reason the use of these airfoils have been found inexpedient.

Another reason could be marketing considerations. Wind turbines having a lower rotor loading have a slightly lowered maximum C_P and are likely to produce more noise, since their tip speed is higher for the same rotational speed. A possible trade off between the annual production and the manufacturing costs is likely to result in less annual production than possible, leading to poorer performance compared to competitors if annual production is the only criterion to be judged. Finally, the search for the optimum trade off requires advanced optimization since the aim is not necessarily the optimum seen from an aerodynamic point of view.

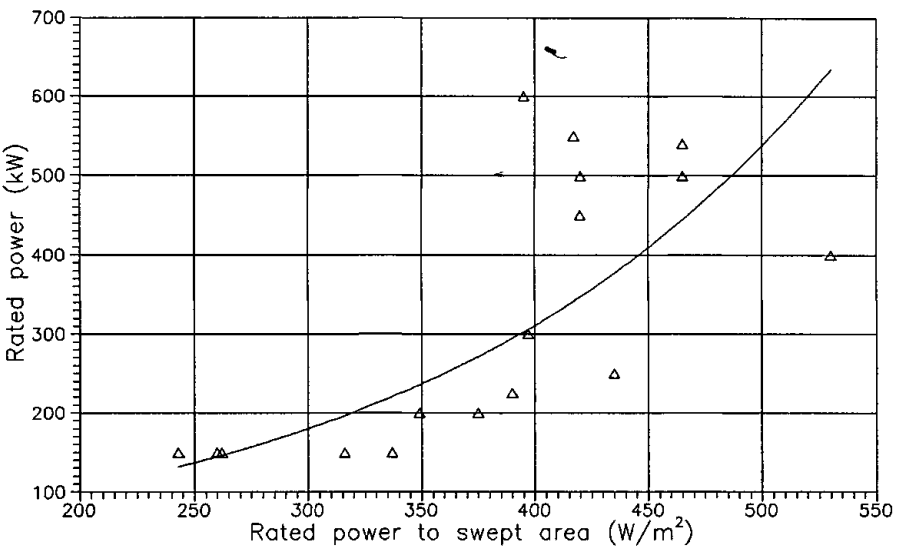

Figure 3.1 The variation of the rated power as a function of the ratio of rated power to swept area (specific power) for Danish wind turbines [24]. The full line is a best fit.

3.2 Introductory investigation

To investigate the fundamental variation of the annual production and important loads with specific power, optimizations of the maximum annual production have been performed for different specific powers (200 W/m^2 to 600 W/m^2) according to Table 3.1. The results of these optimizations will be the aerodynamic optimum as a function of the specific power because of no constraints on loads. Results are presented in Appendix A.

The optimized blade geometries are shown in Figure A1 to Figure A4. There is some degree of similarity between the different chord distributions in Figure A1 despite the variation from the different diameters. The blade mid sections have a relatively small chord, whereas the tip sections are scaled down steeply towards the tip. The root sections have a large chord, even though the root section has only minor influence on the produced power. For a final design a constraint would be applied to the blade root section chord. Compared to existing wind

turbines the nature of the optimized chord distributions is more complex. Traditionally, the chord is almost linear decreasing towards the tip.

Table 3.1 Preliminary optimizations at different specific powers with no constraints on loads. All rotors have a rated power of 1 MW.

	1	2	3	4	5
Specific power (W/m^2)	200	300	400	500	600
Rotor diameter (m)	79.8	65.1	56.4	50.5	46.0
Max. Angular vel. (rpm)	14.4	17.6	20.3	22.7	24.9

The twist distributions in Figure A2 compare quite well with existing designs. Towards the root, the twists have almost the same value for all specific powers. At the tip region however, the twist slope drops with the specific power. The tip pitch angles are gradually reduced as the specific power is decreased (Figure A3) to prevent the maximum rated power from being exceeded. It is notable that the bound on the tip speed has not been active for any of the optimizations.

There is some irregularity between the different optimizations, especially seen on the tip pitch angle (Figure A3) and on the tip speed variation (Figure A4). This is probably because the topology of the design space is flat around the optimum. Probably, a number of calculation conditioned local minima are found and these have almost the same performance, since there exist a rather weak coupling between some of the design variables and the objective function. This means that the optimization results will be slightly sensitive to the initial guess. However, influence from this is not found significant concerning the overall impression of the parameter variations. No optimization results have had significant deviations and different initial guesses have resulted in almost identical solutions.
The rotor performance is shown in Figure A5 to Figure A11 and in Figure 3.2.

The annual production in Figure A5 is seen to increase considerably as the specific power is lowered. The power curves all have a decent stall and some degree of uniformity (Figure A6). When the specific power is lowered, the slope of the power curve before stall is increased due to a larger swept area. The wind speed where the power curve is stalled decreases. The C_p curves show some difference (Figure A7). The width of the curves is decreased when the specific power is lowered and the wind speed with maximum C_p is lowered. This is necessary in order to keep the bound on the maximum rated power. The C_p curves at higher specific powers have a wider and flatter characteristic than what is usually obtained with optimization at a single design wind speed, because of the constraint on the rated power. Hereby, they reveal one of the advantages by using the present numerical optimization algorithm. All thrust curves show a high thrust at lower wind speeds, whereas thrust is reduced when the specific power is lowered to keep the bound on the rated power (Figure A8). Finally both calculated mean and extreme loads show a progressive increase towards lower rotor loading (Figure A9 - A11).

In Figure 3.2 the variation of the annual production, the extreme blade root moment at rotor stand still, the mean blade root flapwise moment and rotor thrust force are shown as function of the specific power. All figures are presented relative to the values at 500 W/m^2. It appears that a substantial increase in the annual production is obtained if the specific power is lowered. However, both blade and rotor loads also increase significantly.

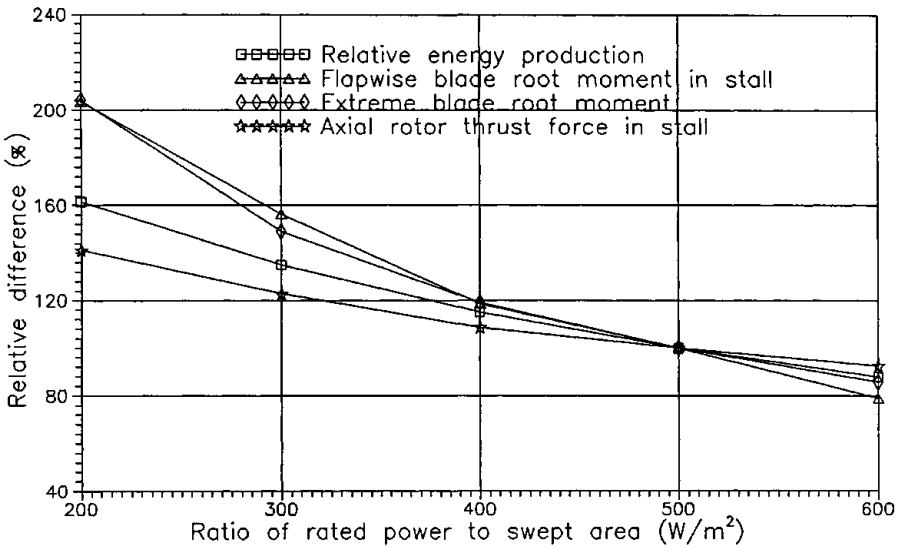

Figure 3.2 Relative variation of annual production, extreme blade root flapwise moment at rotor stand still, mean blade root flapwise moment and mean rotor thrust force for the different optimizations.

3.3 Constraints on the blade root flapwise moments

The performed introductory optimizations have shown, that the aerodynamic optimum is quite different for different specific powers. When solving optimization problems, it is often seen, that forcing the improvement of the objective function (in this case the annual production) to the limit, has a bad influence on other parameters such as loads. Therefore, it will often be preferable to have constraints on e.g. the loads even though this reduces the design space and in the most cases the objective function. The trade off between constraints on loads and the obtainable annual production will therefore be dealt with in this Section.

In the following, different constraints will be put on the following loads:

1) The mean blade root flapwise moment at stall (Section 3.3.1).

2) The extreme blade root flapwise moment at rotor stand still (Section 3.3.2).

The design variables are the chord and twist distributions, the tip pitch angle and the angular velocity.

The optimization tool can not handle constraints on the fatigue loads, since these are found far too time consuming to be calculated within the optimization process. Instead it has been chosen to apply a constraint on the mean blade root flapwise

moment at the windspeed where the entire blade is stalled corresponding to maximum power (Figure 3.3). It is expected that this mean load to some extend is correlated with the fatigue loads since reducing the mean load will lower the slope of the mean load as function of the wind speed before stall. This will be further investigated in Section 3.4.

In order to be able to investigate the variation of different performance parameters with the degrees of constraints, optimizations are run with constraints from 100% (unconstrained) to 60% of the resulting unconstrained loads from the aerodynamic optimum rotors in Section 3.2 as explained in Table 3.2. The rotors having the 60% constraint are constrained most. This results in 30 optimizations for the mean and the extreme loads, respectively.

Table 3.2 30 optimizations are performed with different degrees of constraints at different specific powers.

Specific power (W/m^2)	200	300	400	500	600
Unconstrained (100%)					
Constrained to 95%					
Constrained to 90%					
Constrained to 80%					
Constrained to 70%					
Constrained to 60%					

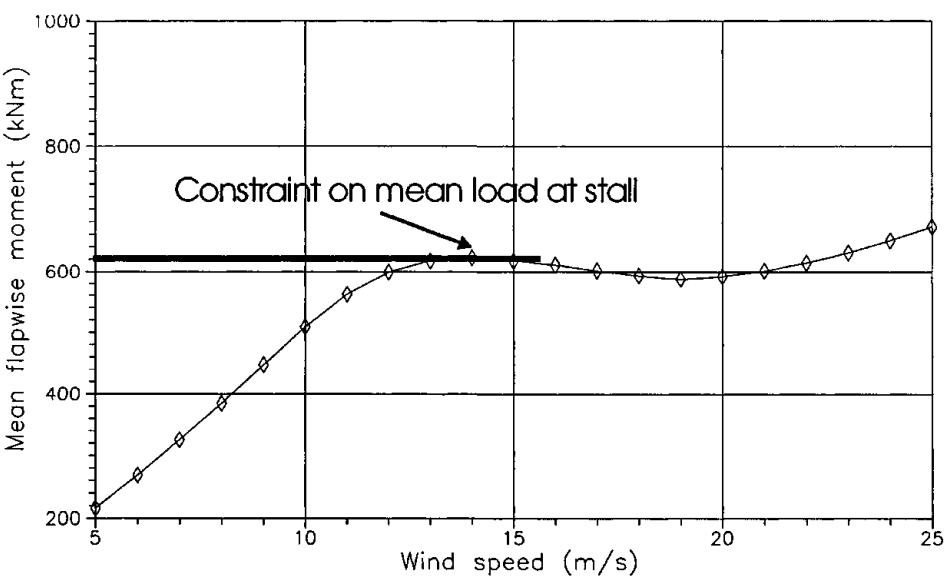

Figure 3.3 The constraint on the mean blade root flapwise moment is introduced to the wind speed at maximum power, where the entire rotor is stalled.

3.3.1 The mean blade root flapwise moment

The constraints considered in this Section are the maximum value of the mean blade root flapwise moment at the wind speed where the blade stalls, as indicated in Figure 3.3. Results from the optimizations at 500 W/m^2 are found in Appendix B.

Figures in Appendix B express the variation of the different optimization parameters, loads and performance with the change in the constrained load at the specific power, 500 W/m^2, whereas figures shown within this Section reveal differences between the different specific powers.

The optimized blade geometries are shown in Figure B1 to Figure B4. The constraint on the load is primarily satisfied by reducing the solidity. The chord distributions (Figure B1) show a remarkably decrease towards the tip section when the constrained load is decreased, whereas the root sections are practically unaltered. The root section has only minor influence on as well the power as on the blade root flapwise moment and apparently the influence from the chord on the constrained load is even less than the influence on the power.

The twist distributions are in fair agreement in Figure B2. A small increase in twist towards the blade root for decreased constrained load is seen. The tip speed (Figure B4) is increased to the bound when the constrained load is lowered to 80%. The lower solidity allows the tip pitch angle (Figure B3) to be increased without exceeding maximum power. However, to keep the constrained load the angular velocity is also increased. The reason for the sudden change in the tip pitch angle at 80% is therefore that the bound on the tip speed is reached.

The rotor performance is shown in Figure B5 to B11 and further information about different specific powers are presented in Figure 3.4 to Figure 3.7.

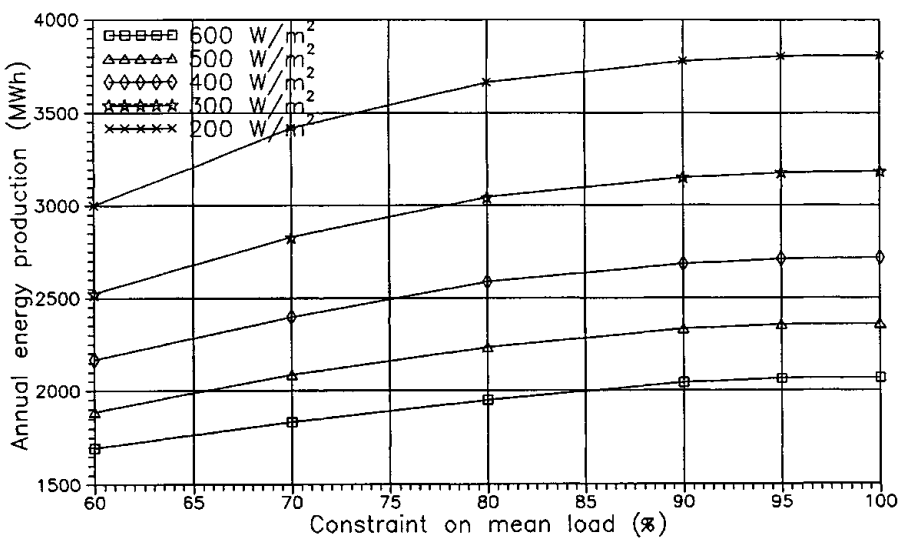

Figure 3.4 Annual production for optimized rotors with constraints on the mean blade root flapwise moment for different specific powers. 100% corresponds to no constraint on the mean load.

In Figure 3.4 the annual production is shown as a function of the constrained load for different specific powers. It can be seen, that the annual production is lowered with the constrained load. However, the annual production is lowered just a few percent when the constraint is lowered from 100% to 90%. This is an important result because it means, that a trade off between the annual production of energy and the loads might be possible, remembering that the mean load is linearly reduced. It can be seen that the loss in annual production is larger for the lower specific power.

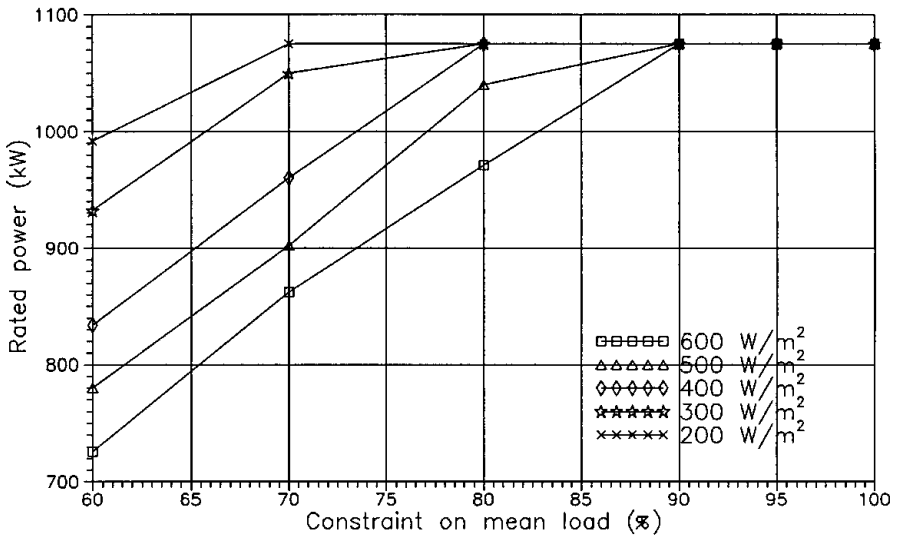

Figure 3.5 Rated power for optimized rotors with constraints on the mean blade root flapwise moment for different specific powers.

The reason for the progressive variation in the annual production with the constrained load is seen in Figure 3.5 and Figure B6. When the constrained load is decreased it becomes problematic to keep the rated power on 1 MW, especially for high specific powers. The mechanisms behind this can be seen on the C_P and C_T curves (Figure B7 and B8). The wind speed for C_{Pmax} and the value of C_{Pmax} is decreased both with the constrained load and with the specific power.

C_T is equally decreased, especially at low wind speeds. The influence from this is most severe at high specific power, where the Betz limit corresponds to a lower attainable power. The optimum rotor design is therefore gradually departed from the aerodynamic optimum with both decreasing constrained load and specific power.

The variation of the extreme blade load and the rotor thrust force is seen in Figure 3.6 and Figure 3.7, respectively. It can be seen that the linear reduction in the constrained mean blade load results in a reduction of both the extreme blade load and the rotor thrust force, which is almost linear. The negative slopes of both load variations are higher towards lower rotor loading.

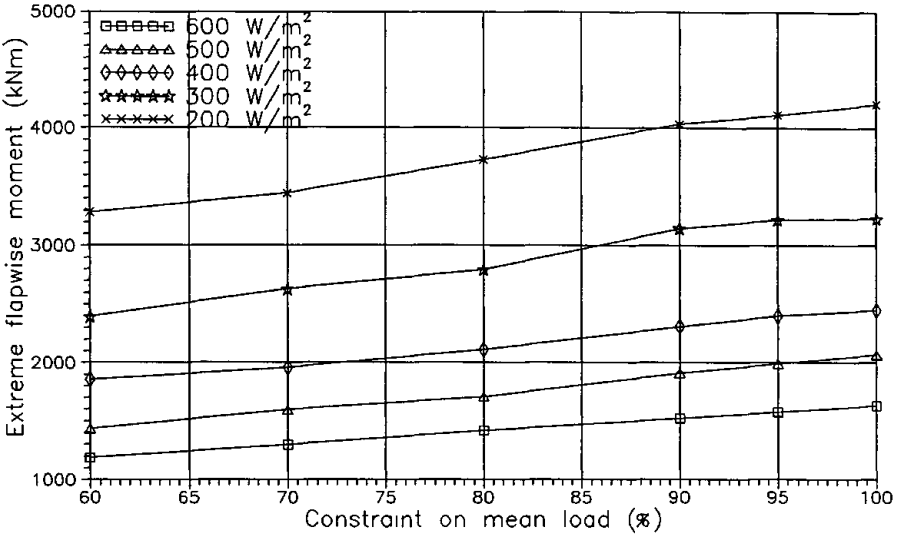

Figure 3.6 Extreme blade root flapwise moment for optimized rotors with constraints on the mean blade root flapwise moment for the different specific powers.

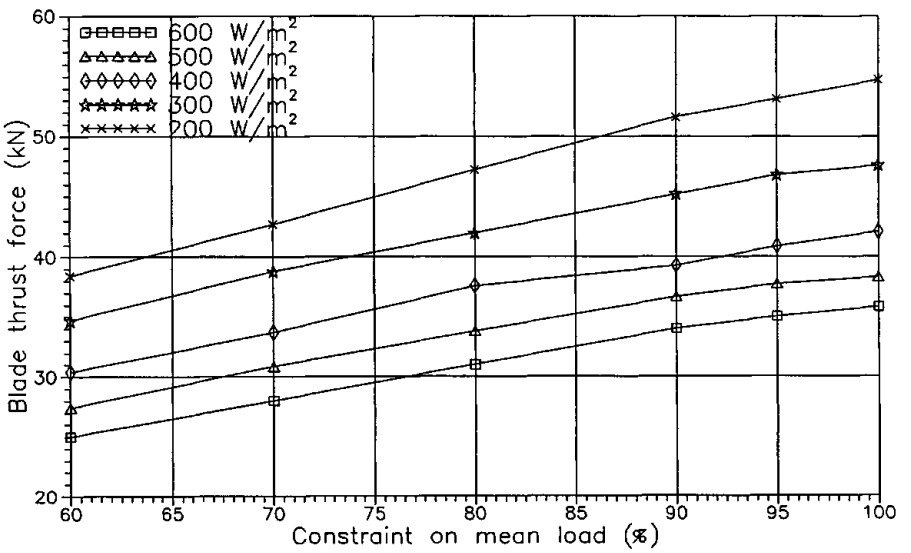

Figure 3.7 Rotor thrust force on one blade for optimized rotors with constraints on the mean blade root flapwise moment for different specific powers.

3.3.2 The extreme blade root flapwise moment

The constraints treated in this Section are the extreme blade root flapwise moments at rotor stand still, calculated from the German Lloyds design code [8]. Results from the optimizations at 500 W/m^2 are found in Appendix C. These figures show the variation with the change in the constrained load, whereas figures revealing differences between the different specific powers are shown within this Section. Since the optimization results have many points of resemblance with the optimizations from the previous Section, focus will be put only on the differences.

Figure C1 to C4 contain the optimized geometries. As in the previous Section, the twist (Figure C2) is almost unaltered except in the root region. On the other hand, the change in the chord (Figure C1) is primarily in the root region in contrast to the previous Section. This is because, the extreme load calculation from the design code results in a larger contribution from the root region compared to the mean load calculation. The optimization algorithm then reduces solidity where the contribution to the power is minimum.

The tip pitch angle (Figure C3) is gradually reduced and the rotational speed increased until the tip speed (Figure C4) reaches its bound. After that the tip pitch angle is increased. This is opposite of the constraint on the mean load. The increase in the tip pitch angle increases the annual production but has no influence on the extreme load since this is being calculated at stand still.

The performance for the optimized rotors is shown in Figure C5 to C11 whereas figures representing the variation of the performance with specific power is shown in Figure 3.8 to Figure 3.11.

Figure 3.8 and Figure 3.9 show the variation of the annual production and the rated power, respectively. The tendencies are the same as in the previous Section. The slope of the annual production curves are less negative and the rated power is generally closer to the bound at lower constrained load values. This means that the constraint on the extreme load acts weaker on the annual production than the constraint on the mean load. The design can therefore be constrained more on the extreme load for a similar reduction in the annual production.

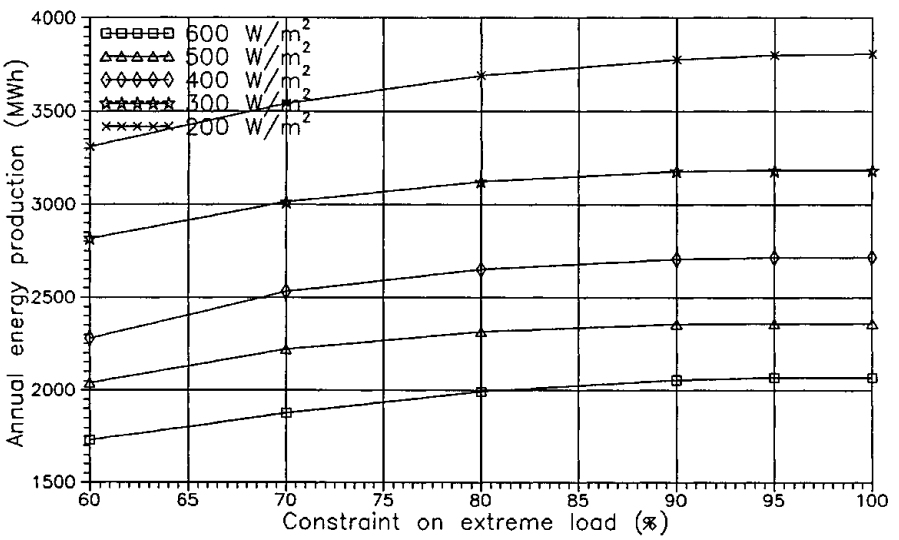

Figure 3.8 Annual production for optimized rotors with constraints on the extreme blade root flapwise moment for different specific powers.

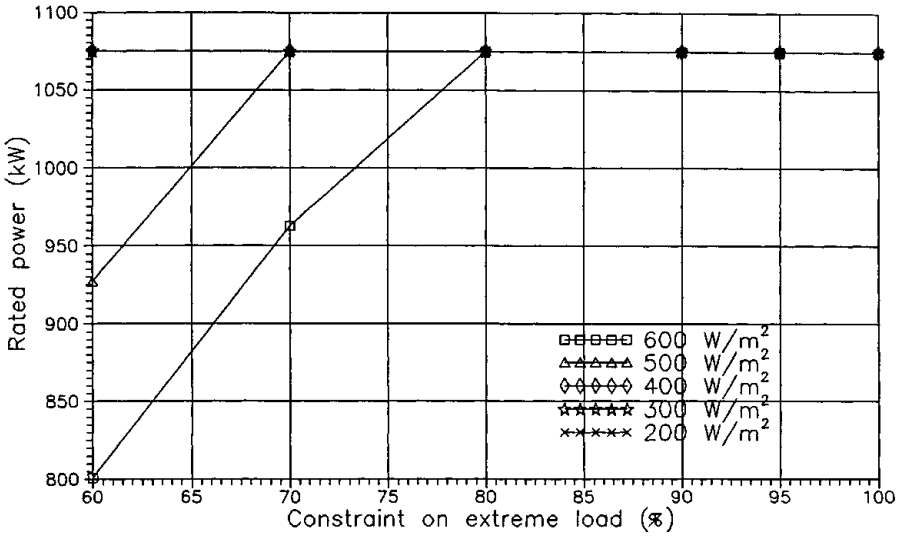

Figure 3.9 Rated power for optimized rotors with constraints on the extreme blade root flapwise moment for different specific powers.

In Figure 3.10 and Figure 3.11 the mean blade root flapwise moment and the mean rotor thrust force on one blade are shown, respectively. Clearly, the constrained load has only minor influence on the mean blade root flapwise moment and the same holds for the blade thrust force at higher rotor loadings. The tendency however, is the same regarding the reduction of the mean loads.

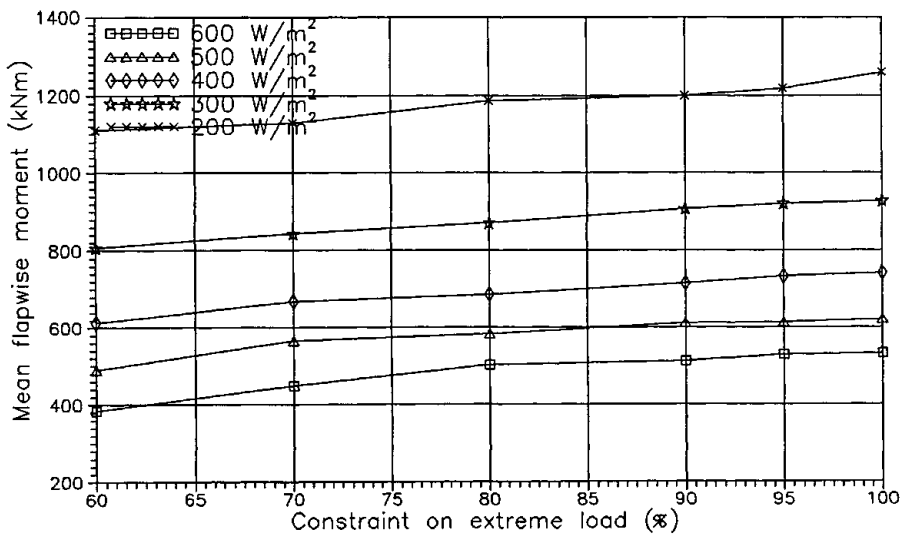

Figure 3.10 Mean blade root flapwise moment for optimized rotors with constraints on the extreme blade root flapwise moment for the different specific powers.

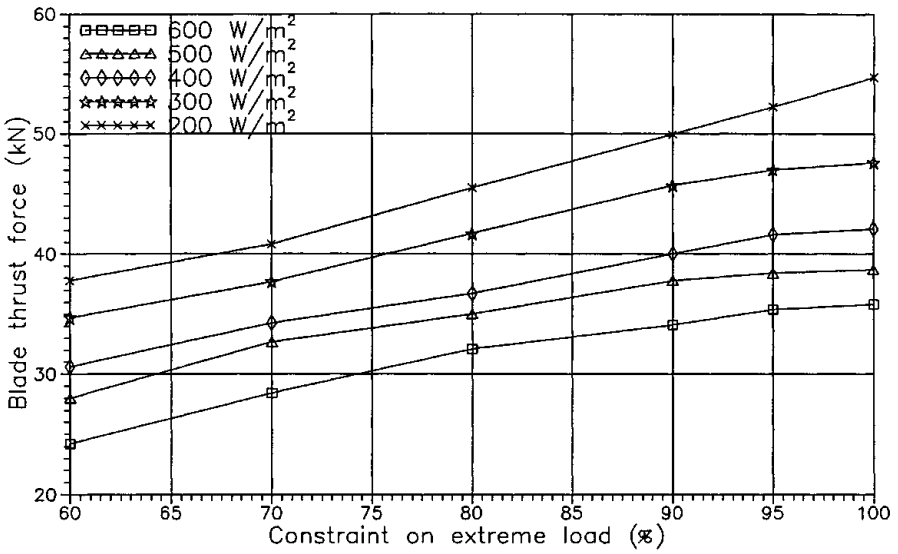

Figure 3.11 Rotor thrust force on one blade for optimized rotors with constraints on the extreme blade root flapwise moment for different specific powers.

3.3.3 Summary

The investigations in this Section have shown a large degree of similarity when constraining mean and extreme loads. It seems though like the constrained mean load has a larger influence on the extreme load than the opposite case. Reducing the constrained mean load has turned out to result in a reduction of other loads. In reality constraints would be put on both mean and extreme loads at the same time.

The key design variable has been the chord, where less solidity has been the main parameter for the reduced loads. Constraints on both mean and extreme loads is likely to result in an overall reduction of the solidity, along the entire blade span.

The limited reduction in the annual production with the constrained load indicates, that a trade off between a lower annual production and lower loads might be possible. However, we still have to verify how the constrained mean loads correlate with the life time equivalent fatigue loads.

3.4 Equivalent fatigue loads

The purpose with this Section is to investigate how the different aerodynamic designs from the optimizations with constrained loads in Section 3.3.1 and Section 3.3.2 compare as concerns the fatigue loads. To ensure a firm comparison, all optimized rotors will be assumed to have equal dynamic qualities concerning the structural design. This means that the eigenfrequencies are identical relative to the rotational speed. Since the constraints on the mean loads were limiting the extreme loads as well, attention will primarily be paid to the constraint on the mean load.

It has turned out, that maintaining equal dynamics at specific power, 200 W/m^2 is impossible. Compared with existing wind turbines, 200 W/m^2 is too different from

these designs. Reliable aeroelastic calculations have therefore not been possible on this family of rotors.

Aeroelastic calculations of time series are simulated at different wind speeds for each of the optimized rotors between 300 and 600 W/m^2. The life time spectra are then found from Rainflow counting assuming linear damage accumulation. Comparison is finally based on expressing the life time spectra as lifetime equivalent fatigue loads at 10^7 cycles having equal S-n curve exponents. The theory used is explained in Section 2.2.

3.4.1 Calculation procedure and assumptions

The equivalent fatigue loads are calculated from 5 minute time series at 7 different wind speeds covering an operational interval from 4.5 m/s to 25.5 m/s. All calculations are calculated with wind input generated with the same random seed to ensure that a relative comparison between different designs is possible even though the time series are short. The life time spectrum will be based solely on these calculations whereas shut down and start up sequences as well as other life time events will not be included.

Operational conditions will be the Danish roughness class 1. Assuming the hub height to be 50 m and the roughness length to 0.01 m gives the Weibull parameters, A = 7.92 and k = 1.9. The design turbulence intensity is 8.5% defined by the Danish code of practice [17]. The turbulence intensity is then corrected for wind farm conditions assuming a distance of 5 rotor diameters between each wind turbine. The wind speed intervals, wind speed probability and the corrected turbulence intensities can be seen in Table 3.3 based on [17] and [18].

Table 3.3 The normal operational interval is divided into 7 wind speed intervals with probability and turbulence intensity from [17] and [18] based on the Danish roughness class 1.

Wind speed interval (m/s)	4.5-7.5	7.5-10.5	10.5-13.5	13.5-16.5	16.5-19.5	19.5-22.5	22.5-25.5
Wind interval probability (%)	42.89	31.64	16.53	6.46	1.94	0.45	0.08
Turbulence intensity (%)	17.2	17.2	17.2	15.3	12.9	11.9	11.9

The structural degrees of freedom (DOF) are: 2 flapwise mode shapes and first edgewise mode shape for each blade (9 DOF), 2 tower bendings, tilt, yaw, 2 main shaft bendings and shaft rotation. A total of 15 degrees of freedom. Compared to the available options in the "Flex4" code, the second edgewise mode shape has been found unimportant and it has been chosen to leave out shaft torsion. The latter choice has been taken in order to avoid misleading results from coupling between the edgewise blade bending modes and the transmission system torsional modes, since the transmission system is kept unchanged for all calculations even though there is a considerable change in the applied torque from the rotor due to the change in the rotational speed. The shaft torsional DOF is believed not to be

important at normal conditions for the loads considered, whereas it would be important in the transient phases of stopping and starting the rotor.

The wind turbine dynamic design is based on an existing wind turbine of equal size concerning the different components as tower, hub, generator, nacelle etc. The important eigenfrequencies for each of the optimized families of rotors (each family is the optimized rotors with the same specific power) are adjusted to be almost identical seen relative to the rotational frequency 1P. This ensures that primarily aerodynamic changes on the different rotor designs are revealed in the analysis of the different overall wind turbine time simulations.

For each family of rotors, the dynamics are adjusted in the following manner, so that no unfavourable amplifications of eigenfrequencies happen:

First the blade mass, the blade centre of gravity and the blade centre of mass inertia is adjusted to reasonable values.

Next, the following non rotational eigenfrequencies are chosen on basis of a number of typical Danish wind turbines.:

1) The first blade flapwise bending eigenfrequency is chosen to be within 3.8P to 4.0P.

2) The first blade edgewise bending eigenfrequency is chosen to be approximately 7P.

3) The first tower bending mode is chosen to be 1.6P.

These are found by adjusting the blade flapwise and edgewise stiffness, blade mass and tower bending stiffness.

Finally, the following rotor eigenfrequencies at rotor stand still are chosen, so that the dynamics of the entire coupled system is a local optimum according to the guidelines in [19]:

4) The asymmetric rotor flapwise bending mode that is coupled with tower torsion (yaw) is chosen within 3P to 3.2P.

5) The asymmetric rotor flapwise bending mode that is coupled with the second tower bending mode (tilt) is chosen within 3P to 3.2P.

These eigenfrequencies are adjusted by changing the shaft bending stiffness and the tower torsional stiffness. When the rotor is rotating these eigenfrequencies are shifted approximately ± 1P due to gyroscopic coupling [19]. This means that the area around 3P, where the turbulence input is, is avoided.

3.4.2 Time series

Appendix D contains an example of a calculated time series at 15 m/s for the unconstrained optimized rotor at specific power, 500 W/m^2. Focus has been directed towards the flapwise and edgewise blade root moments, the rotor thrust force and the rotor tilt and yaw moments, since these are used in Section 3.5 in the material consumption calculation.

It is seen that most of the figures in Appendix D reveal a significant stochastic variation caused by the turbulent wind field, except for the edgewise blade root moment which is primarily deterministic driven from the blade gravity. Bad proportioned dynamics would appear as oscillations having either large load ranges caused by negative damping or long oscillation periods from very little positive damping. All time series have been judged in this qualitative manner.

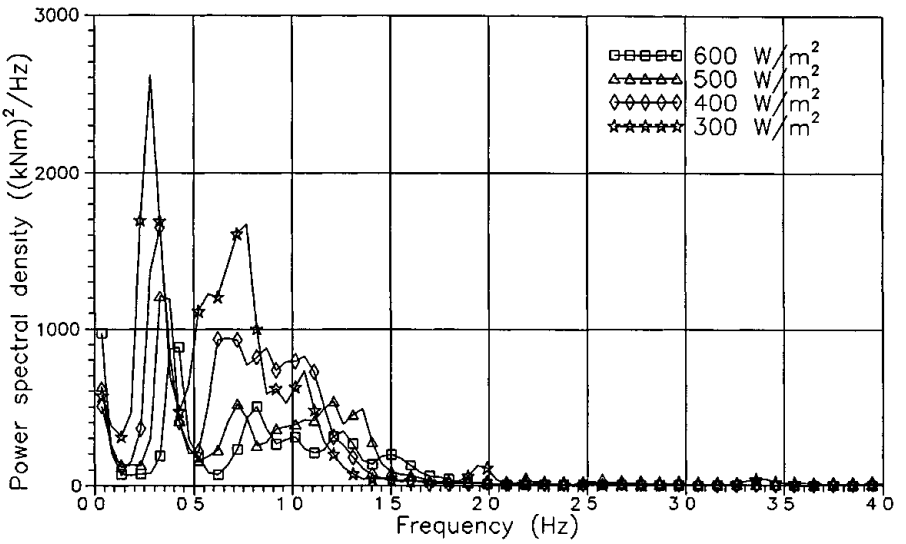

Figure 3.12 *Power spectral density of the blade root flapwise bending moment for the unconstrained optimizations at different specific powers.*

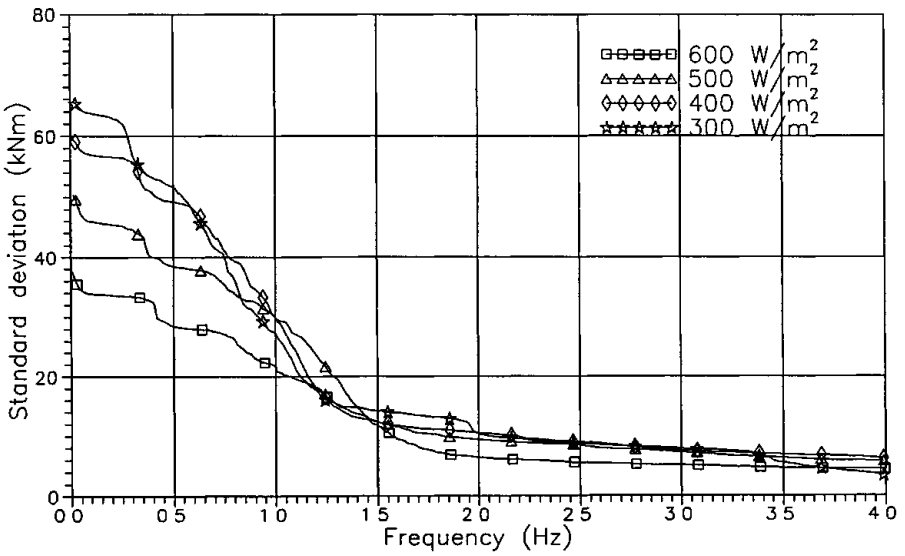

Figure 3.13 *The standard deviation found by integration of the power spectral density of the blade root flapwise bending moment for the unconstrained optimizations at different specific powers.*

Because it is difficult to reveal the exact dynamic nature of the loads just from the time series, the power spectral density (PSD) has been calculated with Fast Fourier Transformation. The dominating amplified frequencies have all been

compared with the rotational frequency, 1P, and have been found acceptable, though the rotors at specific power, 300 W/m^2 have some amplification at other frequencies than 1P and 3P This is probably because this specific power is on that limit where it becomes impossible to obtain equal dynamics

To justify that the dynamic adaptation is applicable for rotors with different specific power, the PSD's for the unconstrained rotors are compared in Figure 3 12 and Figure 3 14 for the blade root flapwise moment and the rotor yaw moment, respectively

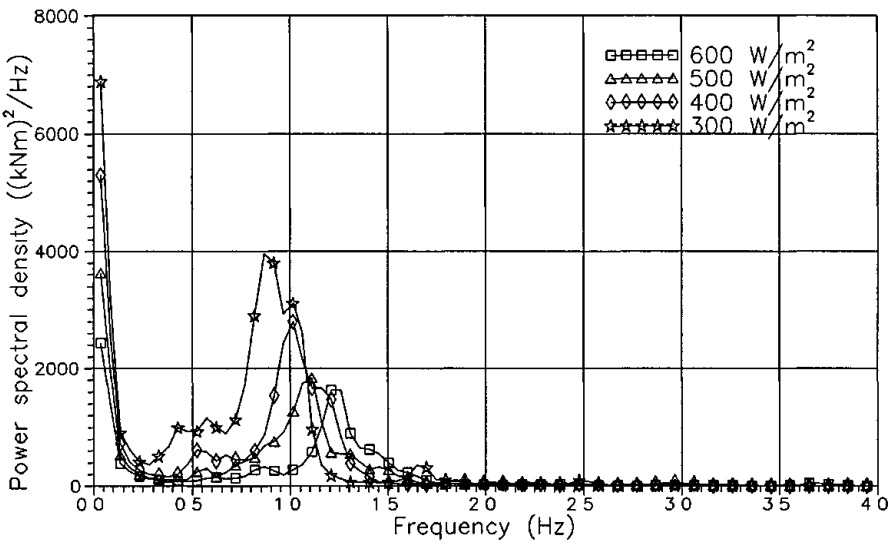

Figure 3 14 *Power spectral density of the rotor yaw moment for the unconstrained optimizations at different specific powers*

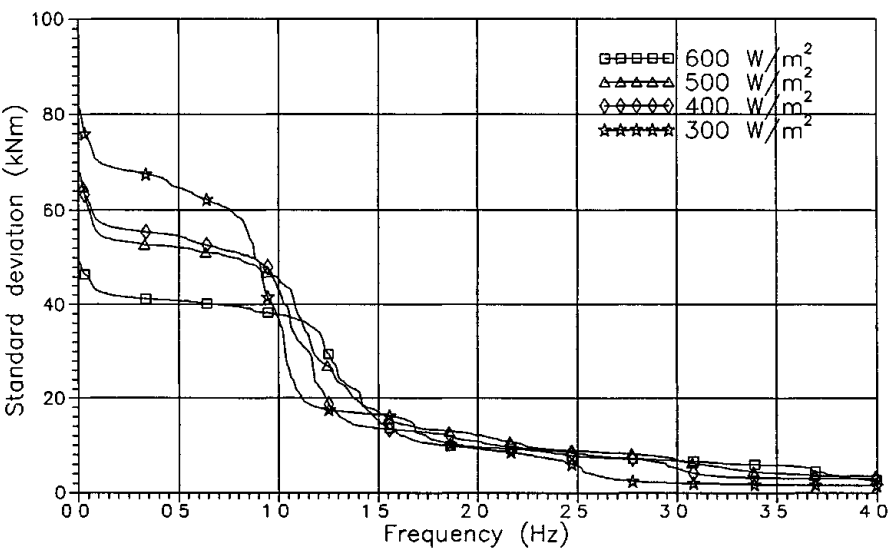

Figure 3 15 *The standard deviation found by integration of the power spectral density of the rotor yaw moment for the unconstrained optimizations at different specific powers*

The standard deviation, σ^2, has been found by integration of the PSD from ∞ to 0:

$$\sigma_i^2 = \sum_{j=\infty}^{j=i} 2PSD_j \tag{10}$$

where i,j are frequency nr.

In Figure 3.13 and Figure 3.15. the standard deviation as a function of frequency is shown. The direction of integration has been chosen so that differences at low frequencies does not offset the curves at higher frequencies, since this is likely to occur.

The blade root flapwise moment in Figure 3.12 has a large peak at the 1P frequency, which varies from 0.29 Hz to 0.43 Hz depending on the specific power. This comes from deterministic input from wind shear and tower shadow and stochastic input from turbulence which is shifted downwards as the specific power is lowered. The standard deviations in Figure 3.13 show the 1P frequency as a jump. From about 2 Hz down to 1P the standard deviation is gradually increased equally for the different specific powers.

The rotor yaw moment in Figure 3.14 has a peak at the 3P frequency, which varies between 0.87 Hz and 1.29 Hz, from stochastic wind turbulence and deterministic wind shear and tower shadow. No other frequencies are amplified significantly. The standard deviations in Figure 3.15 show the 3P frequency clearly as the primary turbulence input.

All calculated time series have been spectral analyzed and no inexpedient amplifications have been found. In general, the PSD's for the different specific powers show good agreement and the standard deviations show no signs of unexpected amplifications of frequencies. This validates the chosen procedure for comparison of the rotors at different specific powers.

3.4.3 Life time equivalent fatigue loads

On basis of the calculated 5 minute time series at 7 windspeeds, Rainflow counting has been performed of the blade root bending moments, the rotor thrust force and the rotor bending moments. This has resulted in life time spectra for each of the optimized rotors with constraints on the mean load. For comparison, the life time spectra have been expressed as equivalent loads. The S-n curve exponent for the blade moments has been chosen to m = 10 for fibreglass. For the rotor loads, m = 4 has been chosen for welded steel.

In Figure 3.16 the equivalent blade root flapwise moment is shown as a function of the constrained mean load for the different specific powers. It is seen, that the constraining of the mean load has been beneficial to the magnitude of the equivalent fatigue load and, that the relation between the loads is almost linear. A constraint on the mean load of 60% corresponds to a drop in the fatigue load to about 65%. Having in mind the amount of calculations on which the results are based, the small deviations are found insignificant.

The slopes of the equivalent loads as function of the constrained load seem to be only little negative at the rotors near 100%. The deviations around 90% - 95% could be caused by small changes of the rotational speed until the bound on the

tip speed is reached about 80%. For rotors constrained to 80% or more, the linear tendency is very clear.

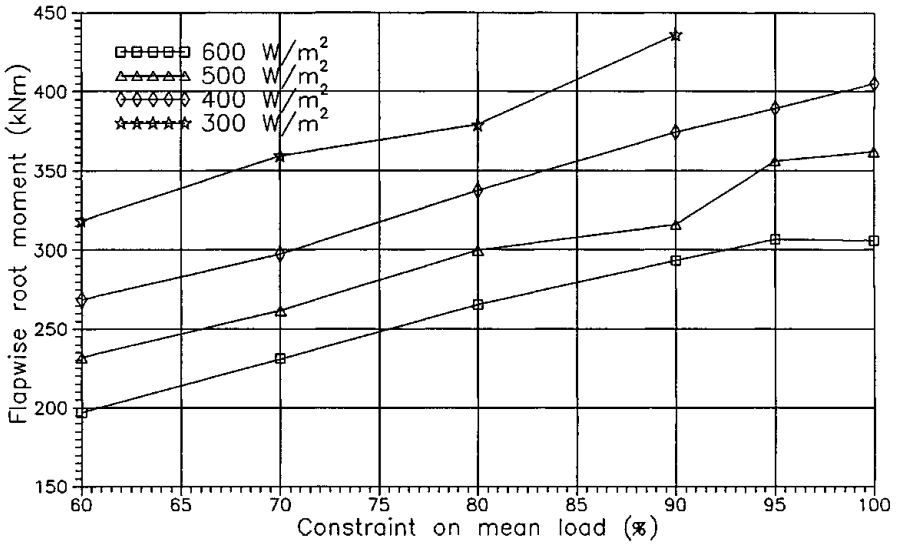

Figure 3.16 *Equivalent flapwise blade root moment, N_{eq} = 10^7, m = 10, as a function of the constrained mean blade root flapwise moment for the different specific powers.*

The rate of decrease in the equivalent fatigue loads seems to be independent of the actual specific power whereas the load range level increases with lower specific power as it is expected. At specific power, 300 W/m^2 results between 90% and 100% constraint was found unreliable and the specific power, 300 W/m^2 seems to be on the limit of the correctness of the assumptions of equal dynamics since the curve is slightly irregular.

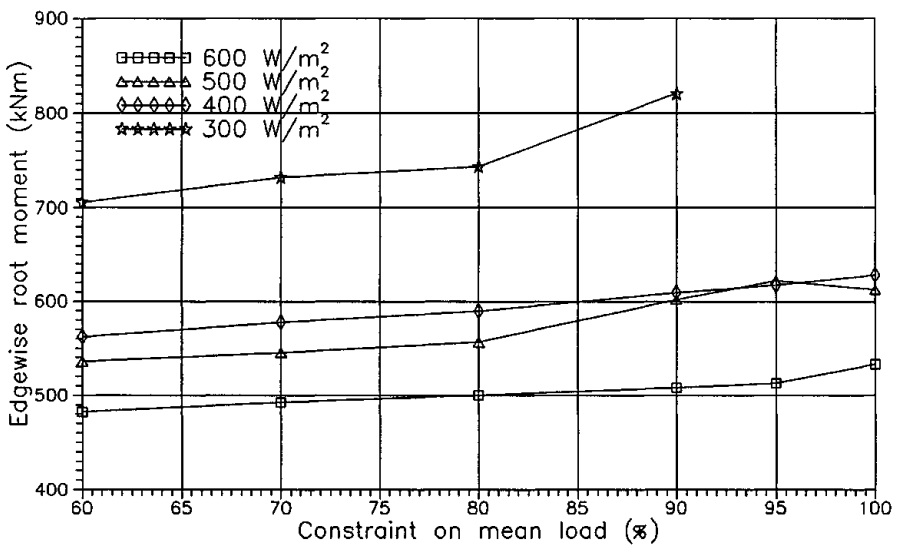

Figure 3.17 *Equivalent edgewise blade root moment, N_{eq} = 10^7, m = 10, as a function of the constraint on the mean blade root flapwise moment for the different specific powers.*

In Figure 3.17 the equivalent blade root edgewise moment is shown as a function of the constrained mean load for the different specific powers. The variation of this load with the constrained mean load is also almost linear, but the rate of change is smaller than that of the equivalent blade root flapwise moment. This is because the edgewise moment is primarily deterministic driven by the gravitational forces from the blade mass. Since all rotors in a family (at the same specific power) have equal blade masses and static moment, the decrease in the equivalent edgewise load is due to a reduction in the stochastic part of the load. A constraint on the mean load of 60% corresponds to a drop in the fatigue load to about 90%.

One reason for the difference between the different specific powers could be due to the total mass of the blades, since this is only roughly estimated in the dynamic adjustment of the eigenfrequencies. However, this has insignificant influence on the size of the other equivalent fatigue loads and the blade mass used in the aeroelastic calculations is not used in the calculation of the material factor in Section 3.5.

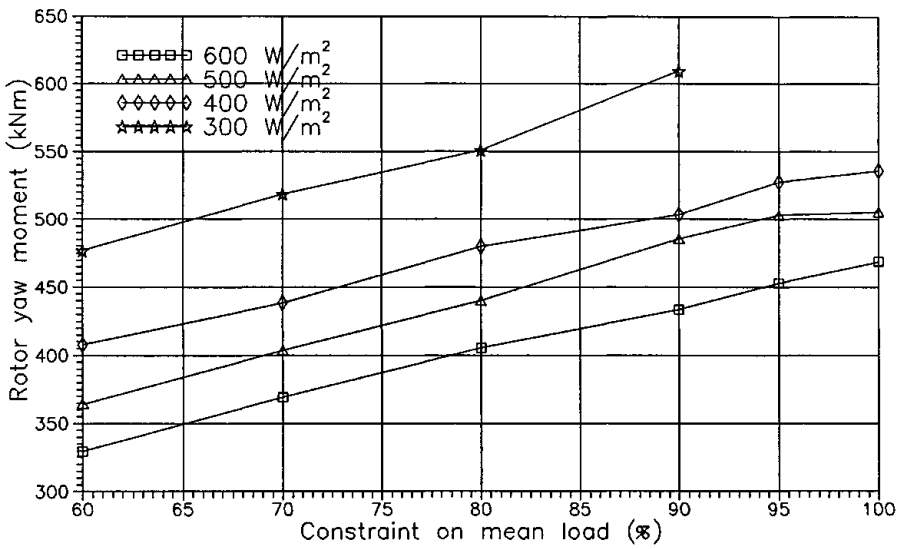

Figure 3.18 *Equivalent rotor yaw moment, $N_{eq} = 10^7$, $m = 4$, as a function of the constrained mean blade root flapwise moment for the different specific powers.*

In Figure 3.18 and Figure 3.19 the equivalent rotor yaw and tilt moments as a function of the constrained mean load at different specific powers are shown, respectively. A good linear correlation between the constrained mean load and the equivalent fatigue loads is again seen. The agreement is even better than for the blade moments. The slopes of the curves are almost identical indicating independence of specific power and a large degree of similarity between equivalent rotor yaw and tilt moments. Furthermore, the levels of the yaw and tilt moments are about the same, the tilt moment being slightly higher. The constraint on the mean load of 60% corresponds to a drop in the fatigue loads to about 75%. However, it seems like the variation in yaw moment with specific power increases towards lower specific power, while the opposite is valid for the tilt moment.

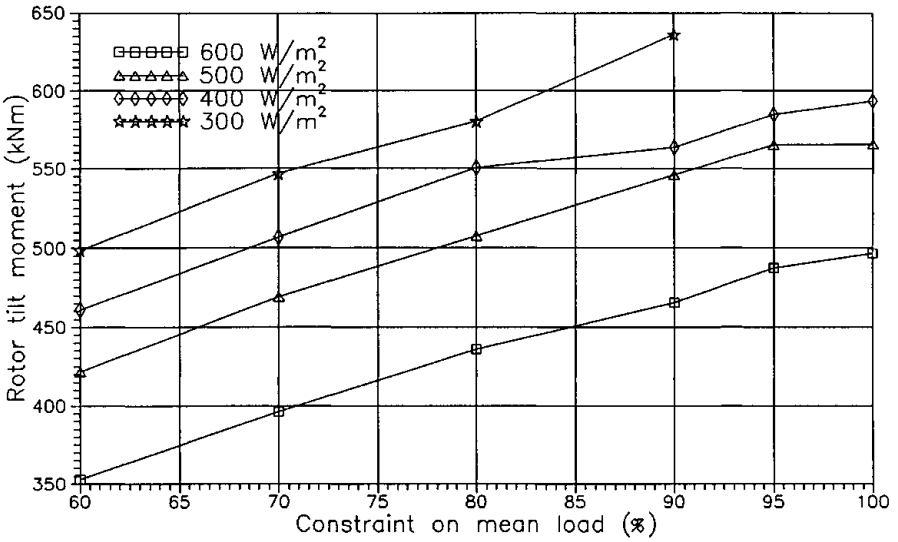

Figure 3.19 *Equivalent rotor tilt moment, N_{eq} = 10^7, m = 4, as a function of the constrained mean blade root flapwise moment for the different specific powers.*

Finally in Figure 3.20 the equivalent rotor thrust force is shown as a function of the constrained load for different specific powers. In contrast to the previously mentioned fatigue loads, no clear linear tendency is seen when the constrained load is lowered even though the level of the loads is decreased with the constrained load.

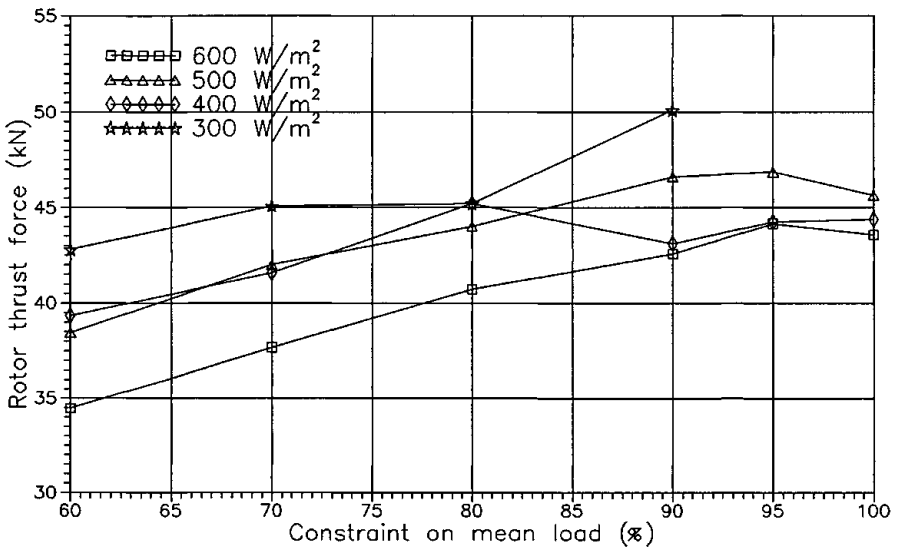

Figure 3.20 *Equivalent rotor thrust force, N_{eq} = 10^7, m = 4, as a function of the constrained mean blade root flapwise moment for the different specific powers.*

The equivalent thrust force increases with the decrease in the specific power probably because the swept area is increased. The size of the rotor thrust force is primarily given from the rotor solidity. At the root section this was almost unaffected by the constraint on the mean load, whereas it was decreased by the

constraint on the extreme load as shown in Section 3.2. This is probably the main reason for the irregularities in Figure 3.20. It emphasizes that the design phase should involve contemporary constraints on both mean as well as extreme loads.

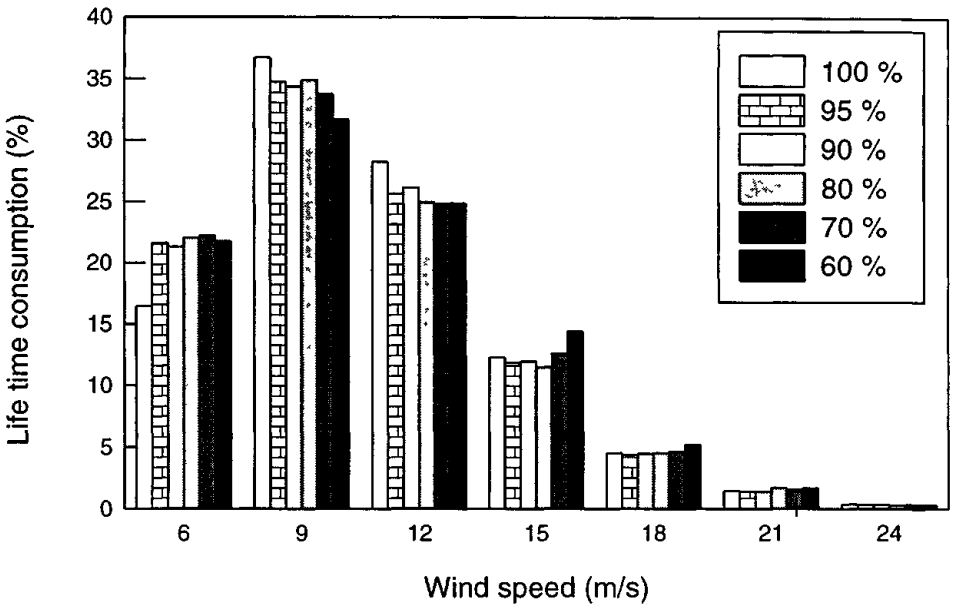

Figure 3.21 Distribution of life time consumption for the flapwise blade root moment for the family of rotors at specific power, 500 W/m².

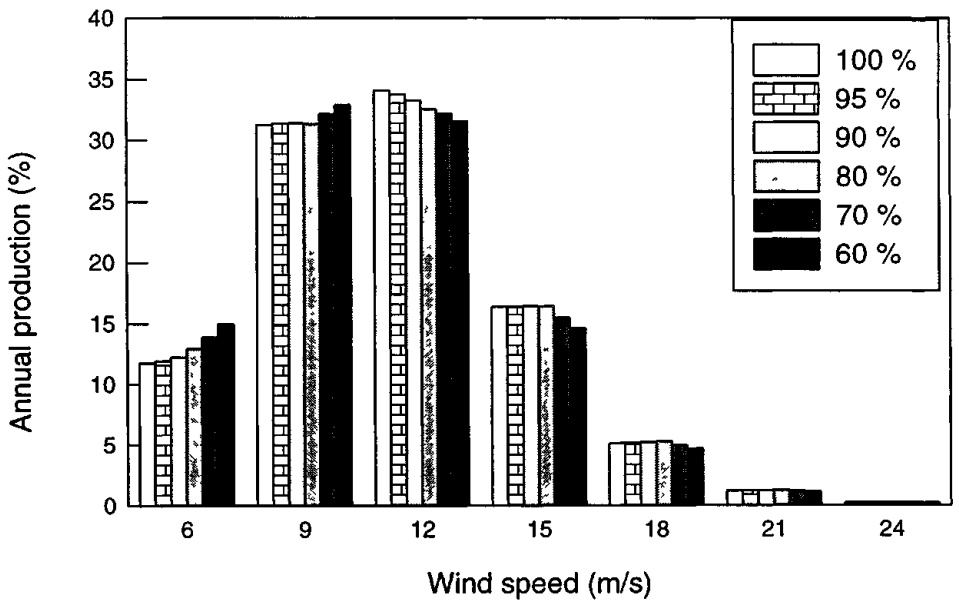

Figure 3.22 Relative annual production distribution for the family of rotors at specific power, 500 W/m².

In Figure 3.21 the distribution of life time consumption in percent is shown as a function of the wind speed for the family of rotors at specific power, 500 W/m². The majority of the life time is spent at the wind speeds before stall, whereas higher wind speeds do not contribute significantly. This would probably change if other life time events than the normal operation were included in the life time

calculations. It can be seen that the life time consumption is pushed primarily towards lower windspeeds but also towards higher wind speeds as the constraint approaches 60%.

In Figure 3.22 the annual production distribution in percent is shown corresponding to the life time distribution in Figure 3.21. When the constrained load is lowered, the relative annual production at lower windspeeds is increased. It is beneficial, that at 6 m/s there is an increase in the life time consumption together with an increase in the relative annual production.
It should be noted that lowering the cut off wind speed to 20 m/s becomes more attractive when the constraint is lowered since the relative annual production at high windspeeds is decreased and the life time consumption is increased. Furthermore, the life time consumption from operation at high windspeeds would be reduced.

3.4.4 Summary

The results in this Section have shown, that applying a constraint on the mean loads at stall has proven to be very suitable for limiting the fatigue loads calculated for an operating wind turbine rotor. Equivalent fatigue loads have been found to vary linearly with the constrained mean blade root flapwise moment for both blade and rotor moments. This is summarized in Figure 3.23 for the specific power equal to 500 W/m^2. Appendix E contains this variation for the other specific powers.

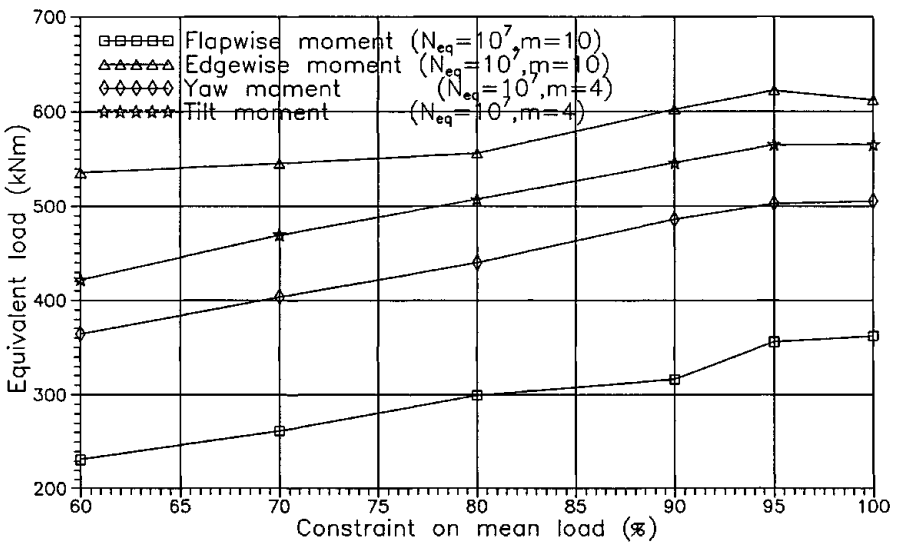

Figure 3.23 *Equivalent fatigue loads as a function of the constrained mean blade root flapwise moment for specific power, 500 W/m^2.*

The findings in this Section are in good agreement with results from [25], that concerns gear box loads. Here, a proportionality between the load standard deviation and the slope of the mean loads versus wind speed was found. The standard deviation correlates with the equivalent fatigue loads used in this Section.

These good correlations between the mean loads and the equivalent fatigue loads are encouraging and very important for future work with numerical optimization algorithms since the approximately linear correlations between mean and fatigue

loads give several opportunities for including constraints on fatigue loads without having to include the time consumable aeroelastic calculations directly in the optimization process.

3.5 Material consumption

The almost linear correlation between the life time equivalent fatigue loads and the constrained mean loads, found in the previous Section, indicates a possible trade off between a loss in the annual production and a decrease in the fatigue loads from the constraint on the mean load. However, to achieve the final basis for comparison, the reduction of the cost from the reduction of the fatigue loads should be quantified.

Since the size of the fatigue loads affect the entire wind turbine, it would be defective just to look at the rotor. In this Section, the material consumption for the entire wind turbine is calculated on basis of the equivalent blade and rotor moments together with the rotor thrust force. The calculation of the material consumption is explained in Section 2.3.

The material consumption will be derived as the percentage expense relatively to a reference wind turbine. This reference rotor has been chosen to be the optimized rotor at specific power, 500 W/m^2 with the mean load constrained to 90%. This is then given the material consumption, mc = 100%.

The material factor, mf, is shown for different wind turbine components as a function of the constrained mean load in Figure 3.24. All components show a drop as the constrained load is lowered. The blade decreases linearly with the constraint, probably because of the decrease in solidity. The shaft and the hub together with the blade show the most significant drop. The gearbox and the tower is reduced less, probably because the blade root edgewise moment is less reduced compared to the other fatigue loads.

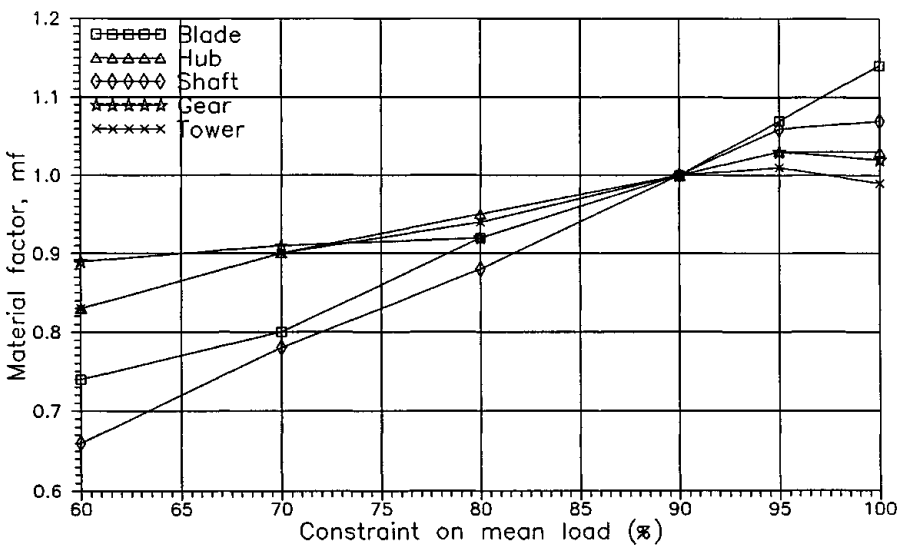

Figure 3.24 The material factor, mf, at specific power, 500 W/m^2 for different components as a function of the constrained mean blade root flapwise moment.

In Figure 3.25 the material consumption, mc, is shown as a function of the constrained mean load for different specific powers. A linear tendency with the constrained mean load is seen. Most of the component dimensions depend nearly linearly on the fatigue loads as it was shown in Figure 3.24, and this explains the linear behaviour of the material consumption. The values at specific power, 300 W/m^2 seem partially unreliable due to the problems explained in Section 3.4 concerning the equal dynamic properties.

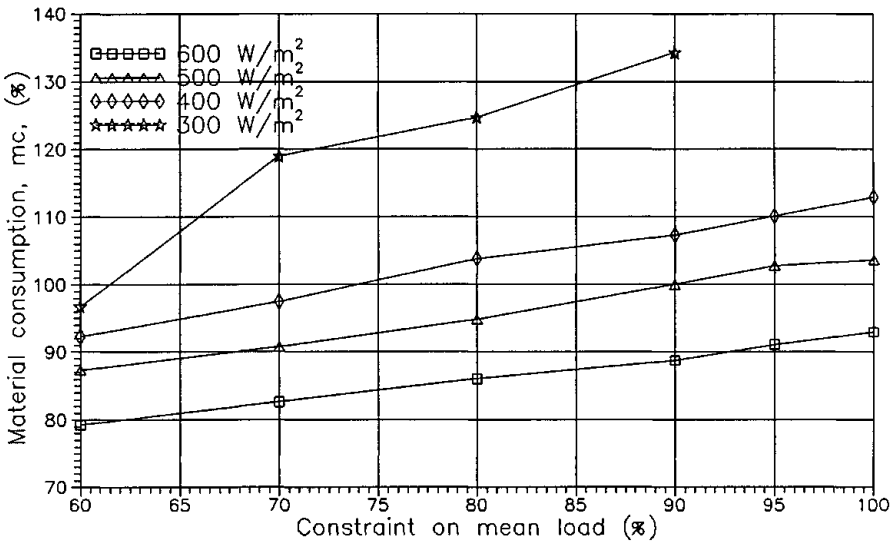

Figure 3.25 The material consumption, mc, as a function of the constrained mean blade root flapwise moment for different specific powers.

The calculation of the material consumption is based on the cost function originating from analysis of existing wind turbines. This means that the accuracy decrease when the actual design is departed from the reference rotor both concerning the constraint on the load and the specific power. However, this difference evolves gradually and quite different rotors will to some extent still have a reliable material consumption calculated. Furthermore, it is not likely that rotors that are very different from the common design of today are suitable.

3.6 Performance factor

In this Section, the performance factor, pf, is calculated. pf is defined as the relative annual energy capture, re, divided by the material consumption, mc:

$$pf = \frac{re}{mc} \tag{11}$$

The relative annual energy capture is the percentage annual production related to the reference rotor. Higher performance factor means improved competitiveness and the choice of specific power should be reflected by an optimum performance factor.

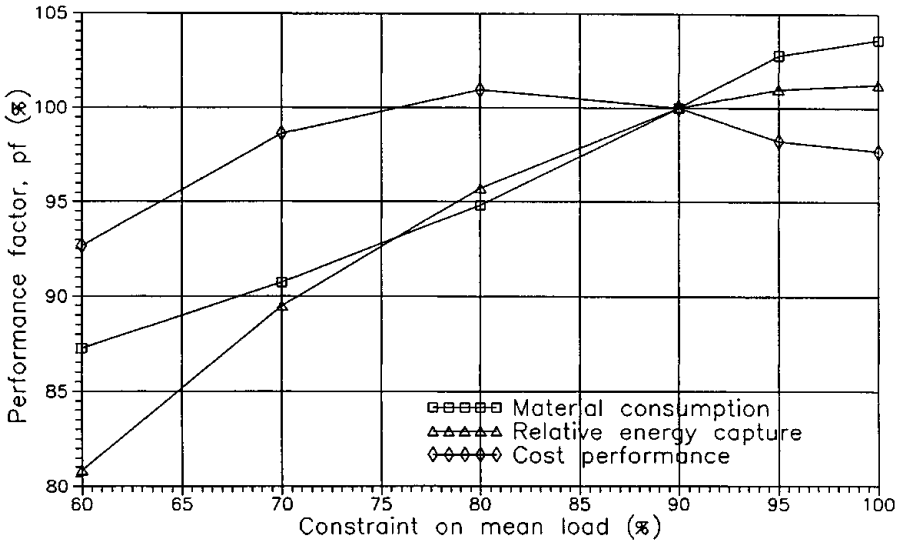

Figure 3.26 The performance factor, pf, as a function of the constrained mean blade root flapwise moment for specific power, 500 W/m².

In Figure 3.26 the performance factor for the family of rotors having specific power, 500 W/m² is shown together with the relative annual production and the material consumption. Point of origin is the specific power, 500 W/m² with a constraint of 90% on the mean load. An optimum is revealed at the constrained mean load equal to 80%. This indicates that it is beneficial to bound important loads and then optimize for the achievable gain in the annual production instead of optimizing without constraints even though the improvement in the annual production would be larger. However, before final conclusions are made the other specific powers should be investigated.

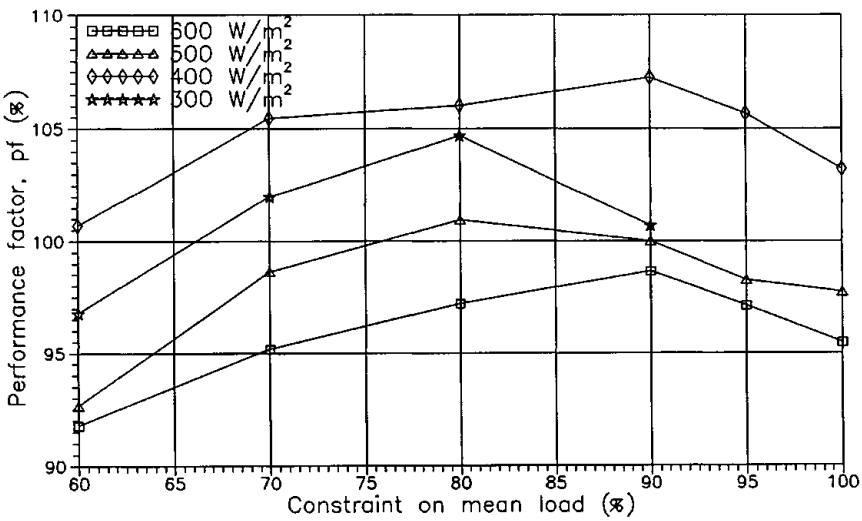

Figure 3.27 The performance factor, pf, as a function of the constrained mean blade root flapwise moment for different specific powers.

In Figure 3.27 the performance factor is shown for the different specific powers. It is seen that all curves have an optimum at around 80% to 90% constraint. However, there is a tendency that lowering the specific power implies that the

loads should be more constrained. The improvement of the performance factor is about 5% compared with the unconstrained rotors.

The optimum specific power appears to be around 400 W/m^2. The slope of the performance factor in the area around and especially below 400 W/m^2 seems to be flat but because both the assumptions of equal dynamics and the material consumption calculation becomes weaker as the specific power is lowered, 400 W/m^2 seems to be a sensible choice.

3.7 Constraint on extreme load

Investigations in this Section have until now been with focus on the constrained mean blade root flapwise moment, since this was found to lower the extreme load as well. In this Section the variations of the equivalent fatigue loads with the constraint on the extreme loads are shown in Figure 3.28 for the specific power, 500 W/m^2.

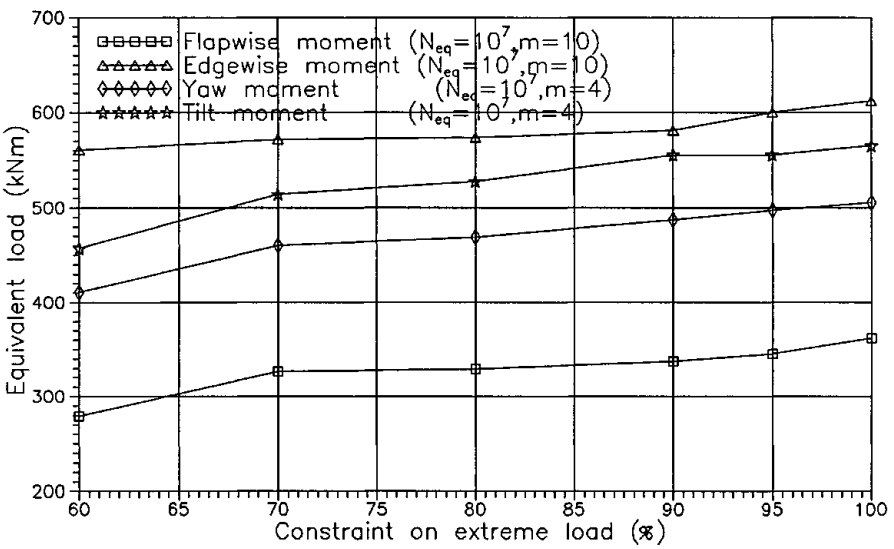

Figure 3.28 *Equivalent fatigue loads as a function of the constrained mean blade root flapwise moment for specific power, 500 W/m^2.*

In general, the equivalent loads are lowered with the constrained extreme load. The slope is however smaller than with the constrained mean load. This compares well with the limited influence from the constraint on the extreme load on the mean loads. It does not give rise to further investigations on the constrained extreme load since this should be evaluated simultaneously with the constrained mean load.

3.8 Roughness class dependency

The objective of this Section is to investigate the influence on the optimum trade off between the annual production and the material consumption, from a change in roughness class from 1 to 2. The optimized family of rotors having specific power, 500 W/m^2 and constraints on the mean load will be used as input for aeroelastic calculations in roughness class 2.

Even though this family of rotors was originally optimized for maximum annual production in roughness class 1, previous investigations in [5] have shown, that the choice of the roughness class for the annual production of energy as objective function has very little influence on the resulting rotor.

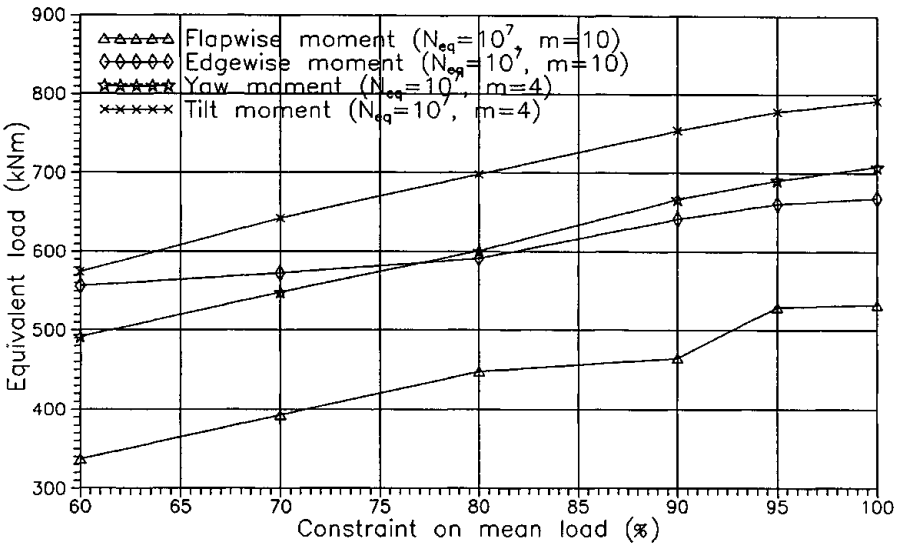

Figure 3.29 Equivalent fatigue loads as a function of the constrained mean blade root flapwise moment for specific power, 500 W/m², roughness class 2.

In Figure 3.29 the variations of the equivalent fatigue loads in roughness class 2 with the constrained mean load are shown. This compares to Figure 3.23. The overall tendency between the two roughness classes is the same. However, the equivalent fatigue loads in roughness class 2 are generally higher at the same constrained mean load. The slopes of the blade moments compare very well between the two roughness classes, whereas the slopes of the rotor moments are less negative with decreasing constrained mean load for roughness class 2.

Even though the higher turbulence intensities from the higher roughness class increase the load ranges, this influence is primarily seen on the rotor yaw and tilt moments. This is probably because of the difference in the S-n curve exponents. The higher exponent chosen for the blades implies that the life time consumption is mainly due to the large load ranges, whereas the lower S-n curve exponents for the rotor moments result in a stronger contribution to the life time consumption from the intermediate load ranges influenced mainly from turbulence and not so much from the large load ranges.

In Figure 3.30 the performance factor for the family of rotors having specific power, 500 W/m² is shown together with the relative annual production and the calculated material consumption corresponding to Figure 3.26. Values have been shown relative to the performance of the optimized rotor with 90% constraint on the mean load in roughness class 2.

Compared to roughness class 1, the variation in the annual production with the constraint in roughness class 2 is quite similar with a slightly higher relative annual production towards the 60% constraint. The material consumption has a

larger slope in roughness class 2 than in roughness class 1 due to the increased fatigue loads.

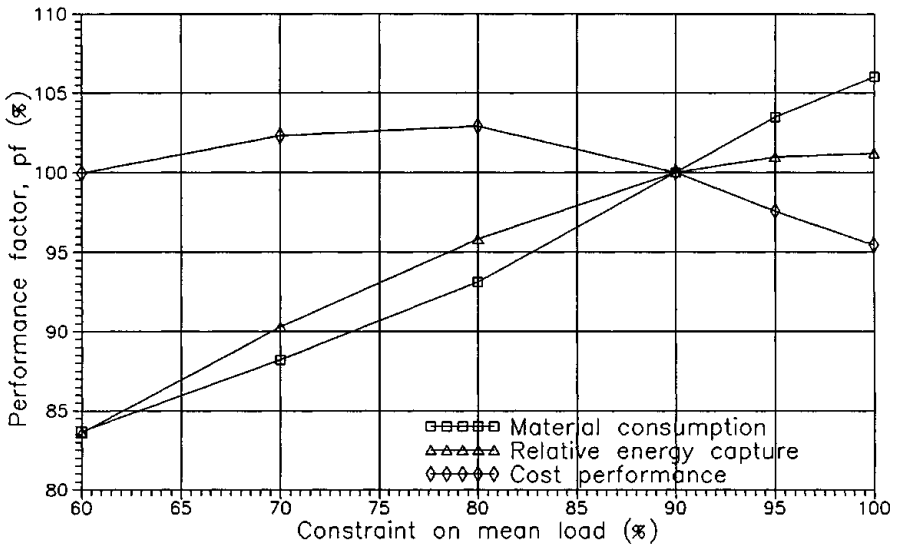

Figure 3.30 The performance factor, pf, as a function of the constrained mean blade root flapwise moment for specific power, 500 W/m², Danish roughness class 2.

This results in a slightly different cost performance variation. The optimum is again found at 80% constraint but the variation towards the unconstrained optimization shows a larger drop in the cost performance whereas the cost performance curve is more flat towards 60% constraint because of the better relative annual production in roughness class 2. This means that it might be even more beneficial to constrain the mean load in roughness class 2 than in roughness class 1.

It is likely that the choice of specific power, is dependent on the choice of the roughness class. However, since the optimum cost performance graph is quite flat in the area around 400 W/m² this would probably be a fairly good choice even for roughness class 2. The increased fatigue loads indicate that the optimum specific power should not be pushed towards lower specific power, than for roughness class 1.

3.9 Summary

In this Chapter, two main aspects in design of numerical optimized wind turbines have been considered:

1) The optimum ratio of rated power to swept area (specific power) and

2) The optimum constraints on the mean or extreme blade root flapwise moment leading to lower fatigue loads.

The procedure has been to investigate the variation of extreme, mean and life time fatigue loads with the constraint on the mean load. The equivalent fatigue loads have been calculated by assuming equal dynamic behaviour for the different

optimized rotors. On basis of these fatigue loads the material consumption has been calculated from a simple model where the relative cost of each of the wind turbine components have been estimated. The material consumption has then been compared with the annual production.

It has been found beneficial to constrain the mean loads at maximum rated power and hereby obtain a trade off between a small loss in the annual production and a corresponding larger reduction in the life time equivalent fatigue loads. The value for the constraint should be between 80% and 90% of the unconstrained mean load, depending on specific power and roughness class. Constraining the mean loads also has an influence on limiting the extreme loads at rotor stand still.

The optimum ratio of rated power to swept area (specific power) has been found in the area of 400 W/m^2.

The investigation has involved many assumptions and simplifications, and the accuracy of the findings should not be over estimated. However, the findings show a trend towards lower specific power, than what is used in todays design of 500 - 1000 kW wind turbines.

4 Optimum airfoil characteristics

The objective of this Chapter is to find optimum airfoil characteristics with different constraints on loads and geometry. This means that parameters describing the airfoil characteristics are included as design variables in the optimization problem as parametric airfoil characteristics, as explained in Section 2.1.3. First, an overview of the present status of special tailored airfoils for wind turbines is given. Next the optimum airfoil characteristics are found with different degrees of constraints on the mean and extreme loads, respectively. The flatness of the design space at the optimum design point with respect to the airfoil characteristics is investigated by optimizing chord, twist and tip pitch angle, while having fundamentally different airfoil characteristics. Furthermore, the importance of minimum drag is discussed. Finally optimum airfoil characteristics are found with different constraints on tip pitch angle and tip chord.

The optimization objective function will be the annual production of energy in Danish Roughness Class 1. Design variables will be the chord and the twist distributions represented by 8 and 5 points, respectively, the tip pitch angle and the maximum lift coefficient, C_{Lmax}, along the blade span represented by 5 points. The angular velocity is not a design variable. Except for the optimizations with different degrees of constraints on mean and extreme loads, all optimizations concern the specific optimized design from the previous Chapter having an 80% constraint on the mean blade root flapwise moment at stall. All rotors have a ratio of rated power to swept area of 400 W/m^2, together with a rated power of 1 MW.

For simplicity it has been chosen to restrict the investigation of the airfoil parameters to C_{Lmax} even though the parametric airfoil characteristics include several other parameters (Section 2.1.3). Previous investigations in [5] have shown that C_{Lmax} is the most important parameter and that by varying C_{Lmax} different airfoils can be represented well. It does not make much sense to optimize in the post stall area since this area is associated with large uncertainties. Therefore, the parameters describing the stall and post stall characteristics will be set and fixed to sensible values so that realistic airfoil characteristics are obtained.

Since the post stall characteristics are somewhat different from the airfoil data used in Chapter 3, comparison on the magnitude of loads with results from this Chapter should not be carried out. However, it has been investigated that the different post stall behaviour does not affect the findings in Chapter 3 concerning the optimum degree of constraint on about 80% and the correlation between the slope of the mean loads and the fatigue loads.

4.1 Background

The development of special tailored airfoils for wind turbines was initiated in the early 80'ties. The leading institute has been the American Solar Energy Research Institute, SERI (now National Renewable Energy Laboratory, NREL) [20]. Their goal was to retrofit older blades that had very poor performance because of both poor airfoils and an insufficient blade design leading to generator burn outs and blade damage. In the following years other research institutes such as FFA in Sweden [21] and Risø [2] also developed new airfoils.

The trend of these developments was to increase C_{Lmax} for airfoils aimed for the inboard blade section whereas airfoils for the tip section should have a low C_{Lmax} compared to the NACA airfoils. This allowed a larger blade length for the same rated power, and the annual energy production could be increased. A tendency that follows quite well with the findings in the previous Chapter.

The tools used for finding the optimum airfoil characteristics have until now been a single design point method, based on the classical Glauert theory [4] extended to include airfoil drag and tip loss [1]. On an existing blade planform, the airfoil characteristics has in [1] been optimized for maximum power coefficient at wind speeds below rated power. The improvement in the annual energy production by application of optimum airfoils was then found to be about 12%.

The method has also been used in the design of a new blade planform in [2]. At a number of wind speeds, the ideal power coefficient was found by varying the product of the lift coefficient and the chord ($C_L \cdot c$). Since the variation of this product with wind speed decreased towards the blade tip, it could be seen, that choosing a constant design C_L would lead to a decreasing C_{Lmax} from root to tip. Having found C_L at some design wind speed, chord and twist could then easily be found. This trial and error like design process did however not include the simultaneous variation of the entire rotor geometry which is one of the advantages by using the numerical optimization algorithm.

With the use of the optimization algorithm a number of investigations have in [5] and [6] been performed concerning optimum airfoil characteristics together with the blade planform. All of these optimizations have been without constraints on loads and geometry.

The investigations in [6] have in all cases verified the advantage of a high C_{Lmax} at the root region. If the entire blade geometry is optimized, C_{Lmax} at the tip region has in general not been found to be lowered significantly. If the airfoil characteristics are the only design variables, an increase in the swept area will lead to a lower C_{Lmax} at the tip in order to keep the rated power constant. It appears that when the airfoil characteristics are optimized together with the overall blade design, C_{Lmax} should not be lowered at the tip. Instead the solidity is reduced and the twist is adjusted for maximum annual production.

The potential improvement has in [6] been found to be lower than in [1]. When the airfoil characteristics are restricted to a continuous variation along the blade span and realistic bounds are set, the attainable improvement has been found to be about 4% when both the blade planform and the airfoil characteristics are included as design variables, compared to optimizations of the blade planform with traditional NACA airfoils.

An important result is that the unconstrained optimum appears to be flat when the entire geometry is optimized. This means that different airfoil characteristics can lead to almost identical annual productions. This is important because airfoil design includes other considerations than C_{Lmax}. If C_{Lmax} can be selected within a broader region, more attention can be paid to other important airfoil qualities that can not be included directly in the optimization of the C_L and C_D characteristics.

Among these are:

- Design lift coefficient
- Reliable stall behaviour
- Insensitivity to surface roughness
- Low noise emission

Even though the unconstrained optimum has been found to be flat, the optimum airfoil characteristics are believed to depend on the different constraints on both loads and geometry, that are investigated in the following Sections.

4.2 The parametric airfoil characteristics

In this Section the adjustment of the parametric airfoil characteristics, that was explained in Section 2.1.3 is presented. The characteristics have been defined according to the following:

1) The angle of attack for zero lift is set constant to -3 deg. Since the twist is included as design variable, a variation in this corresponds to a change of the airfoil angle of attack for zero lift.

2) The slope of the lift curve before stall is fixed to 0.11 deg [1].

3) The post stall slope, curvature at stall and the rate of increase from C_{Dmin} are fixed at all radial positions so that realistic post stall characteristics are ensured. The angle of attack for the transition to post stall drag is coupled to C_{Lmax} as shown in Figure 4.1, that shows a parametric airfoil having C_{Lmax} = 1.60 and C_{Dmin} = 0.0065

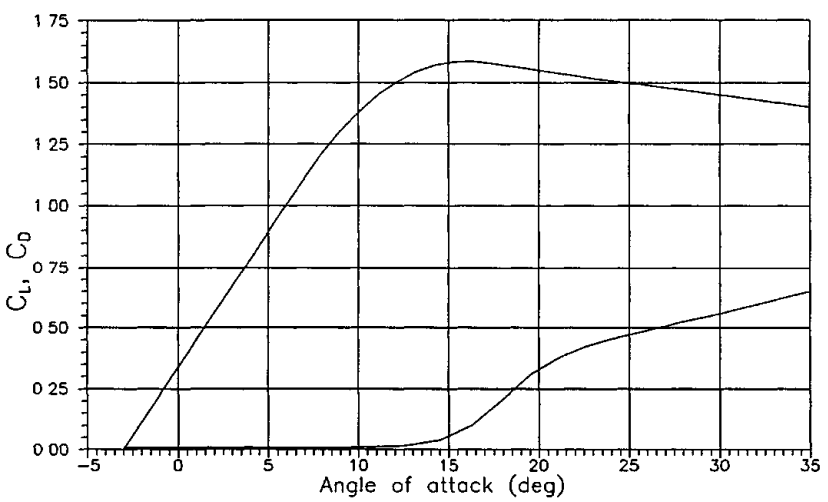

Figure 4.1 Example of a parametric airfoil characteristic having C_{Lmax} = 1.60 and C_{Dmin} = 0.0065.

4) C_{Dmin} is given a linear variation from 0.0080 to 0.0065 from root to tip to compensate for the change in blade relative thickness.

5) Finally the C_{Lmax} distribution is a cubic spline with 5 design variables at equally distributed radial positions. All optimizations have been run with 3 different initial guesses from 1.1 to 1.6. To ensure realistic results C_{Lmax} has been bounded to be less than or equal than 1.6.

In Appendix F, the figures F1 to F3 show corresponding values of C_L and C_D for C_{Lmax} values from 1.0 to 1.6. It is seen that a smooth variation is obtained. In Figure F1, the post stall region has been adjusted to the assumed 3D behaviour of the airfoil characteristics. Only airfoils with high C_{Lmax} have a region with negative slope until the common deep stall curve value of 1.4 is reached at 35 deg. C_{Lmax} might be even larger at the inner part of the blade, but this is not taken into account since it is of only minor importance to the overall power from the blade.

In Figure F2, the increase from C_{Dmin} to the common deep stall C_D curve is seen to be pushed to higher angles of attack as C_{Lmax} is increased. The transformation area is seen more clearly in Figure F3 showing C_L versus C_D. It is seen here that the transition is quite abrupt. This has been chosen because a low drag should be obtained at the highest possible angle of attack as possible for an optimum design. Since the transition is not optimized it has been assumed that this is nearly optimum even though it might be hard to achieve for airfoils having a high C_{Lmax}.

4.3 Optimum airfoils with constraints on loads

Corresponding to Section 3.3.1 and 3.3.2, a number of optimizations with different degrees of constraints on the mean and extreme loads have been carried out on a rotor having specific power, 400 W/m^2. The aim has been to investigate how the optimum C_{Lmax} distributions depend on the constraints. Both the extreme and the mean loads have been constrained from 100% until 60% of the unconstrained values.

The constraint on the extreme blade root flapwise moment at rotor stand still resulted in an unambiguous and obvious result. All optimizations showed a C_{Lmax} = 1.6, which is the upper bound, at all radial positions. Since the angle of attack at the extreme load calculation is nearly 90 deg it is preferable to reduce the extreme loads by reducing the solidity. Maintaining a high C_{Lmax} then gives the highest energy production.

Somewhat surprising, the constraint on the mean blade root flapwise moment resulted in an equally uniform C_{Lmax} = 1.6 along the blade span for all optimizations, independent on the value of the constraint. Since reducing the solidity was the driving action in the previous Chapter as the constrained load was lowered, one could expect that C_{Lmax} would be increased as the constrained load was lowered. However, even an unconstrained optimization resulted in a uniform C_{Lmax} = 1.6.

These results might change if additional constraints are added to the optimization problem and this will be investigated below. First, the optimum rotor having an 80% constrained mean load is compared with optimized rotors having fundamentally different fixed C_{Lmax} distributions. Next, a number of additional constraints will be added to the optimization problem to investigate how bounds on tip pitch angle and chord affect the results.

4.4 The design space topology

When the airfoil characteristics are included in the optimization problem as design variables, the number of dimensions in the design space increases and one could expect that the optimum becomes more flat because of the increased number of feasible solutions and because some of the design variables overlap with respect to the power production, e.g. chord and C_L. The purpose with this Section is to investigate the design space topology for an optimum rotor to clarify the flatness of the optimum. This is done by comparing two fundamentally different C_{Lmax} distributions with the optimum from the previous Section. All rotors have parametric airfoils with different fixed C_{Lmax} distributions and an 80% constraint on the mean blade root flapwise moment.

1) The optimum blade from Section 4.3 with $C_{Lmax} = 1.6$.

2) A blade with a traditional NACA 634xx C_{Lmax} distribution

3) A rotor with a low lift style C_{Lmax} distribution.

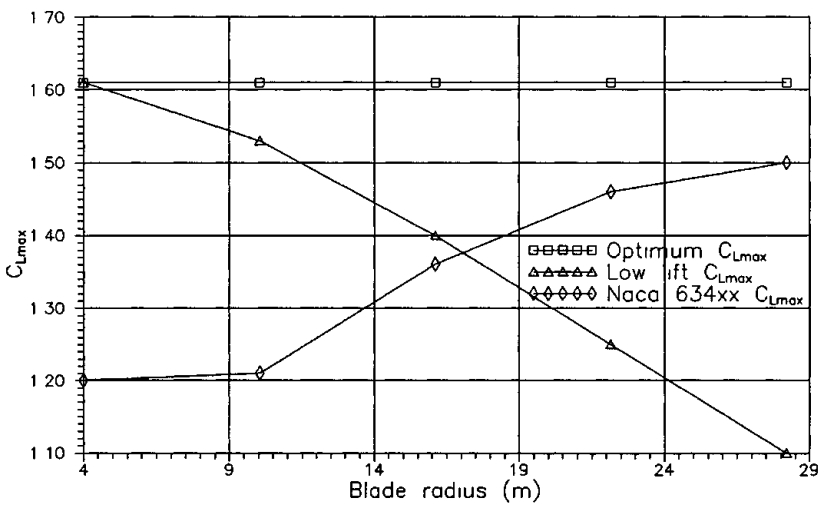

Figure 4.2 *C_{Lmax} variation along the blade span for the different optimizations. In all three cases, the parametric airfoil characteristics are used with different fixed values of C_{Lmax}*

The different C_{Lmax} distributions are shown in Figure 4.2. These distributions are used in the parametric airfoil characteristics with fixed values. Chord, twist and tip pitch angle have been optimized for each of these rotors. Since all blades have parametric airfoil characteristics with identical parameters except for C_{Lmax}, there will be no influence on the optimization result from different post stall characteristics.

Appendix G contains figures of the optimization results. Some key values are given in Table 4.1. It is seen, that the blade with optimum C_{Lmax} produces 4% more energy than the other blades. This is in agreement with earlier findings [5]. More interesting is, that the NACA C_{Lmax} and the low lift C_{Lmax} distributions result in almost equal annual production even though they are fundamentally different.

Because of the lowered solidity for the optimum C_{Lmax} blade (Figure G1), the extreme blade root moment at rotor stand still is lowered compared to the other blades. The extreme loads for the NACA C_{Lmax} and the low lift C_{Lmax} blades are almost equal even though the low lift C_{Lmax} planform is increased towards the tip. However, a reason for the slightly low extreme load for the low lift C_{Lmax} blade compared to the NACA C_{Lmax} blade is that the NACA blade has a larger chord towards the root together with a more negative tip pitch angle. The twist distributions are shown in Figure G2. Remembering the differences in the tip pitch angle, the low lift C_{Lmax} fall in between the other blades.

Table 4.1 Comparison between the optimizations with different C_{Lmax} distributions.

	Optimum C_{Lmax}	NACA 634 C_{Lmax}	Low lift C_{Lmax}
Annual production (MWh)	2679	2610	2595
Relative energy production (%)	100	96.0	95.4
Tip pitch angle (deg)	-4.25	-4.40	0.5
Tip chord (mm)	84	153	211
Extreme blade root flapwise moment (kNm)	1884	2371	2309

The power coefficients and thrust coefficients are shown in Figure G3 and Figure G4, respectively. The NACA C_{Lmax} and the low lift C_{Lmax} blades have similar qualities, whereas the optimum C_{Lmax} blade has a higher C_P before rated power. This is because the parametric airfoil having higher C_{Lmax} implies that C_{Dmin} is kept until higher angles of attack. C_T is correspondingly higher for the optimum C_{Lmax} blade.

The aerodynamic forces and the angle of attack versus wind speed at different blade positions are shown in Figure G7 - Figure G11 for the optimum C_{Lmax} blade. C_L versus wind speed in Figure G7 reveal a very harmonic variation. Over the entire blade, C_{Lmax} is reached exactly when the power curve (Figure G5) starts to bend off towards rated power. From an aerodynamic point of view this should give a reliable stall, since C_{Lmax} has been passed simultaneously on the entire blade. It could result in bad conditioned structural qualities from negative damping in post stall, but the axial component, C_a, in Figure 10 does not become negative. The tangential component, C_t, shows the nature of the stall, that runs from the root at 13 m/s to the tip at 17 m/s. Stall is advanced on the inner part of the blade because the angle of attack is quickly increased after 13 m/s which is seen in Figure G11.

The aerodynamic forces are shown for the NACA C_{Lmax} blade in Figure G12 - G16. In general there are similarities between this and the optimum C_{Lmax} blade. Due to the lower C_{Lmax} at the root, the slope of C_L versus wind speed (Figure G12) does not become negative and stall is moved to lower wind speeds in the root region (Figure G13). The variation in the tangential force component (Figure

G14) shows that the blade root stalls at 13 m/s, whereas the tip stalls at 17 m/s in a similar manner to the optimum C_{Lmax} blade.

The aerodynamic forces for the low lift C_{Lmax} blade are shown in Figure G17 - G21. This blade is quite different from the other blades. Because of the higher twist and C_{Lmax} in the root region, stall is delayed to a higher wind speed (Figure G17). This means that stall appears on the blade mid section and develop both towards the root and the tip. This could be avoided by allowing a larger C_{Lmax} on the blade mid section leading to a sudden stall over the entire blade, which probably would produce more energy and be more realistic. When more knowledge about the 3D flow effects have been incorporated into the calculation tools, the optimization methodology would be very suitable for obtaining better control of the 3D stall behaviour of the rotor.

The low lift C_{Lmax} blade design does not seem to be very suitable. However, the value of the angle of attack in the tip region is lower to the same wind speed compared to the other blades. This could be an advantage concerning the tip noise, where a reduced angle of attack would reduce the tip noise.

The power curves are shown in Figure G5. Only small variations are revealed before rated power, as it could be expected. The mean blade root flapwise moment is shown in Figure G6. The level of the optimum C_{Lmax} blade is higher than the other blades before rated power whereas it is lowered after rated power. In itself, this is not surprising because of the higher thrust. Because of the constraint on the mean load at stall, the slope of the mean load is reduced compared to the other blades. This gives hope for better fatigue qualities even though the level of the mean load is increased.

Table 4.2 Comparison of equivalent fatigue loads and material consumption for the optimizations with different C_{Lmax} distributions.

	Optimum C_{Lmax}	NACA 634 C_{Lmax}	Low lift C_{Lmax}
Flapwise blade root moment (kNm)	314	358	355
Edgewise blade root moment (kNm)	636	630	630
Rotor yaw moment (kNm)	417	463	455
Rotor tilt moment (kNm)	468	529	515
Rotor thrust force (kN)	38.5	45.5	43.75
Material consumption (%)	100	101.5	101.5
Relative energy prod (%)	100	96.0	95.4
Cost performance (%)	100	94.6	94.0

The magnitudes of the equivalent fatigue loads have been calculated using the same procedure as in Section 3.4. Results are shown in Table 4.2. In general both

equivalent rotor moments and blade root moments have been reduced for the optimum C_{Lmax} blade, except for the edgewise blade root moment. In particular, the rotor thrust force is reduced, primarily due to the reduced solidity. The material consumption has been calculated on basis of the fatigue loads and it turns out that the NACA C_{Lmax} and the low lift C_{Lmax} wind turbine is 1.5% more expensive. The mass of the optimum C_{Lmax} blade is increased compared to the other blades because of the reduction in chord. This is however counterbalanced by lower rotor and blade flapwise moments plus a lower rotor thrust fatigue load. Seen together with the difference in the annual production, the rotor having the optimum C_{Lmax} blades would be about 6% more cost efficient than the other blades.

The reduction in solidity should be counterbalanced by a larger relative thickness to maintain equal stiffness qualities along the blade span. This emphasizes the need for airfoils having high C_{Lmax} and low C_{Dmin} together with a high relative thickness.

Even though there is a difference in the annual production on 4%, the design space is found to be flat around the optimum, since the main part of the improvement comes from a lowered drag before stall.

Until now, the optimization results have not revealed any advantages by having a low C_{Lmax} in the tip region. However, no constraints have yet been added on the blade geometry, but this will be investigated in Section 4.7.

4.5 Variation of minimum drag

One of the obvious potential improvements of the airfoil characteristics is a reduction of C_{Dmin} along the blade span. Earlier findings in [1] showed an increase in the annual production of 3% when C_{Dmin} was lowered 0.002. However, this investigation was carried out with airfoils having an ideal transition from C_{Dmin} to post stall drag. Three optimizations have been performed with different values of C_{Dmin}. C_{Dmin} has been lowered and increased respectively 0.002 along the blade span compared to the optimization result from Section 4.3.

Table 4.3 Comparison between the optimizations with different C_{Dmin} values along the blade span.

	Lowered C_{Dmin}	Medium C_{Dmin}	Increased C_{Dmin}
Annual production (MWh)	2703	2679	2655
Relative energy production (%)	100.9	100	99.1
Tip pitch angle (deg)	-4.25	-4.25	-4.26
Tip chord (mm)	160	160	158
Extreme blade root flapwise moment (kNm)	1881	1884	1887

In Table 4.3 main results are presented. The annual production is changed approximately 1% by changing C_{Dmin}. Despite this, there is hardly no change in both the blade design and in the blade performance. In Figure 4.3 the power coefficient is shown for the different optimizations. Due to the assumed transition from minimum drag to post stall drag, the difference between the different blades is only noticeable at low wind speeds, where a drop in C_{Dmin} corresponds to higher C_P.

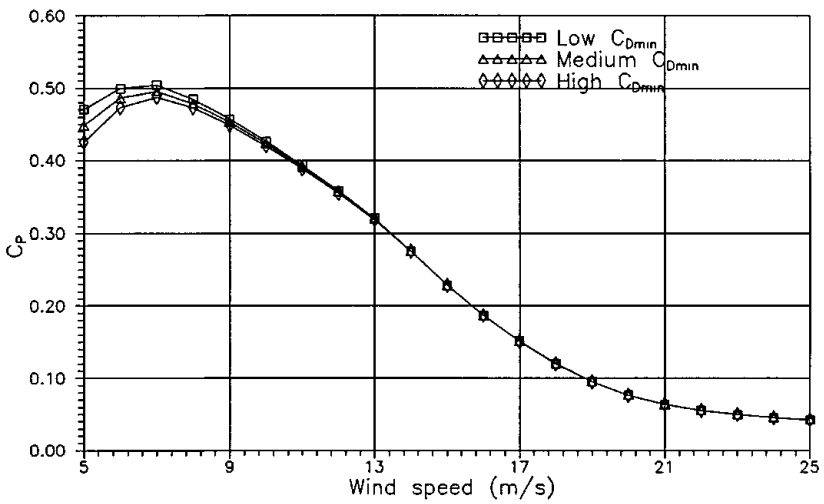

Figure 4.3 Power coefficient versus wind speed for the optimizations with different values of C_{Dmin}.

Since the resulting designs are practically identical, the aim should be to decrease C_{Dmin} as much as possible keeping in mind that this has only a minor influence on the overall performance. However, a more complex model for the variation of C_{Dmin} including the possibility of a low drag bucket might show a potential higher annual energy production.

4.6 Variation of tip pitch angle

One of the advantages by using low C_{Lmax} airfoils in the tip region has been that the tip pitch angle can be increased in positive direction resulting in a lower angle of attack in the tip region compared to blades having a higher C_{Lmax} at the tip.

This is believed to decrease the trailing edge noise emission from the tip.
In this Section, five blades will be optimized with different constraints on the tip pitch angle ranging from -4.3 deg to +4 deg as shown in Table 4.4. Some figures of the results are shown in Appendix H.

It is seen in Table 4.4, that an increase in the tip pitch angle involves a drop in the annual production and an increase of the extreme blade root flapwise moment at rotor stand still. However, the tip pitch angle can be increased to 0.0 deg with only a little drop in the overall performance. The tip chord is seen to be increased with the increase in the tip pitch angle. Whereas the reduction in the tip pitch

angle involves a reduction in the trailing edge noise, the increase in chord involves an increase in the trailing edge noise.

Table 4.4 Comparison between the optimizations with different tip pitch angles.

Tip pitch angle (deg)	-4.3	-2.0	0.0	2.0	4.0
Annual production (MWh)	2679	2677	2664	2630	2576
Relative energy production (%)	100	99.9	99.4	98.2	96.2
Tip chord (mm)	160	176	194	229	246
Extreme blade root flapwise moment (kNm)	1884	1884	1896	1963	2173

The corresponding C_{Lmax} distributions are shown in Figure 4.4. It is seen that when the tip pitch angle is increased, the optimum C_{Lmax} distribution shows a lowered C_{Lmax} at the tip compared to the optimum tip pitch angle. However, the tip pitch angle can be increased to 0.0 deg without a significant drop in C_{Lmax} at the tip. This means that there are other mechanisms for increasing the tip pitch angle than lowering C_{Lmax} at the tip.

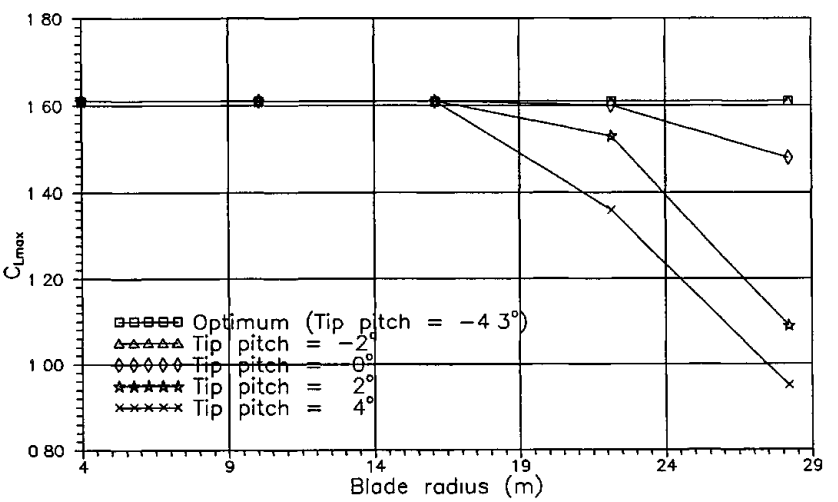

Figure 4.4 C_{Lmax} variation along the blade span for the different optimizations with different tip pitch angles.

The variation in the tip angle of attack versus wind speed is seen in Figure 4.5. The angle of attack is seen to drop linearly with the increase in the tip pitch angle. Since C_{Lmax} at the tip is not lowered until a tip pitch angle of about 0.0 deg, the reason for the drop in the tip angle of attack is that stall in the tip section is delayed to a higher wind speed. This reduces the angle of attack at the tip and

gives the possibility to maintain a high C_{Lmax}. Another advantage of this is, that since stall is no longer occurring simultaneously along the blade span, the slope of C_L at the tip just after rated power is no longer negative.

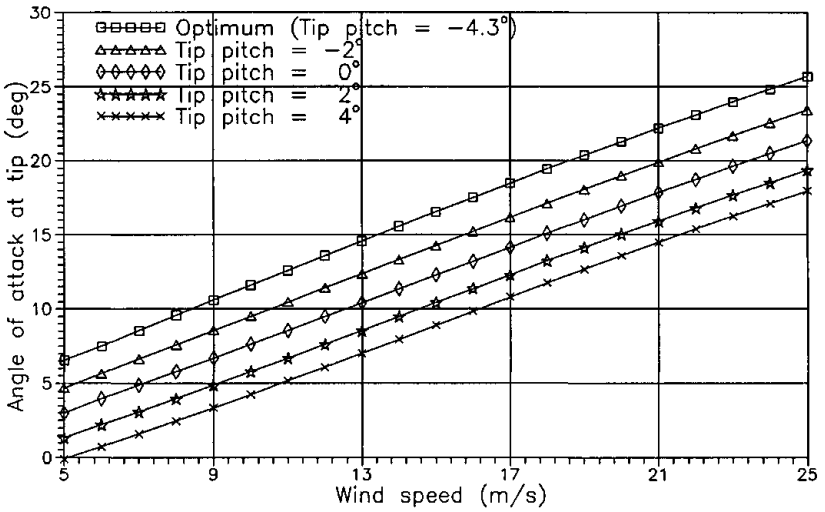

Figure 4.5 The angle of attack as a function of wind speed at the blade tip for the different optimizations having different tip pitch angles.

In Figure H1 and H2 the chord and twist distributions are shown, respectively. The chord is only slightly increased with the tip pitch angle, whereas the twist is quite different for the different optimization results. When the tip pitch angle is increased, the twist on the inboard section is correspondingly reduced to maintain equal aerodynamics. At the tip, this is not possible since the tip pitch twist is locked to be zero degrees. Therefore the twist becomes flat at the tip and even slightly negative on the blade mid section. This is unconventional and it shows that a constraint on the tip pitch angle to be positive acts rather severe on the resulting blade. If more freedom were allowed in the cubic spline representation of the twist distribution, the twist would probably become negative towards the tip and then switch towards positive at the tip.

In Figure H3 and H4 the power and thrust coefficients are shown, respectively. Both are seen to drop at low wind speeds as the tip pitch angle is increased. In Figure H5 and H6 the power and the mean blade root flapwise moment are seen. The slope of the blade root moment is increased when the tip pitch angle is increased resulting in larger fatigue damage.

4.7 Variation of tip chord

Another advantage by lowering C_{Lmax} at the tip region is that the tip chord can be increased without exceeding rated power, since manufacturing considerations might require this. In the previous Section it was shown that the tip chord was increased with the tip pitch angle. In this Section, optimizations have been performed with different constraints on the tip chord along the entire blade.

In Table 4.5, main results are shown. The tendencies are the same as in the previous Section. The performance is lowered and the tip pitch angle is increased with the increase in the tip chord. However, the tip chord can be increased from 160 mm to 400 mm with practically no drop in C_{Lmax} and only a slight drop in performance. This means that manufacturing requirements about a certain value of the tip chord to a large extent can be fulfilled by changing chord and twist and maintaining a high C_{Lmax} at the tip.

Table 4.5 Comparison between the optimizations with different tip chord values.

Tip chord (mm)	160	400	600
Annual production (MWh)	2679	2669	2644
Relative energy production (%)	100	99.6	98.7
Tip pitch angle (deg)	-4.25	-3.0	-0.4
C_{Lmax} at blade tip	1.61	1.59	1.29
Extreme blade root flapwise moment (kNm)	1884	1876	1889

4.8 Summary

In this Chapter several questions concerning optimum airfoils for wind turbines have been highlighted.

To gain maximum annual production of energy, C_{Lmax} should be kept high over the entire blade. The value of C_{Lmax} is independent of constraints on both mean (fatigue) and extreme loads ranging from 100% (unconstrained) to 60%.

Comparisons of three fundamentally different C_{Lmax} distributions showed a total difference in the annual production on 4%. The fatigue loads were calculated and the optimum C_{Lmax} distribution has lower equivalent fatigue loads even though the mean loads are increased. This lead to an improved cost performance at about 6%.

When the entire rotor geometry is included as optimization design variables, the choice of airfoil C_{Lmax} becomes less important since the design space is flat in the neighbourhood of the optimum design point. This means that airfoil qualities that are not included in the optimization problem such as e.g. roughness insensitivity can be paid more attention in the design process at the expense of a certain C_{Lmax}.

A reduction of C_{Dmin} on 0.002 has been found to improve the annual production with 1%.

From considerations on tip noise and manufacturing, additional constraints on tip pitch angle and tip chord showed that these to a large extent can be fulfilled without decreasing C_{Lmax} at the tip. Instead the stalling of the blade was changed so that the tip section stalls at a higher wind speed. Both an increase in tip chord

and tip pitch angle could to some extent be obtained with almost no loss in performance.

The reduction in solidity should be counterbalanced by a larger relative thickness to maintain equal stiffness qualities along the blade span. This emphasizes the need for airfoils having high C_{Lmax} and low C_{Dmin} together with a high relative thickness.

5 Comparison with LM 24.0

The objective of this Chapter is to compare an optimized blade that is based on the findings in Chapter 3 with an existing blade having an equal rated power. The LM 24.0 blade has been chosen for comparison, since this blade covers the range from 800 kW to 1100 kW [23]. The aim is to evaluate the potential improvement in the cost performance from lowering the ratio of rated power to swept area and simultaneously having constraints on the mean (fatigue) loads at normal operation.

First, the assumptions will be discussed. Differences in the blade geometry and the performance will be shown. Aeroelastic calculations of both blades will be compared and the material consumption and the cost performance will be calculated.

5.1 Assumptions

The LM 24.0 blade covers a number of different operational conditions. To get the best standard of reference, the adaption to the 1 MW rated power operation has been carried out according to LM's guidelines [23]. The rotor diameter has been chosen to be 52 m. The ratio of rated power to swept area is hereby 471 W/m^2. The blade geometry is the original blade design. On the inboard section the FFA-W3 airfoil family is used, whereas the NACA 634xx airfoil family is used at the outboard section.

To find the optimum tip pitch angle and angular velocity at this configuration, an optimization of the annual production of energy has been performed. The tip pitch angle was hereby found to be -1.9 deg and the angular velocity to be 21.9 rpm (Table 5.1).

The blade flapwise and edgewise eigenfrequencies have in the aeroelastic calculations been kept as the original ones [23]. Seen relative to the angular velocity the dynamic properties of the LM 24.0 are in very good agreement with the values used in Section 3.4.1.

The optimized blade has a diameter of 56.4 m and hereby a ratio of rated power to swept area of 400 W/m^2. The mean blade root flapwise moment has been constrained to 80% of the unconstrained value. The blade chord and twist are optimized whereas the blade relative thickness is chosen equal to the LM 24.0 blade. The root chord has been fixed equal to the root chord of the LM 24.0 to prevent the inboard solidity to be decisive different. The angular velocity is 20.3 rpm corresponding to a tip speed of 60 m/s.

Because the optimum airfoil characteristics from Chapter 4 has not yet resulted in the development of new airfoils, airfoils for the optimized blade will be the same as for the LM 24.0 blade. This ensures also that differences in the performance from the two concepts is not caused by airfoil characteristics that perhaps only partially can be realised. Furthermore, the post stall airfoil characteristics are similar for the two blades.

The extreme rotor thrust force and the extreme blade root flapwise moment at rotor stand still have been constrained to the values of the LM 24 0, so that differences in these do not influence the resulting design

The blade mass, static moment and mass moment of inertia have been calculated on a relative basis, so that the consequences on these from the longer optimized blade is revealed in the aeroelastic calculations The actual blade mass for both the optimized blade and the LM 24 0 blade is believed to be lower than the mass used, but this is not crucial since only a relative comparison is performed

The blades have been mounted on the same wind turbine ensuring equal influence from generator, tower, shaft etc

5.2 Geometry

The blade chord distributions are compared in Figure 5 1 The LM 24 0 blade is only slightly nonlinear, whereas the optimized blade has both convex and concave regions Towards the inboard section, the optimized blade has a larger chord On the mid section the optimized blade chord is smaller than the LM 24 0 The tip design is very different since the optimized blade tip chord is only 128 mm compared to the LM 24 0 tip chord of 469 mm (Table 5 1) The increase in solidity is therefore only in the root region One reason for the higher tip chord for the LM 24 0 blade might be because of space needed for the tip brake system

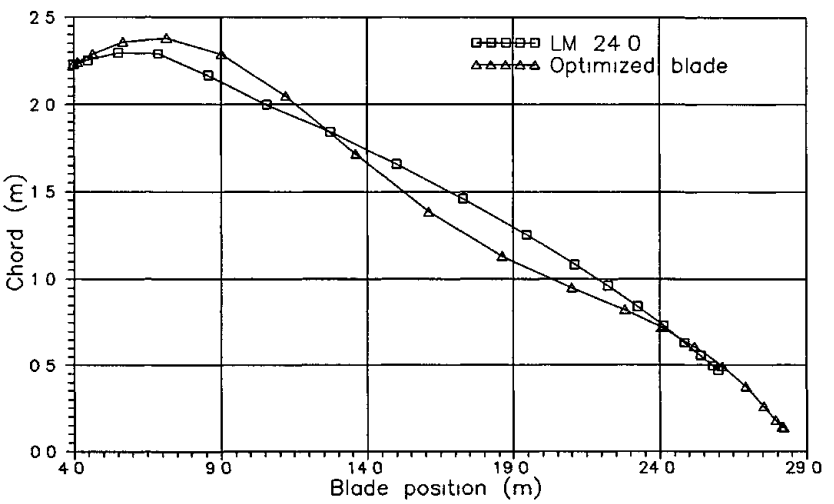

Figure 5 1 Comparison of chord distributions for the optimized blade and the LM 24 0 blade

In Figure 5 2 the planform of both blades is shown in right scaling It is seen that the difference between the two blades is small

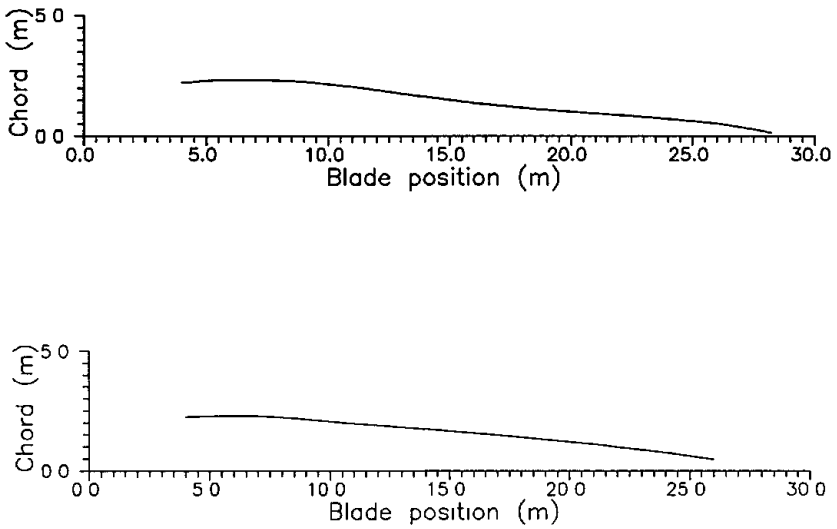

Figure 5.2 Comparison of the blade planform for the optimized blade and the LM 24.0 blade. The optimized blade is on top.

In Figure 5.3 the twist distributions are shown for both blades. It is seen that the optimized blade has a higher twist on the entire blade, except for the tip, where the tip pitch angle is slightly less negative for the LM 24.0 blade. The difference in the twist decreases towards the tip region.

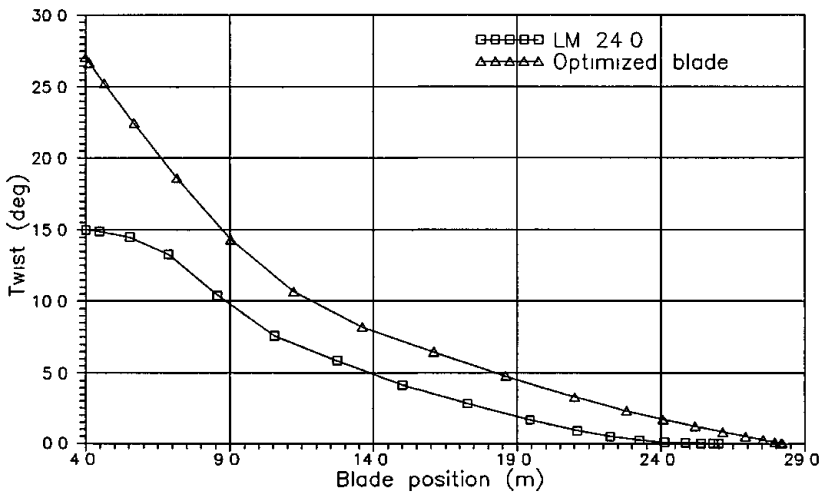

Figure 5.3 Comparison of twist distributions for the optimized blade and the LM 24.0 blade.

At the root section the twist is very different. This is partially because the LM 24.0 blade is designed also to cover smaller values of rated power, than 1 MW. The tip pitch and the rotor diameter are then adjusted to achieve this. The lower twist advances stall especially on the inboard section, where stall appears from 9 m/s compared to 11 m/s for the optimized blade.

On the other hand stall at the tip section is delayed to 19 m/s for the LM 24.0 blade compared to 17 m/s for the optimized blade. Because of the reduction in chord towards the tip for the optimized blade, the induced velocities are reduced from the lowered solidity. The angle of attack is therefore increased and this advances stall to an earlier wind speed.

The optimized blade appears to have higher angles of attack at the tip which amounts to 2.5 deg. This should lead to an increased contribution to tip noise. In contrast, the tip chord is decreased for the optimized blade, which decreases the noise and decreases the local velocity around the airfoil and reduces the strength of the tip vortex. However, tip noise will not necessarily become a problem for an optimized blade, since it was shown in section 4.6, that the tip angle of attack can be decreased with about 4 deg. without significant loss of energy production.

5.3 Annual energy production and loads

In Table 5.1 the overall properties for the two blades are shown. The optimized blade produces 5.8% more energy on an annual basis, than the LM 24.0 blade in the Danish roughness class 1. This increase is primarily obtained by the enlarged swept area as seen in Figure 5.4, where the rotor power versus wind speed is shown. At low windspeeds the power curve is significantly increased for the optimized blade. Both power curves reveal a decent stall and maximum mechanical rated power on approximately 1080 kW at 16 m/s but the calculation results become highly uncertain at these wind speeds.

Table 5.1 Comparison of the optimized blade and the LM 24.0 blade.

		LM 24.0 blade	Optimized blade
Annual energy production	(MWh)	2441	2583
Relative energy production	(%)	100	105.8
Rotor diameter	(m)	52.0	56.4
Tip pitch angle	(deg)	-1.9	-2.4
Angular velocity	(rpm)	21.9	20.3
Tip chord	(mm)	469	128
Extreme rotor thrust force	(kN)	411	410
Extreme blade root flapwise moment	(kNm)	1740	1740

The extreme blade root flapwise moment and rotor thrust force at rotor stand still are seen to be equal for both blades. The longer optimized blade does not have increased extreme loads, since the solidity has been lowered on a large part of the blade.

The mean blade root flapwise moment is shown in Figure 5.5 for both blades. Though the swept area is increased, the mean blade root flapwise moment is

lowered for the optimized blade compared to the LM 24.0 blade because of the constraint in the optimization. Equally important is it, that the slope of the mean blade root flapwise moment appears to be slightly decreased. This is believed to have a positive influence on the fatigue loads. In reality the slopes of the mean flapwise blade root moments should increase more after 16 m/s than they do in Figure 5.5. This is because the post stall airfoil characteristics probably does not compensate sufficiently for 3D effects and dynamic stall. However, since this comparison is based on a relative basis this has no influence on the result.

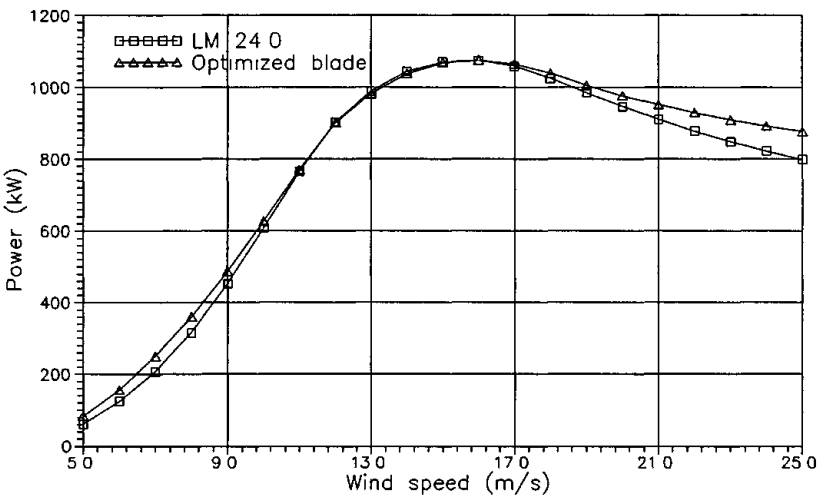

Figure 5.4 Comparison of the power curves for the optimized blade and the LM 24.0 blade.

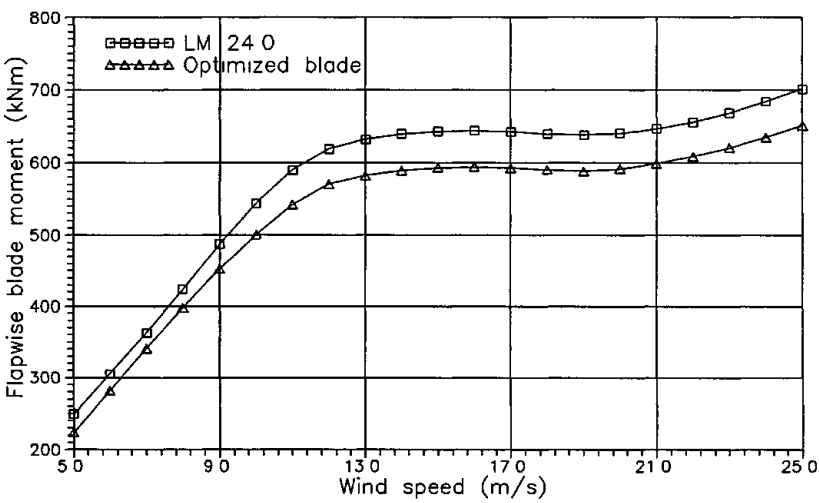

Figure 5.5 Comparison of the mean blade root flapwise moment curves for the optimized blade and the LM 24.0 blade.

The fatigue loads have been calculated following the procedure that was explained in Section 3.4. The dynamic properties for the two blades are shown in Table 5.2.

The difference in the rotational frequency implies different values for the individual eigenfrequencies, however, seen relative to the rotational frequency (1P) a good correlation have been ensured.

The LM 24.0 blade eigenfrequencies are the original ones [23]. The asymmetric rotor flapwise bending modes (yaw and tilt) have been adjusted to exactly follow the values from Section 3.4 by changing the tower and shaft stiffness.

The optimized blade eigenfrequencies have been adjusted relative to 1P and this has resulted in insignificant differences compared to the LM 24.0 blade.

Seen in absolute values however, there is a substantial difference, since the tower and shaft stiffness have been changed. Both the blade bending and the shaft bending/ tower torsion has to be more flexible to obtain the eigenfrequencies in Table 5.2. However, it is assumed in this comparison that the proper eigenfrequencies are obtainable.

The blade masses have been found to be equal for both blades. However, because of the increase in the blade length, the blade static moment has been increased 8.5% and the blade mass moment of inertia has been increased 17%.

Table 5.2 Comparison of dynamic design for the optimized blade and the LM 24.0 blade.

	LM 24.0 blade	Optimized blade
Rotational frequency (Hz)	0.365	0.338
First flapwise bending eigenfrequency (Hz)	1.45 (4.0P)	1.35 (4.0P)
First edgewise bending eigenfrequency (Hz)	2.65 (7.3P)	2.46 (7.3P)
First tower bending frequency (Hz)	0.58 (1.6P)	0.58 (1.7P)
Blade mass (kg)	3761	3761
Blade static moment ($kgm \cdot 10^3$)	25.9	28.1
Blade mass moment of inertia ($kgm^2 \cdot 10^3$)	318	372
Asymmetric rotor flapwise bending coupled with tower torsion (yaw) (Hz)	1.11 (3.0P)	1.00 (3.0P)
Asymmetric rotor flapwise bending coupled with second tower bending (tilt) (Hz)	1.18 (3.2P)	1.04 (3.1P)

The equivalent fatigue loads are shown in Table 5.3. The equivalent blade root flapwise moment is seen to be reduced by 7% for the optimized blade. This is primarily because of the constraint on the mean load at stall. The equivalent edgewise blade root bending moment is seen to increase 5%. This is because of the increased blade length that increased the blade static moment and mass moment of inertia. The rotor yaw and tilt moments have been reduced by 5% each. These are less sensitive to the increase in the blade length, but depend more on the solidity of the blades. As it can be seen, the equivalent rotor thrust force

has been reduced and this has been beneficial to the rotor moments. In general the fatigue loading of the LM 24.0 blade is slightly larger compared to the optimized blade even though the optimized blade has a larger swept area.

Table 5.3 Comparison of equivalent fatigue loads for the optimized blade and the LM 24.0 blade. $N_{eq} = 10^7$.

		LM 24.0 blade	Optimized blade
Flapwise blade root moment	(kNm)	346	319
Edgewise blade root moment	(kNm)	602	632
Rotor yaw moment	(kNm)	384	362
Rotor tilt moment	(kNm)	433	412
Rotor thrust force	(kN)	38.6	36.6

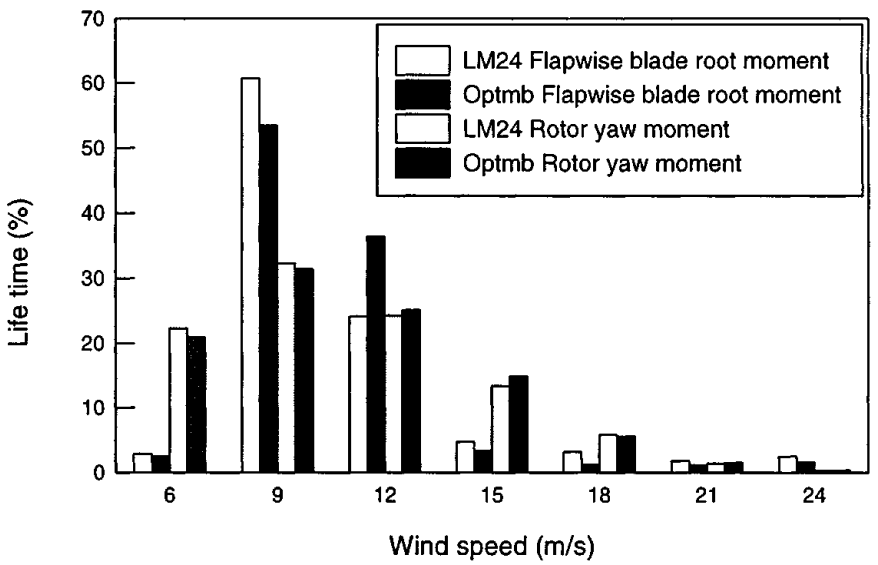

Figure 5.6 Distribution of life time consumption for the flapwise blade root moment and the rotor yaw moment for the optimized blade (Optmb) and the LM 24.0 blade.

In Figure 5.6 the distribution of life time consumption for the blade root flapwise moments and the rotor yaw moments for the optimized blade and the LM 24.0 blade are shown, respectively. This kind of comparison should be looked upon with care since the individual values in the life time distributions to some degree depend on the wind speeds chosen. This can be seen on the flapwise blade root moments at 9 and 12 m/s, where the LM 24.0 blade and the optimized blade, respectively spend a considerable part of their life time. Having calculated more wind speeds, this difference might have been smoothed out. In general there is only smaller differences and no indications of bad behaviours for either of the blades.

5.4 Material consumption

The material consumptions have been calculated on basis of the equivalent fatigue loads and are shown in Table 5.4. The material factor and the material consumption for the optimized blade are shown relative to the LM 24.0 blade.

Table 5.4 Comparison of material factor and material consumption for the optimized blade and the LM 24.0 blade. Material factors shown relative to the LM 24.0.

	LM 24.0 material factor	Optimized blade material factor	LM 24.0 material cost	Optimized blade material cost
Blades	1.00	0.99	24.5	24.3
Hub	1.00	0.95	3.20	3.03
Main shaft	1.00	0.95	3.30	3.19
Main gear, generator and brake.	1.00	1.06	25.4	26.8
Machine foundation	1.00	1.02	4.50	4.55
Yaw system	1.00	0.94	4.00	3.77
Tower	1.00	0.96	17.6	17.2
Remaining components	-	-	17.5	17.5
	-	-	100.0	100.3

Most of the components have an almost equal material factor for the two blades. The slightly higher rotor loads for the LM 24.0 blade have increased the hub, shaft, yaw system and tower just a few percent, whereas the increase in the edgewise blade root moment and the shaft torque for the optimized blade has increased the main gear, generator, brake and machine foundation. In total, the optimized blade has been found to be 0.3% more expensive than the LM 24.0 blade.

The calculations of the necessary blade shell thicknesses and hence the resulting blade masses are carried out at the wind speed where the entire blade is stalled. Here, the section moment perpendicular to the local chord is calculated, Figure 5.7. This is the windspeed where the constraint on the mean blade root flapwise moment is added as explained in Section 2.3. This means that the estimation of mass is associated with some uncertainty, since the mean load is not directly an expression for the fatigue load. The reason for not using the fatigue load has been the mutual dependency between the blade mass and the fatigue load leading to an iterative and time consuming evaluation of the fatigue loads.

Another source of uncertainty is whether the extreme loads should determine the blade mass distribution. Even though the extreme blade root moments are identical the section moments on the outer part of the optimized blade would be increased compared to the LM 24.0 blade.

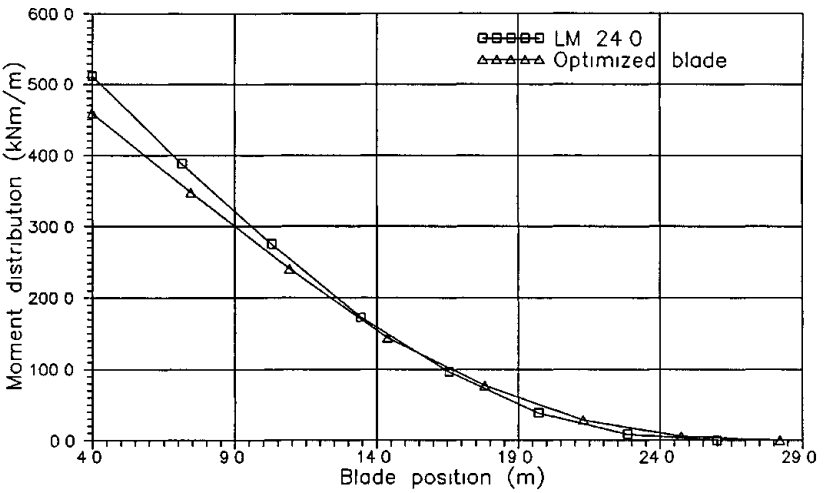

Figure 5.7 Section moments perpendicular to the local chord axis calculated inward from the tip for the optimized blade and the LM 24.0 blade at the wind speed having the constraint on the mean load.

5.5 Cost performance

Based on the material consumption and the relative annual production, the cost performance has been calculated both with and without the difference in blade mass. In Table 5.5 the results are shown. The optimized blade is found to have an increased cost performance of about 5.5% since the annual production has been increased by 5.8% whereas the material cost has only been increased by 0.3%.

Table 5.5 Comparison of cost performance for the optimized blade and the LM 24.0 blade. Values are shown relative to the LM 24.0 blade.

		LM 24.0 blade	Optimized blade
Relative energy production	(%)	100.0	105.8
Material consumption	(%)	100.0	100.3
Cost performance	(%)	100.0	105.5

5.6 Summary

In this Chapter, the design guidelines found in Chapter 3 have been tried out and the resulting optimized blade has been compared with the LM 24.0 blade.

The optimized blade has an increased annual production of energy on 5.8% compared to the LM 24.0 blade. The extreme blade root flapwise moment and the extreme rotor thrust force are fixed to be identical. An optimum constraint has not been found for the extreme loads and future work should include more attention to extreme loads.

The mean blade root flapwise moment has been reduced for the optimized blade, leading to lower equivalent fatigue loads, except for the blade root edgewise moment, which has been increased because of the increase in blade length. The rotor yaw and tilt moments and the rotor thrust force have been reduced leading to a drop in the material consumption, counterbalanced by an increase from the edgewise blade root moment leading to a total increase in the material consumption on only 0.3% for the optimized blade. This has lead to an increased cost performance on 5.5%

The main factors for the improved performance is a larger annual production from larger swept area, slightly lowered rotor fatigue loads from the constraint on the mean load and equal blade mass caused by the reduced solidity in the tip region.

The material consumption calculation has been used on optimization results instead of being directly incorporated in the optimization process. This means that an additional improvement might be possible, since a simultaneous variation of all design parameters could reveal smaller beneficial adjustments to the design guidelines found.

The performed comparison should be seen as a comparison between two different concepts rather than two blades, since the optimized blade is a design in an early stage that might have some bad properties not yet discovered, whereas the LM 24.0 blade is already being produced. However, it seems like a substantial improvement in the cost performance can be achieved by the use of the design guidelines derived in Chapter 3.

The calculation of the cost performance is connected with some uncertainty, since the modelling of the determining component dimensions and masses are simple. The importance of the extreme loads and demands on space for the tip brake system have not been sufficiently investigated. Furthermore, it has not yet been proven that the eigenfrequencies used in the aeroelastic calculations can be achieved with the requirements this has to the blade bending stiffness and to the tower torsional and bending stiffness.

6 Conclusion

The main objective of this report has been to design a 1 MW stall regulated rotor including investigations of the potential improvements by using special tailored airfoils. The target has been a rotor which should have an improved cost performance compared to existing rotors, where cost performance is defined as the annual production of energy relative to the material consumption. A newly developed numerical optimization tool and an aeroelastic code have been used in the study. The results indicate that a potential improvement of the cost performance of about 5.5% can be achieved with the use of traditional airfoils. Using optimized airfoil characteristics have indicated an additional improvement on 6% compared to traditional airfoils.

The calculation foundation

The rotor design has been performed with the aid of the numerical optimization code for wind turbine design, "Rotor" [5]. Design parameters have been the blade chord, twist, tip pitch angle, angular velocity and airfoil characteristics. The objective function for the optimization has been the annual production of energy in the Danish roughness class 1. Within the optimization process constraints have been added to mean and extreme blade root flapwise moments, rated power, tip speed and blade geometry.

A number of parameter investigations have been performed whereby the optimum rotor has been found at different operational conditions and with different requirements to loads and geometry.

To gain information on the fatigue loads for the optimized designs, aeroelastic calculations have been performed with the code, "Flex4" [11], with a large number of degrees of freedom and a full 3D three component turbulent wind input. A life time spectrum based on loads from normal operation has been calculated using Rainflow counting and equivalent fatigue loads have been calculated for comparison.

Based on blade and rotor equivalent fatigue loads, the relative material consumptions of the individual wind turbine components have been calculated. This allows for a relative comparison of costs of the individual optimization results.

The investigations cover three main subjects:

1) The optimum ratio of rated power to swept area.

2) The optimum airfoil characteristics along the blade span.

3) Evaluation of the derived design guidelines for an optimum blade.

The ratio of rated power to swept area

When the rotor swept area is increased for constant rated power, a substantial increase in the annual production is possible. However, both mean and extreme loads also increase progressively. If a constraint is added to the mean blade root

flapwise moment at stall or to the extreme blade root flapwise moment at rotor stand still, the annual production is reduced nonlinear with a linear drop in the constrained load. When the constrained load is lowered, the blade chord is reduced, leading to a reduction in rotor solidity. Even though the design is no longer at the aerodynamic optimum, the results indicate, that a trade off between the annual production and the loads might be beneficial.

By performing aeroelastic calculations on the optimized designs with different degrees of constraints on the mean blade root flapwise moments, an almost linear correlation between the mean blade root flapwise moment and the equivalent fatigue loads appears. Whereas the edgewise blade root moment is primarily deterministic, and therefore less sensitive to the constraint, the flapwise blade root moment and the rotor yaw and tilt moments show an equal slope primarily dependent on the swept area.

This finding is important, since the linear correlations imply that the fatigue loads can indirectly be included in the optimization process by adding constraints on mean loads instead of performing time consuming aeroelastic calculations within the optimization iteration loop.

The material consumption of the entire wind turbine has also been found to depend nearly linear on the constrained mean blade root flapwise moment. Based on this result together with the found nonlinear relation between constraint and energy yield, an optimum degree of constraint of about 80% to 90% has been found depending on the swept area. It seems therefore preferable to reduce the solidity for an optimum trade off between the annual production and the magnitude of the fatigue loads.

The optimum ratio of rated power to swept area appears to be around 400 W/m^2 with an 80% constraint on the mean flapwise blade root moment.

The airfoil characteristics along the blade span

The distribution of C_{Lmax} along the blade span has been included as design variables besides the blade planform, and optimizations have been performed with different degrees of constraints on the mean flapwise blade root moment. All optimized rotors in this investigation have had the optimum ratio of rated power to swept area of 400 W/m^2.

The maximum annual production of energy has been found for high value of C_{Lmax} over the entire blade. This result is independent on both the degree of constraint and the type of load constrained (extreme or mean load).

The direct improvement from the use of special tailored airfoils has been found to be around 4% on the annual production. By calculating the equivalent fatigue loads a reduction in the material consumption of 1.5% has been found leading to an improvement in the cost performance of about 6%.

Compared with the trend in modern airfoil design [20] the result is somewhat surprising regarding C_{Lmax}. However, because the optimization has involved a simultaneous variation of both the airfoil characteristics and the blade planform, it has been found preferable to reduce the solidity and increase C_{Lmax} instead of the opposite.

The reduction in solidity should be counterbalanced by a larger relative thickness to maintain equal stiffness qualities along the blade span. This emphasizes the need for airfoils having high C_{Lmax} and low C_{Dmin} together with a high relative thickness. Further investigations should include a more detailed cost function for the blade so that the influence from lower solidity on stiffness and thickness could be judged together with a relation between the relative airfoil thickness and C_{Lmax}. This might modify the results somehow.

When the entire rotor geometry is included as optimization design variables, the choice of C_{Lmax} becomes less important since the design space is flat in the neighbourhood of the optimum. This means that airfoil qualities that are not included in the optimization problem such as roughness insensitivity can be paid more attention to in the design process at the expense of a specific C_{Lmax}.

It has been found that a lowering of C_{Dmin} with 0.002 would increase the annual production with 1%. This indicates that it is not profitable to use highly laminar airfoils as they will often be much more sensitive to e.g. surface roughness.

Investigations of additional constraints on the minimum tip pitch angle and the minimum tip chord show that these to some extent can be increased without decreasing C_{Lmax} at the tip and without a significant loss in the annual production. This might be beneficial because of tip noise and manufacturing considerations.

Comparison with LM 24.0

A blade that was optimized using the guidelines found in Chapter 3 has been compared with the existing LM 24.0 blade. Both blades have had an equal rated power on 1 MW, equal airfoils, equal relative thickness, equal extreme loads at rotor stand still and equal dynamic properties. The optimized blade has a ratio of rated power to swept area of 400 W/m^2 and an 80% constraint on the mean load, whereas the LM 24.0 blade has a ratio of rated power to swept area of 471 W/m^2. The increase in blade static moment and mass moment of inertia from the longer blade has been taken into account.

The optimized blade has an increased annual production of energy of 5.8% compared to the LM 24.0 blade. The mean blade root flapwise moment has been reduced for the optimized blade partially leading to lower fatigue loads. The blade root edgewise moment is not reduced, whereas the blade root flapwise moment, rotor fatigue moments and the rotor thrust force have been reduced. This has in total lead to an increase in the material consumption on 0.3% for the optimized blade.

This leads to an improved cost performance of 5.5% compared to LM 24.0. Adding the benefit of optimum airfoil characteristics increases the cost performance to about 11%. However this number might only be partially realistic since the airfoils used already have a high C_{Lmax} over most of the blade.

The performed comparison should be seen as a comparison between two different concepts rather than two blades, since the optimized blade is a design in an early stage that might have some bad properties not yet discovered, whereas the LM 24.0 blade is already being manufactured.

Final remarks

The investigations have involved many assumptions and simplifications, and the accuracy of the findings should not be over estimated, however, it appears that a substantial improvement in the cost performance is available by using the found design guidelines.

The material consumption has only been used on optimization results instead of being directly incorporated in the optimization process. This means that an additional improvement in the cost performance might be possible, since a simultaneous variation of all design parameters could reveal beneficial adjustments on the found design guidelines.

The fatigue load calculations have been based on normal operation only. No considerations have been taken on the importance of other life time events such as stop and start sequences etc.

For the material consumption, it has been assumed that the magnitude of the fatigue loads determine the important dimensions of the individual components, independently of extreme loads. Further investigations should contain a judgement of whether the individual component sizes are determined from either fatigue or extreme loads. Furthermore the calculation of the blade mass should be refined to become more reliable.

Whereas the proposed guidelines have been very beneficial to constrain the fatigue loads, the extreme loads have not been entirely included. However, it has been shown that reducing the mean and fatigue loads has a beneficial influence on the extreme blade root moment at rotor stand still. Further investigations should include additional constraints on extreme loads.

References

[1] Hoadley, D. et al., 1993, "Aerofoil Section design and assessment," *Final report on contract JOUR 0079 for The Commission of the European Communities*, Directorate-General XII, Published by the University of Southhampton.

[2] Madsen, H. Aa., 1994, "Design af en 20 kW - 12.6 m Stallreguleret Rotor," (In Danish), Risø-I-809(DA), Risø National Laboratory, Denmark

[3] Antoniou, I. A., Madsen, H. A., and Kretz, A., 1994, "Afprøvning af en 20 kW - 12.6 m Stallreguleret Rotor," (In Danish), Risø-I-788(DA), Risø National Laboratory, Denmark

[4] Glauert, H., 1963, "Airplane Propellers," In *Aerodynamic Theory*, Durand, W. F. ed., Dover Publications, New York.

[5] Fuglsang, P. L, and Enevoldsen, P. B., 1994, "Aerodynamisk optimering af rotor til vindturbine," (in Danish), *M.Sc. Thesis*, Aalborg University, Denmark.

[6] Fuglsang, P.L., and Madsen, H.A., 1994, "Optimization of stall regulated rotors", Risø-I-830(EN), Risø National Laboratory, Denmark

[7] Vanderplaats, G.N., 1984, "Numerical Optimization Techniques for Engineering Design with applications," McGraw-Hill Book Company.

[8] Germanishe Lloyds, 1993, "GL 150. GL - Vorschriften und Richtlinien, GL Nichtmaritime Technik," part 1, chap. 1 - 10.

[9] Abbott, I. H. and von Doenhoff, A. E., 1959, "Theory of wing Sections," Dover Publications, New York.

[10] Petersen, H., 1986, "Benchmark test on power curve computations on wind turbines - A compendium," Risø National Laboratory. Denmark, Unpublished.

[11] Øye, S., 1992, "FLEX4 - Computer code for wind turbine load simulation," Fluid Mechanics Department, Tecnical University of Denmark.

[12] Madsen, P.H. (Editor) et.al, 1990, "Recommended practices for wind turbine testing and evaluation, 3. Fatigue Loads," Executive Committee of the International Energy Agency Programme for Research and Development on Wind Energy Conversion Systems.

[13] Thomsen, K., 1994, "Notat vedrørende Analyse af udmattelseslaster på vindmøller," (In Danish), Risø National Laboratory, Denmark, Unpublished.

[14] Rasmussen, F. and Kretz, A., 1994,"Dynamics and potentials for the twobladed teetering rotor concept,", In *Proc. Windpower 1994.*

[15] Veers, P.S., 1988, "Three-Dimensional Wind Simulation.", Sandia Report, SAND 88-0152.

[16] Øye, S., 1991, "Dynamic Stall - Simulation as time lag of seperation", In *Proc. IEA 2nd symposion on the Aerodynamics of Wind Turbines.* Ed by K. F. McAnulty, Rome, Italy.

[17] Dansk Ingeniørforening, 1992, "Dansk Ingeniørforenings og IngeniørSammenslutningens norm for last og sikkerhed for vindmøllekonstruktioner," (In Danish), DS 472, Teknisk Forlag, Denmark.

[18] Energistyrelsens regeludvalg for godkendelse af vindmøller, 1992, "Teknisk grundlag for typegodkendelse og certificering af vindmøller i Danmark," (In Danish), Risø National Laboratory, Denmark.

[19] Thomsen, K. et al., 1993, "Loads and dynamics for stall regulated rotors," Risø-R-655(EN), Risø National Laboratory, Denmark.

[20] Tangler, J. et al., 1987, "Status of the Special - purpose Airfoil Families," In *proc. WINDPOWER 1987*, San Francisco, USA.

[21] Björck, A., 1988, "Airfoil Design for Horizontal Axis Wind Turbines," In *Proc. IEA 2nd Symposium on Aerodynamics of Wind Turbines*, Lyngby, Denmark.

[23] Grabau, P., 1994, "Udvikling af rotor til en 1 MW vindmølle.", (In Danish), Final report, ENS project 51171/91-0046, LM Glassfiber A/S, Denmark.

[24] Informationssektretariatet For Vedvarende Energi, 1995, "Vindmølleoversigten," (In Danish), DTI, February.

[25] Thomsen, K. et al., "Experimental Investigation of Gear Box Duration Loads on Stall and Pitch Controlled Wind Turbines," Risø-R-653(EN), Risø National Laboratory, Denmark.

A Introductory investigation

Figures in this Appendix concern optimization results from Section 3.2.

Design variables: Chord is a cubic spline with 8 points
Twist is a cubic spline with 5 points
Tip pitch angle
Angular velocity

Constraints: Rated power < 1 MW
Tip speed < 60 m/s
Zero twist at tip

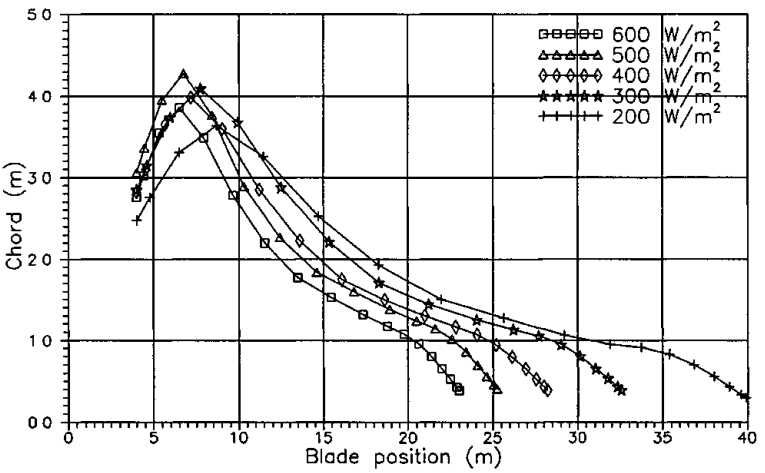

Figure A1 Chord distribution for optimizations at different ratios of rated power to swept area.

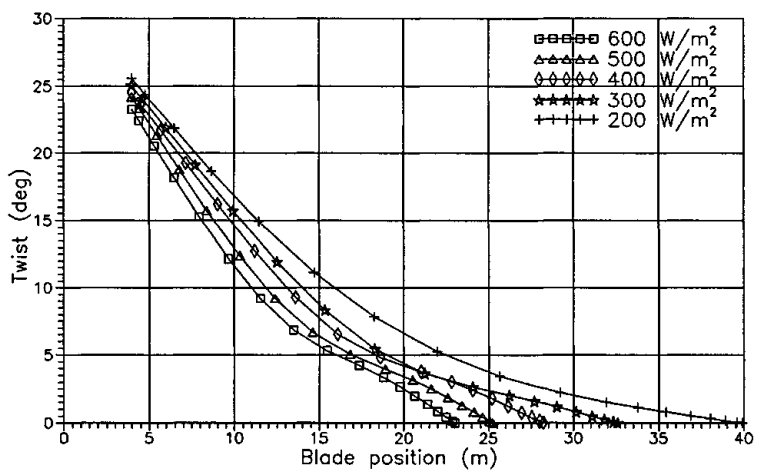

Figure A2 Twist distributions for optimizations at different ratios of rated power to swept area.

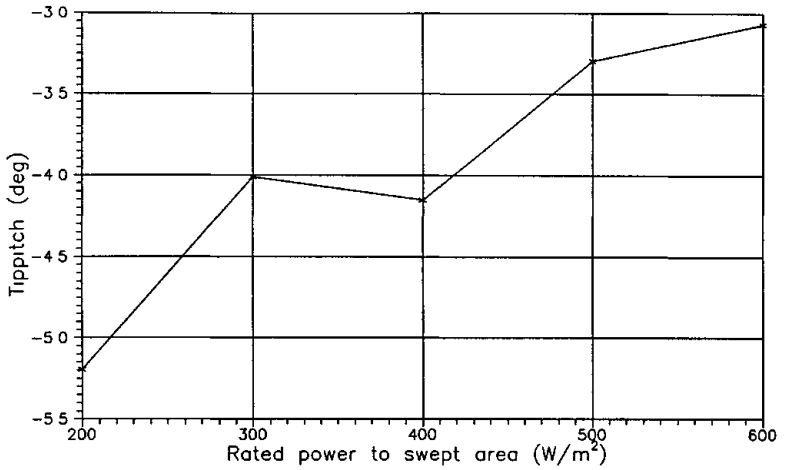

Figure A3 Tip pitch angles for optimizations at different ratios of rated power to swept area.

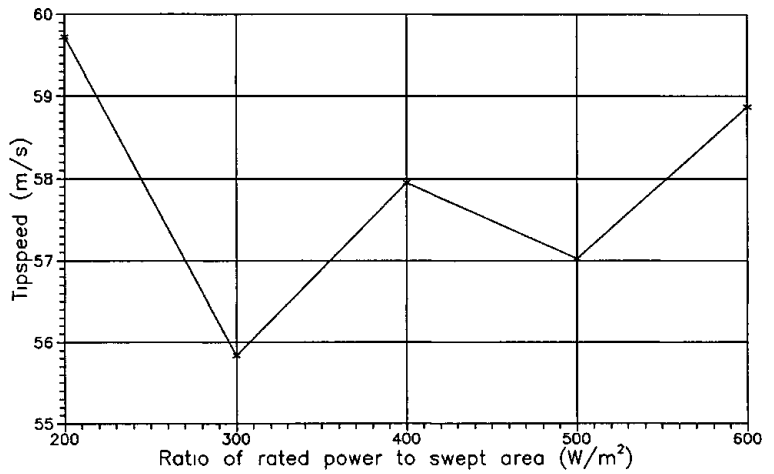

Figure A4 Tip speed for optimizations at different ratios of rated power to swept area.

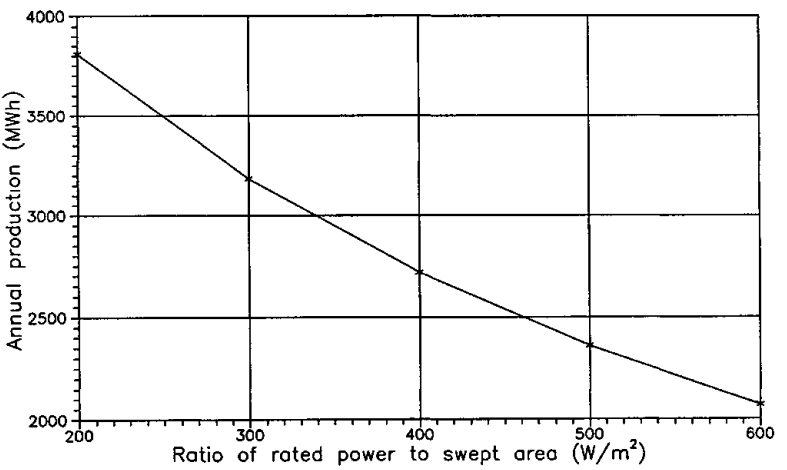

Figure A5 Annual production for optimizations at different ratios of rated power to swept area.

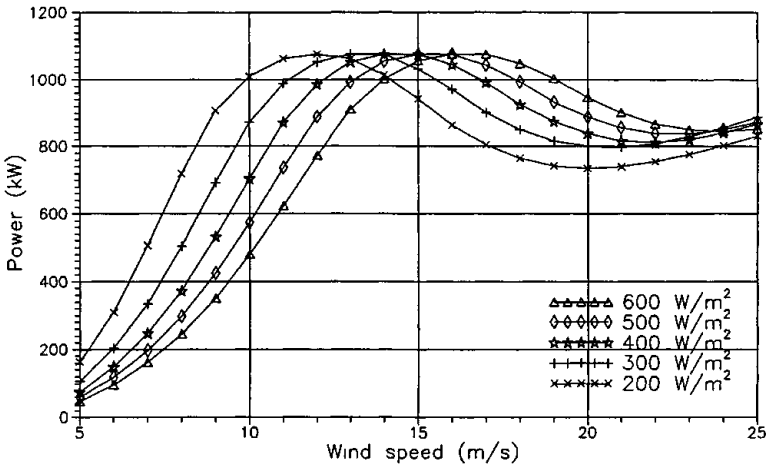

Figure A6 Power curves for optimizations at different ratios of rated power to swept area.

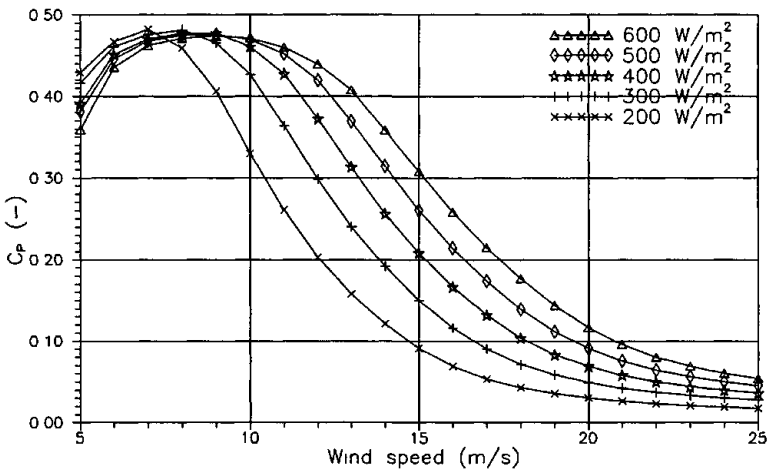

Figure A7 Power coefficient curves for optimizations at different ratios of rated power to swept area.

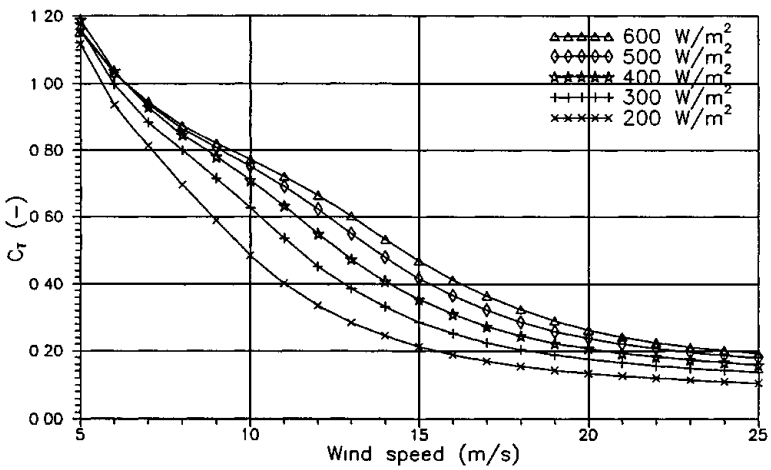

Figure A8 Thrust coefficient curve for optimizations at different ratios of rated power to swept area.

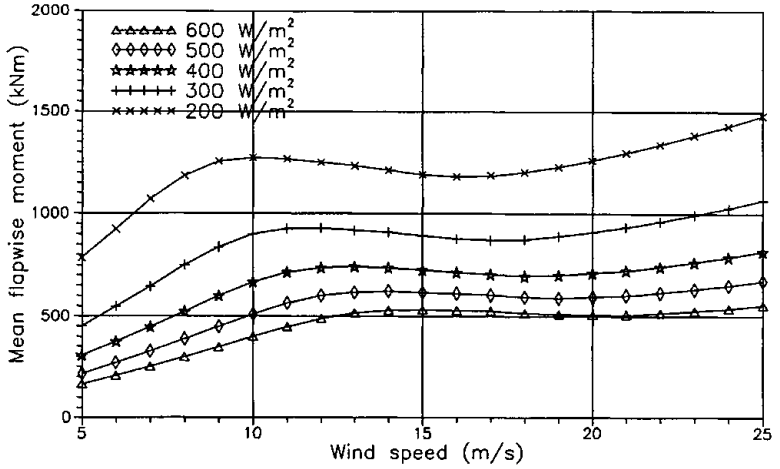

Figure A9 Mean blade root flapwise moment curve for optimizations at different ratios of rated power to swept area.

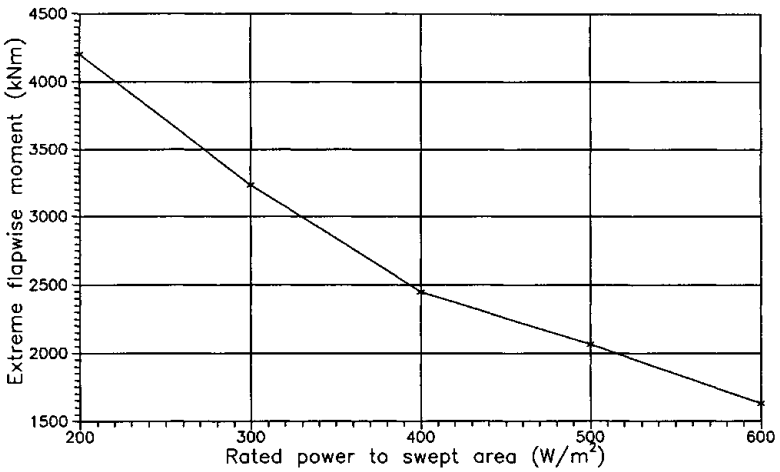

Figure A10 Extreme blade root flapwise moment at rotor stand still for optimizations at different ratios of rated power to swept area.

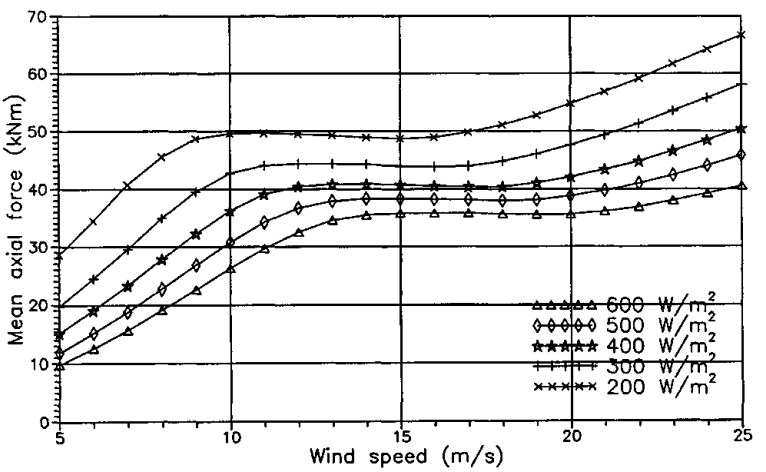

Figure A11 Rotor thrust force on one blade for optimizations at different ratios of rated power to swept area.

B Constraint on the mean blade root flapwise moment

Figures in this Appendix concern optimization results from Section 3.3.1.

Ratio of rated power to swept area: 500 W/m^2

Design variables: Chord is a cubic spline with 8 points
Twist is a cubic spline with 5 points
Tip pitch angle
Angular velocity

Constraints: Rated power < 1 MW
Tip speed < 60 m/s
Zero twist at tip
The mean blade root flapwise moment at stall at 60%, 70%, 80%, 90%, 95% and 100% (unconstrained)

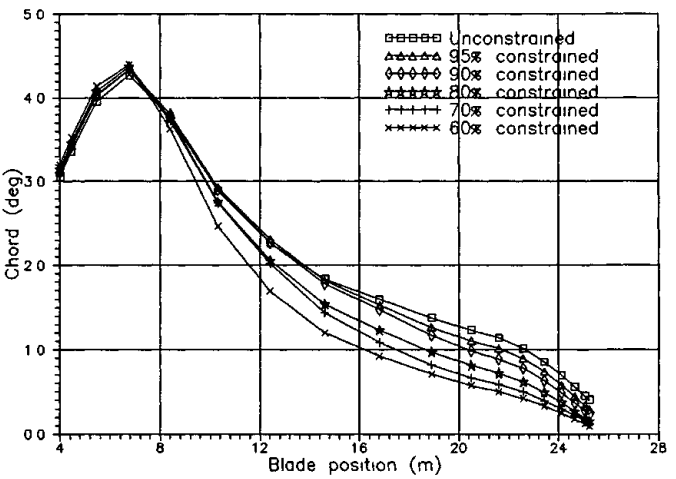

Figure B1 *Chord distribution for optimizations with different constraints on the mean blade root flapwise moment at stall.*

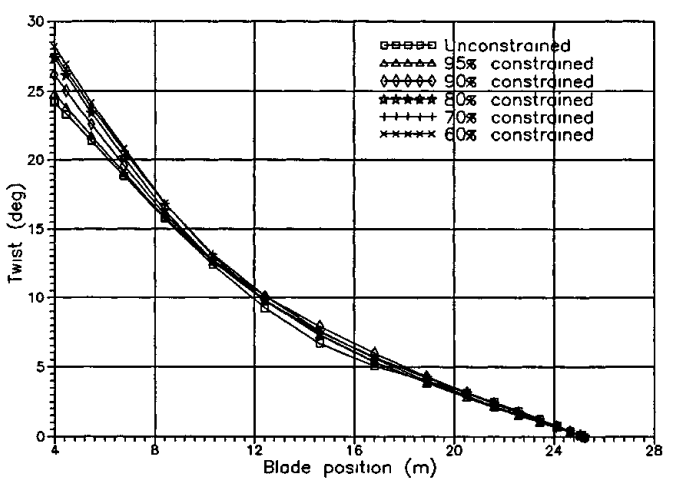

Figure B2 *Twist distributions for optimizations at different constraints on the mean blade root flapwise moment at stall.*

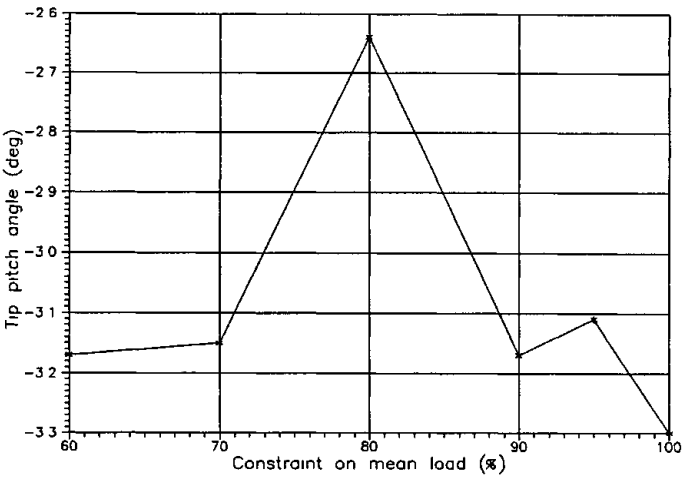

Figure B3 *Tip pitch angles for optimizations at different constraints on the mean blade root flapwise moment at stall*

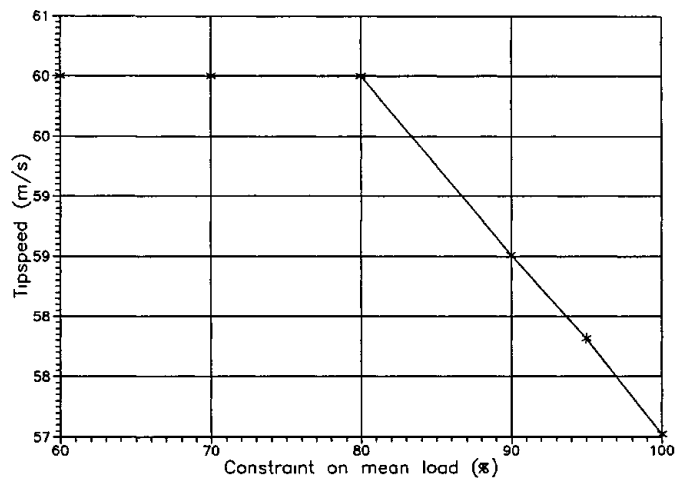

Figure B4 *Tip speed for optimizations at different constraints on the mean blade root flapwise moment at stall.*

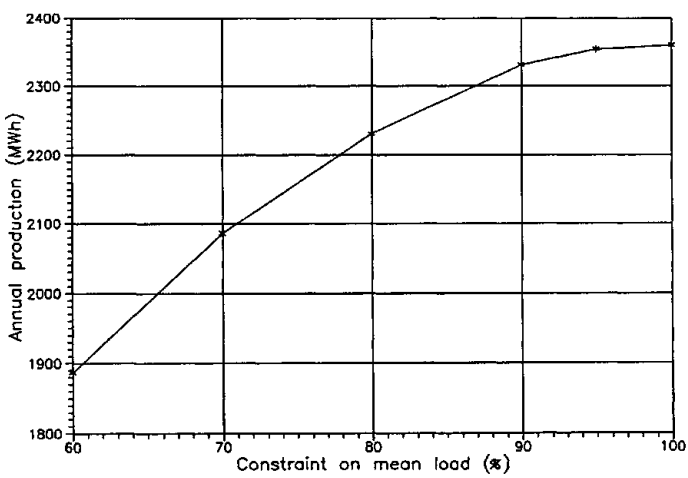

Figure B5 *Annual production for optimizations at different constraints on the mean blade root flapwise moment at stall.*

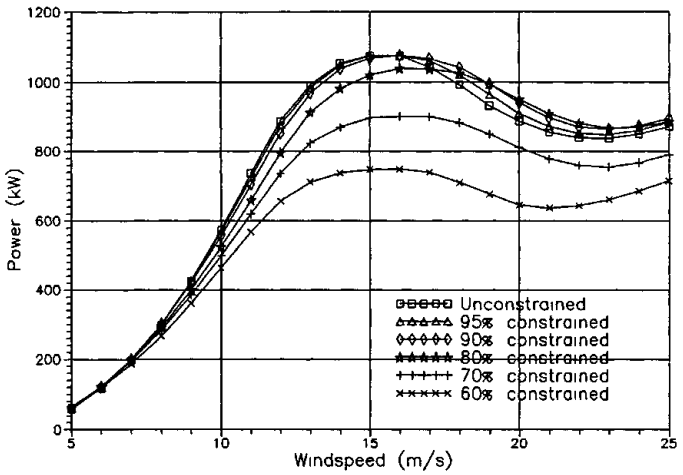

Figure B6 *Power curves for optimizations at different constraints on the mean blade root flapwise moment at stall.*

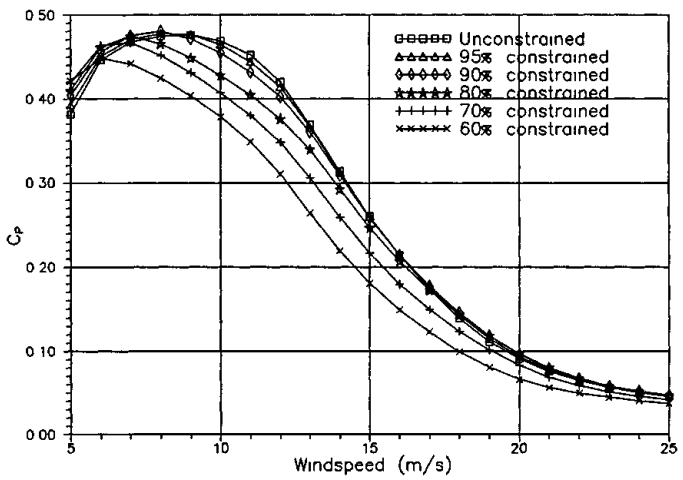

Figure B7 *Power coefficient curves for optimizations at different constraints on the mean blade root flapwise moment at stall.*

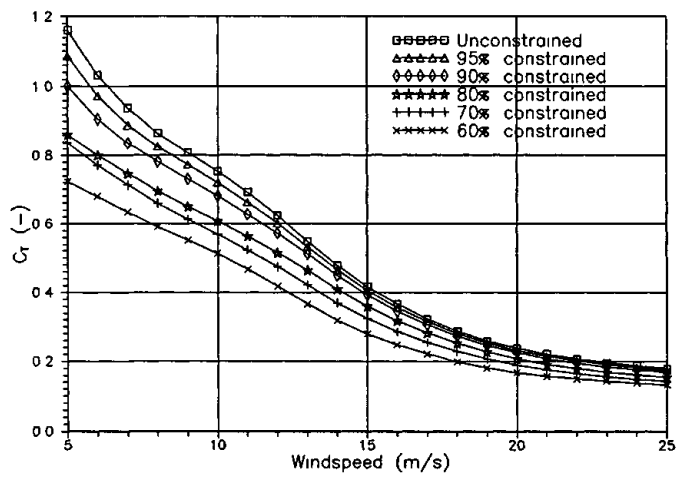

Figure B8 *Thrust coefficient curves for optimizations at different constraints on the mean blade root flapwise moment at stall.*

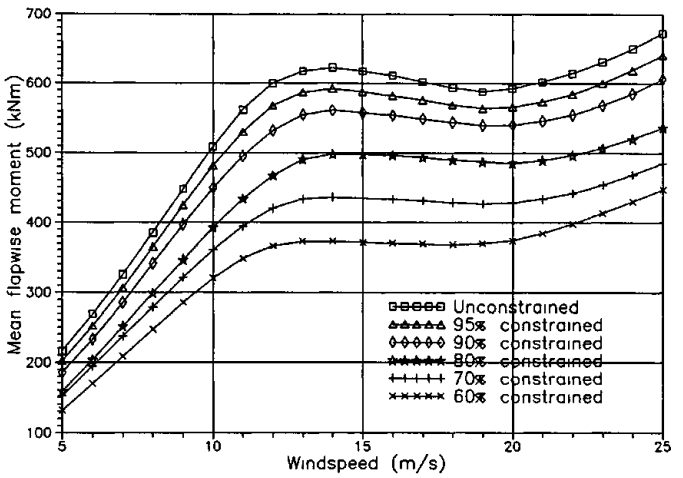

Figure B9 *Flapwise blade root moment curves for optimizations at different constraints on the mean blade root flapwise moment at stall.*

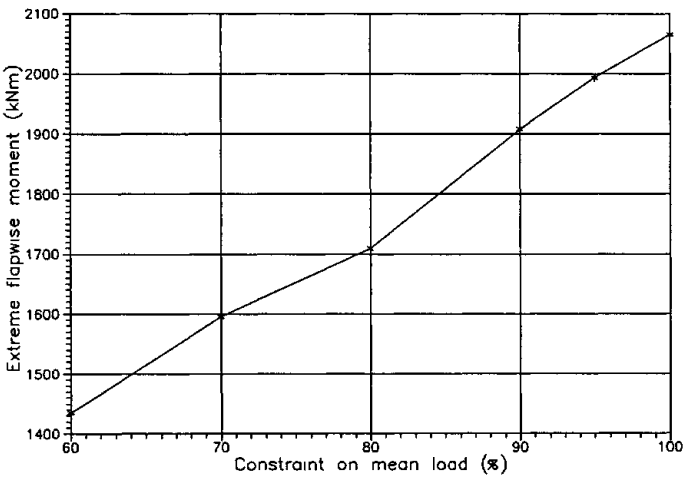

Figure B10 *Extreme flapwise blade root moment at rotor stand still for optimizations at different constraints on the mean blade root flapwise moment at stall.*

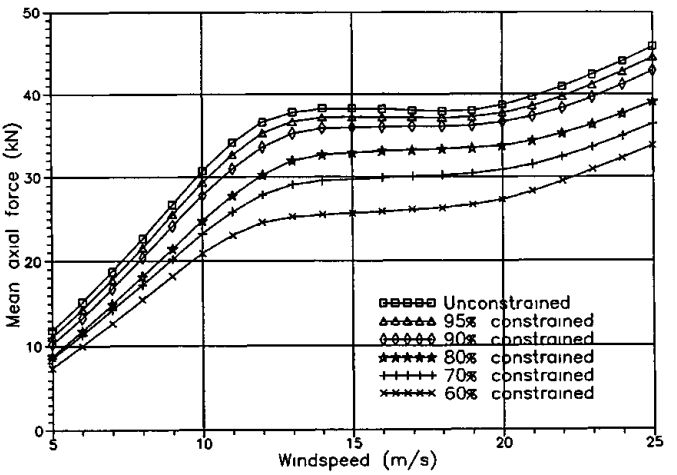

Figure B11 *Thrust force curves for optimizations at different constraints on the mean blade root flapwise moment at stall.*

C Constraint on the extreme blade root flapwise moment

Figures in this Appendix concern optimization results from Section 3.3.2.

Ratio of rated power to swept area: 500 W/m^2

Design variables: Chord is a cubic spline with 8 points
Twist is a cubic spline with 5 points
Tip pitch angle
Angular velocity

Constraints: Rated power < 1 MW
Tip speed < 60 m/s
Zero twist at tip
The extreme blade root flapwise moment at rotor stand still at 60%, 70%, 80%, 90%, 95% and 100% (unconstrained)

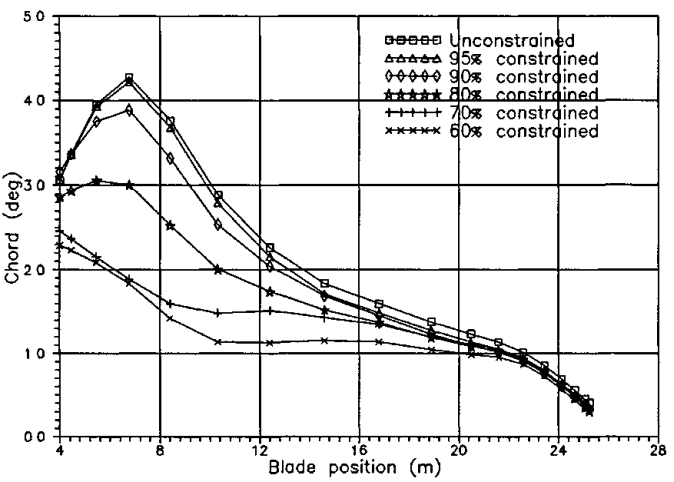

Figure C1 Chord distribution for optimizations with different constraints on the extreme blade root flapwise moment at rotor stand still.

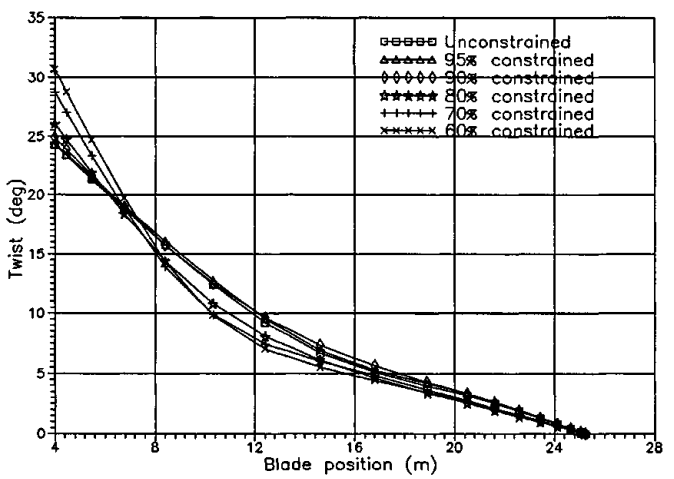

Figure C2 Twist distributions for optimizations at different constraints on the extreme blade root flapwise moment at rotor stand still.

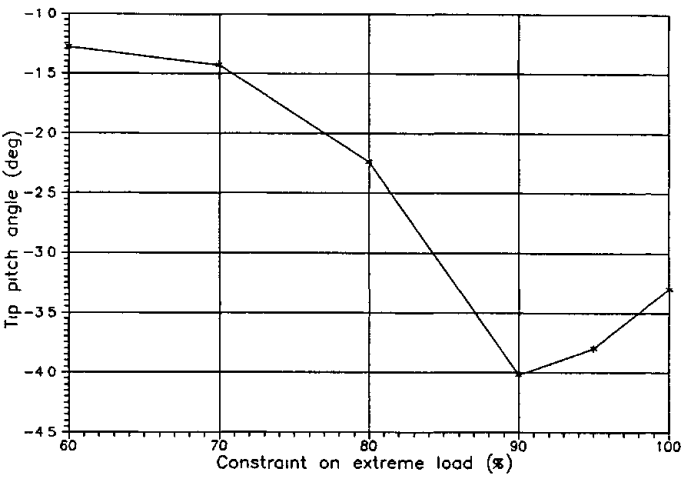

Figure C3 *Tip pitch angles for optimizations at different constraints on the extreme blade root flapwise moment at rotor stand still*

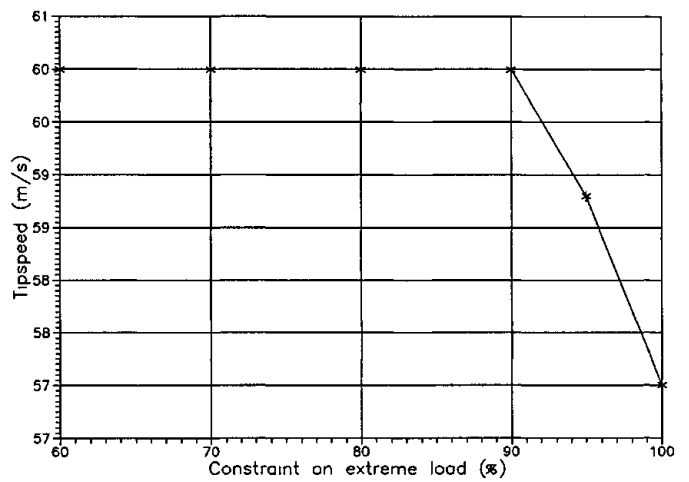

Figure C4 *Tip speed for optimizations at different constraints on the extreme blade root flapwise moment at rotor stand still.*

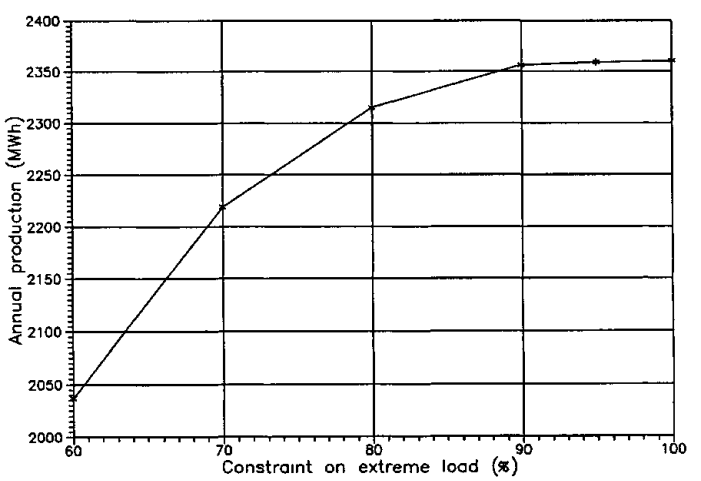

Figure C5 *Annual production for optimizations at different constraints on the extreme blade root flapwise moment at rotor stand still.*

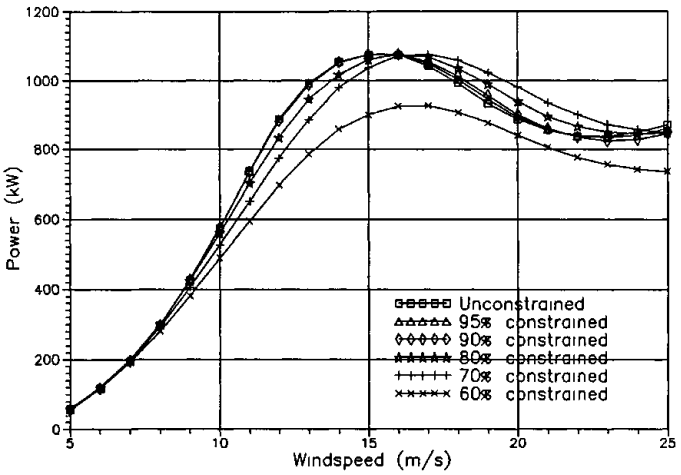

Figure C6 Power curves for optimizations at different constraints on the extreme blade root flapwise moment at rotor stand still.

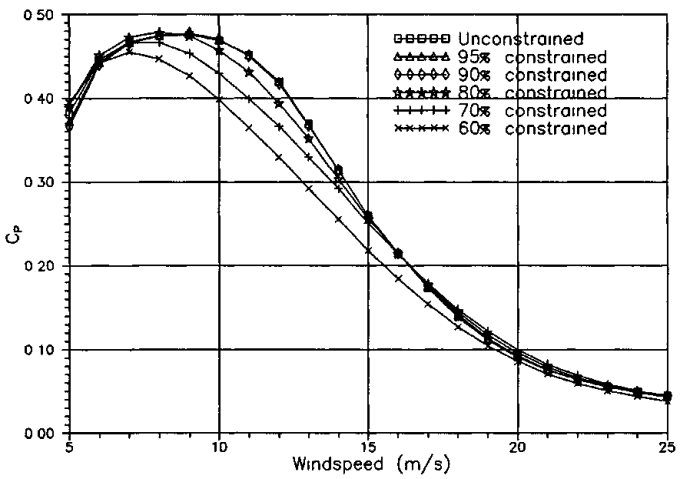

Figure C7 Power coefficient curves for optimizations at different constraints on the extreme blade root flapwise moment at rotor stand still.

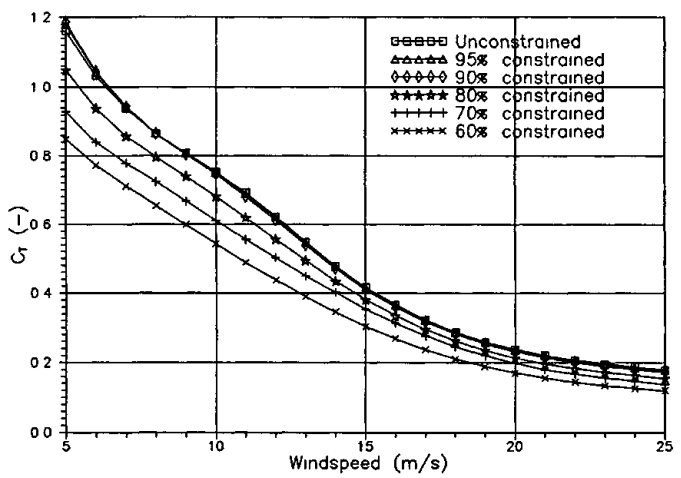

Figure C8 Thrust coefficient curves for optimizations at different constraints on the extreme blade root flapwise moment at rotor stand still.

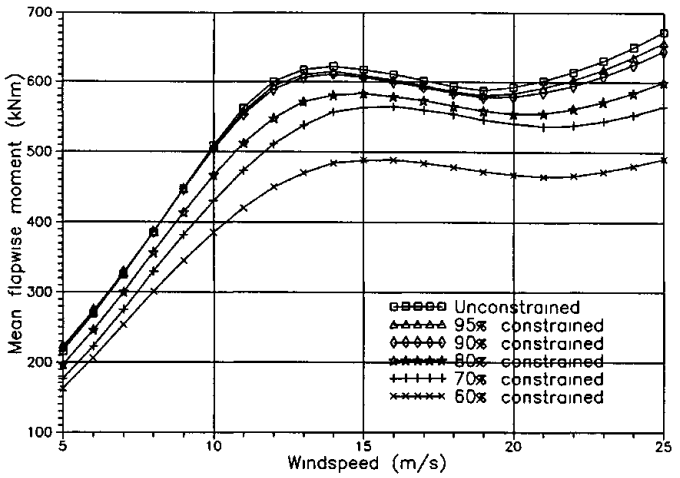

Figure C9 Flapwise blade root moment curves for optimizations at different constraints on the extreme blade root flapwise moment.

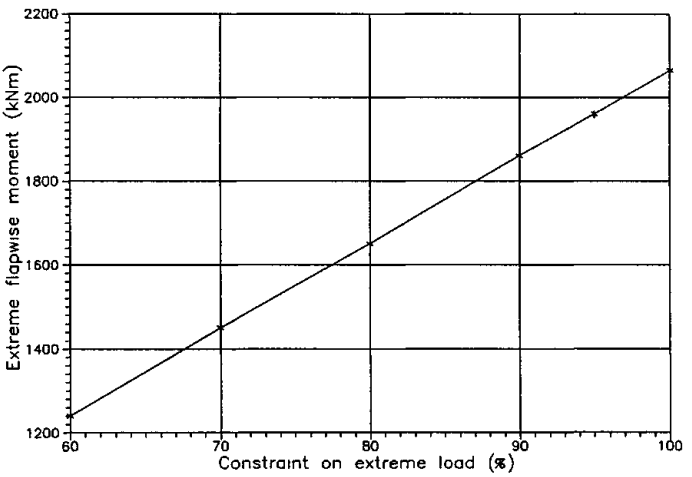

Figure C10 Extreme flapwise blade root moment at rotor stand still for optimizations at different constraints on the extreme blade root flapwise moment at rotor stand still.

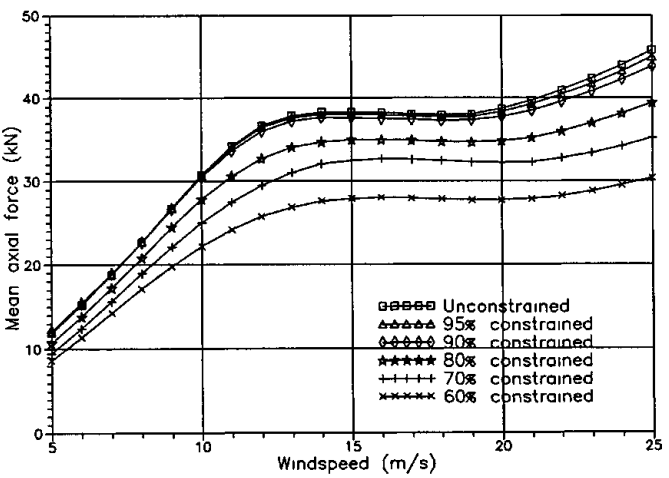

Figure C11 Thrust force curves for optimizations at different constraints on the extreme blade root flapwise moment at rotor stand still.

D Time series

Figures in this Appendix concern time series calculations in Section 3.4.

Ratio of rated power to swept area: 500 W/m^2

Wind speed: 15 m/s

Constraints: Unconstrained

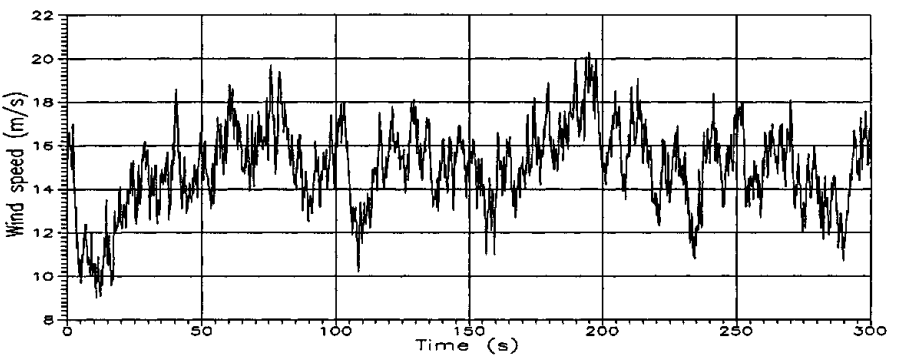

Figure D1 Wind speed time series.

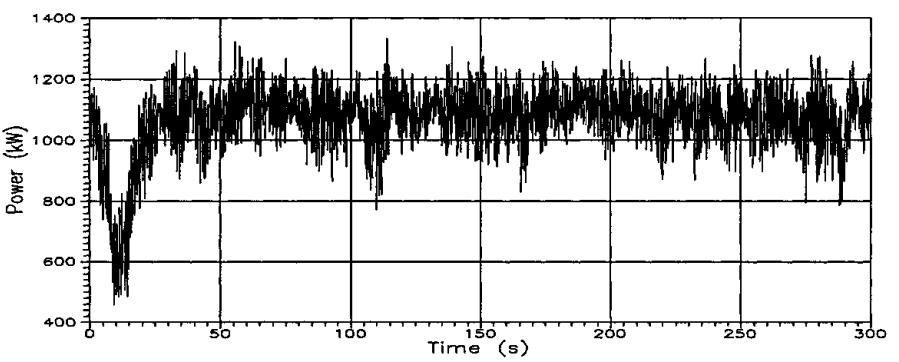

Figure D2 Power curve time series.

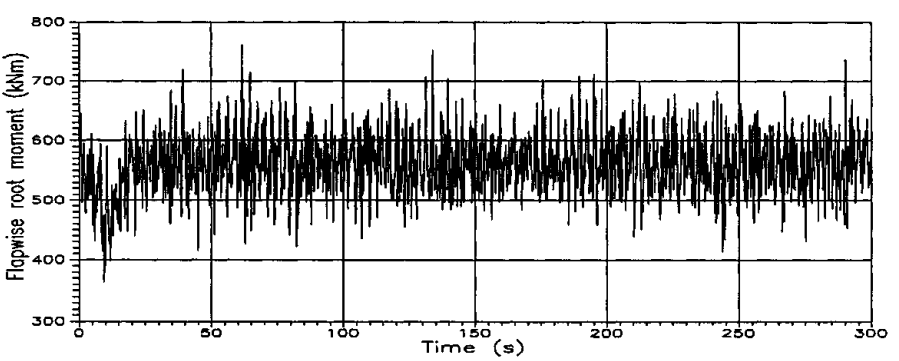

Figure D3 Blade root flapwise moment time series.

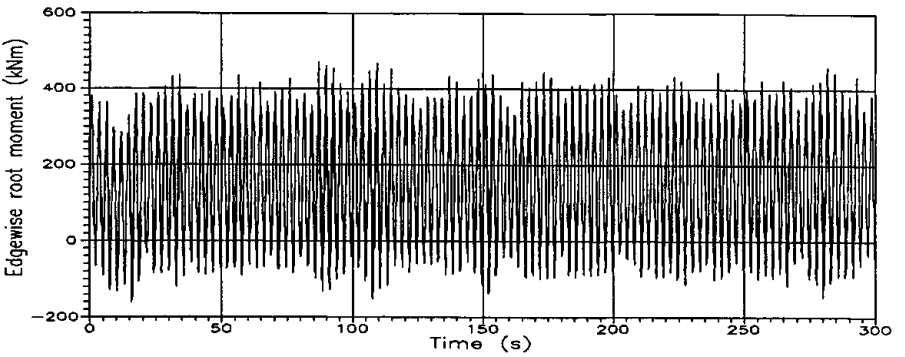

Figure D4 Blade root edgewise moment time series.

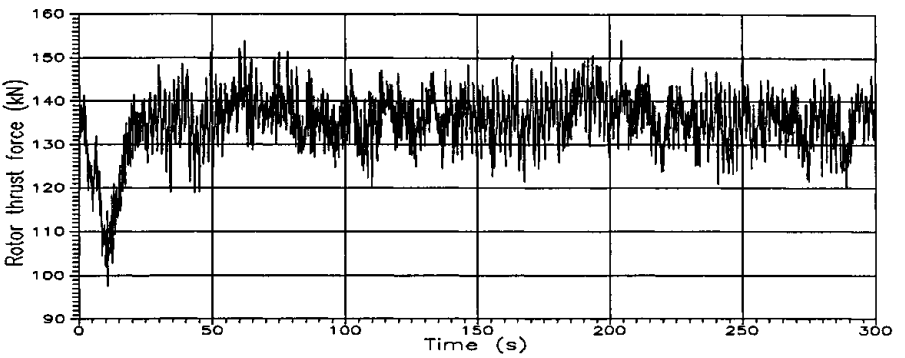

Figure D5 Rotor thrust force time series.

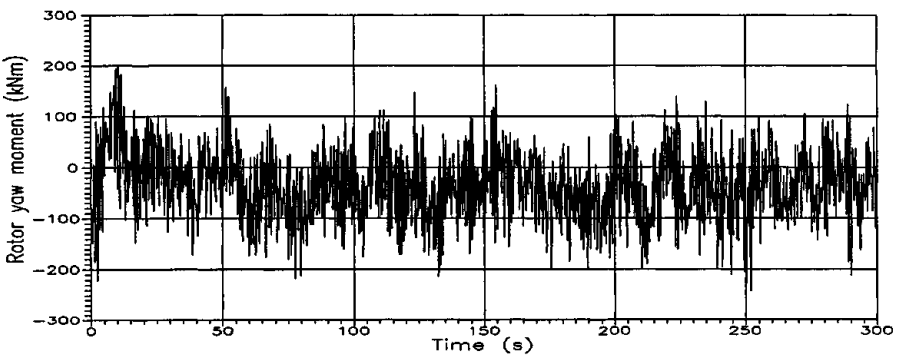

Figure D6 Rotor yaw moment time series.

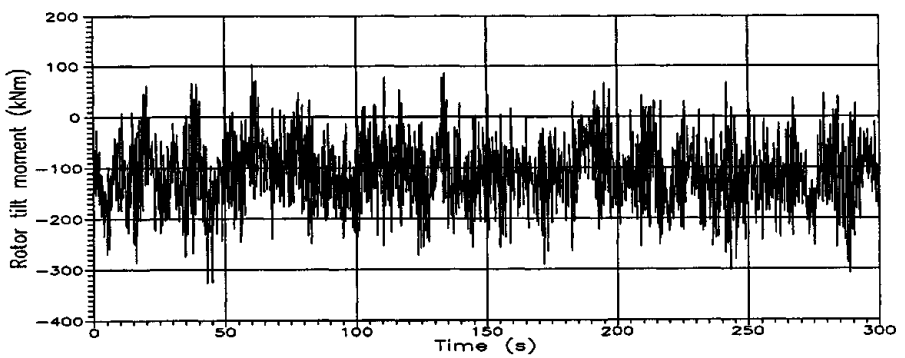

Figure D7 Rotor tilt moment time series.

E Equivalent fatigue loads

Figures in this Appendix concern the equivalent fatigue loads in Section 3.4.3.

Ratio of rated power to swept area: 300 - 600 W/m^2

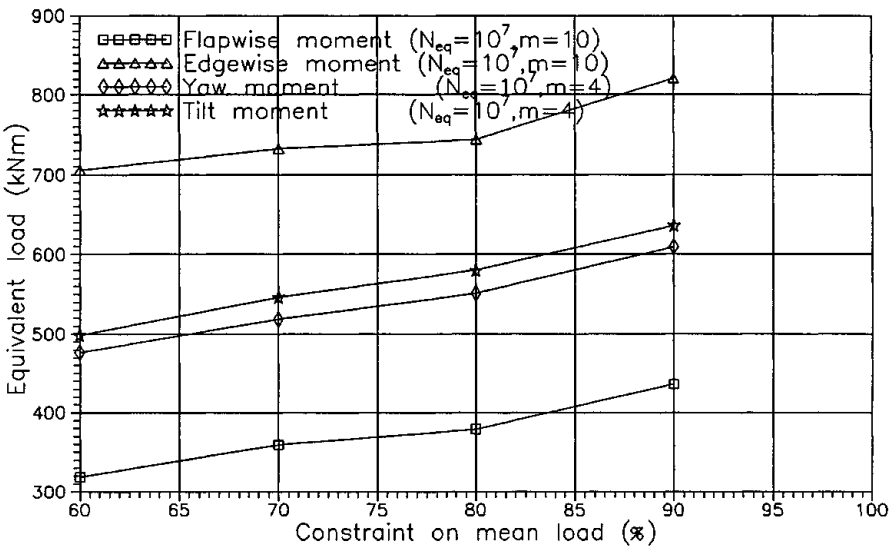

Figure E1 Equivalent fatigue loads as a function of the constrained mean load for specific power, 300 W/m^2.

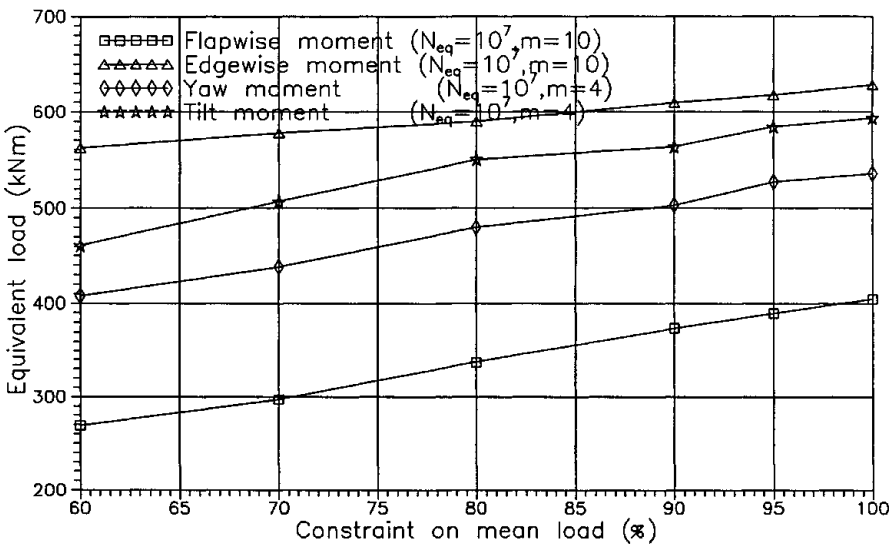

Figure E2 Equivalent fatigue loads as a function of the constrained mean load for specific power, 400 W/m^2.

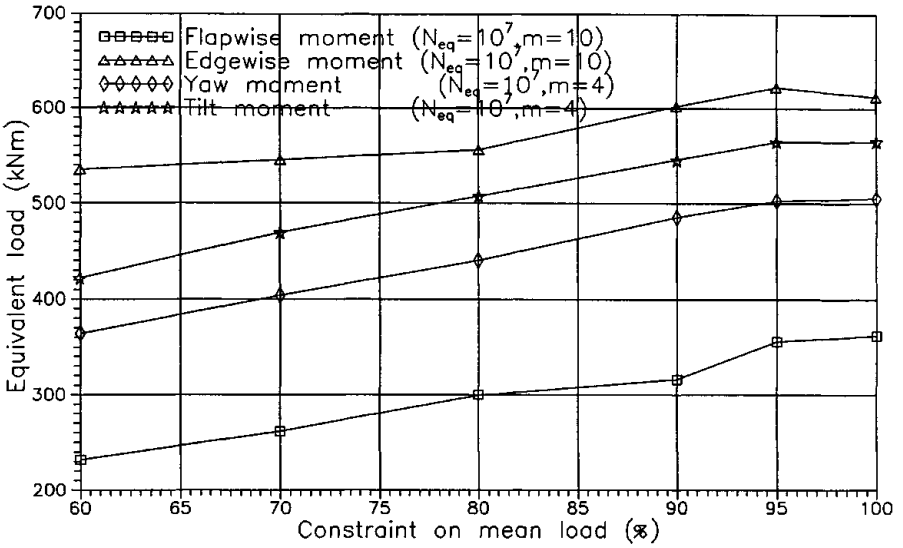

Figure E3 Equivalent fatigue loads as a function of the constrained mean load for specific power, 500 W/m².

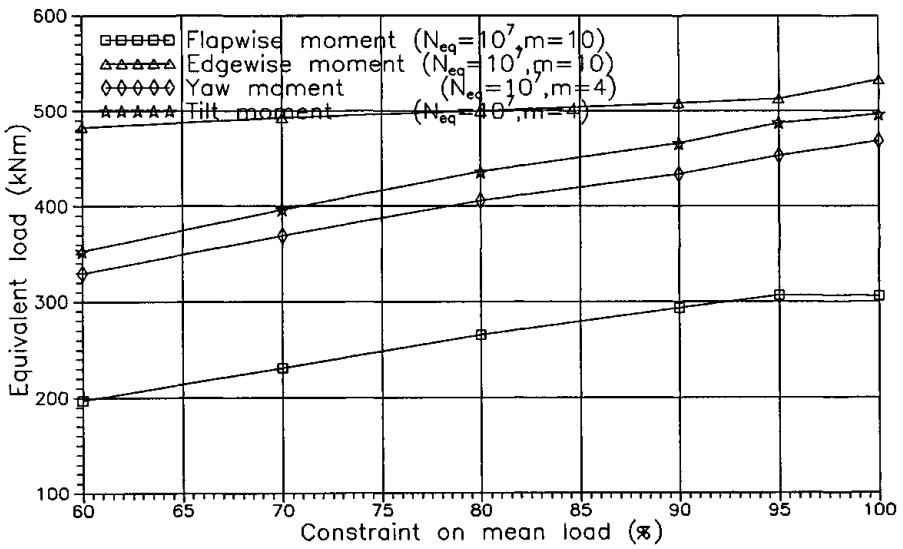

Figure E4 Equivalent fatigue loads as a function of the constrained mean load for specific power, 600 W/m².

F Parametric airfoil characteristics

Figures in this Appendix are examples of the parametric airfoils used in Chapter 4. The only design variable is the maximum lift coefficient, C_{Lmax}, a cubic spline with 5 points along the blade span. The value of C_{Dmin} is lowered from 0.008 to 0.0065 along the blade span to compensate for a loss in the relative thickness.

In this example, C_{Lmax} varies from 1.0 to 1.60 along the blade span. This means that C_{Dmin} is lowered when C_{Lmax} is increased.

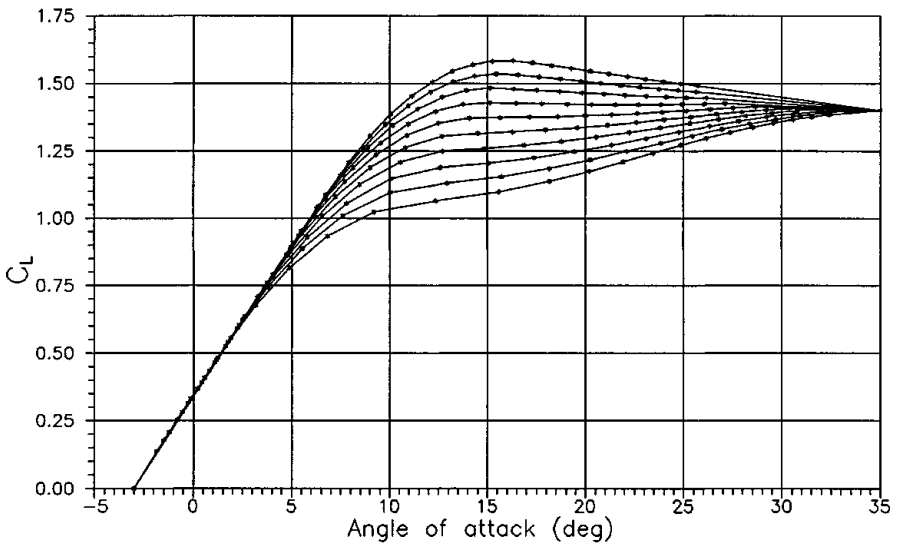

Figure F1 Variation in C_L versus angle of attack.

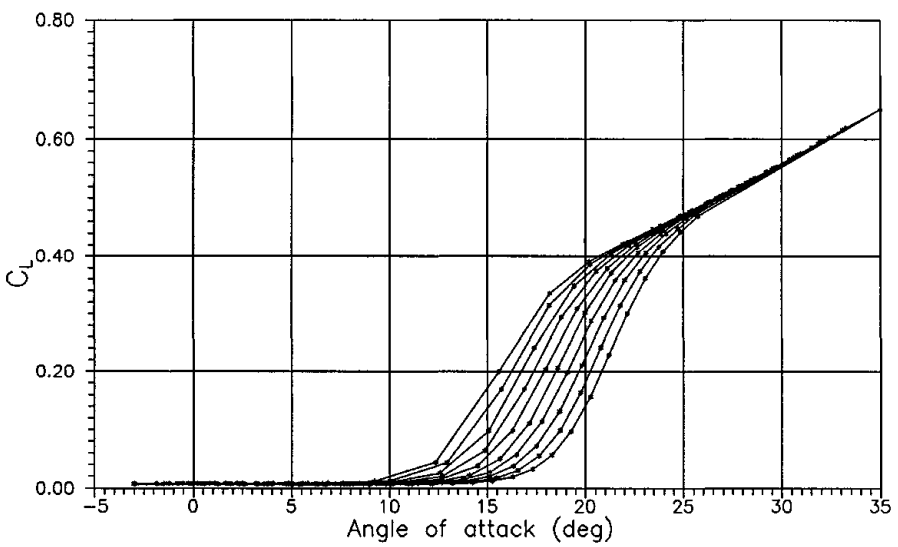

Figure F2 Variation in C_D vs. angle of attack. In this example lower C_{Dmin} corresponds to lower C_{Lmax}

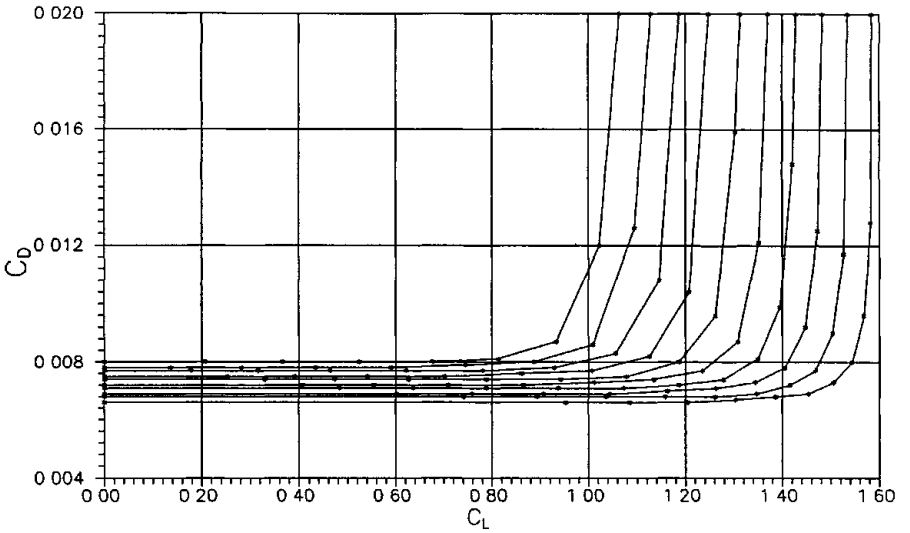

Figure F3 C_D *as a function of* C_L *The increase in drag is pushed to the right as* C_{Lmax} *is increased.*

G The design space topology

Figures in this Appendix concern the optimization results from Section 4 2 and Section 4 3

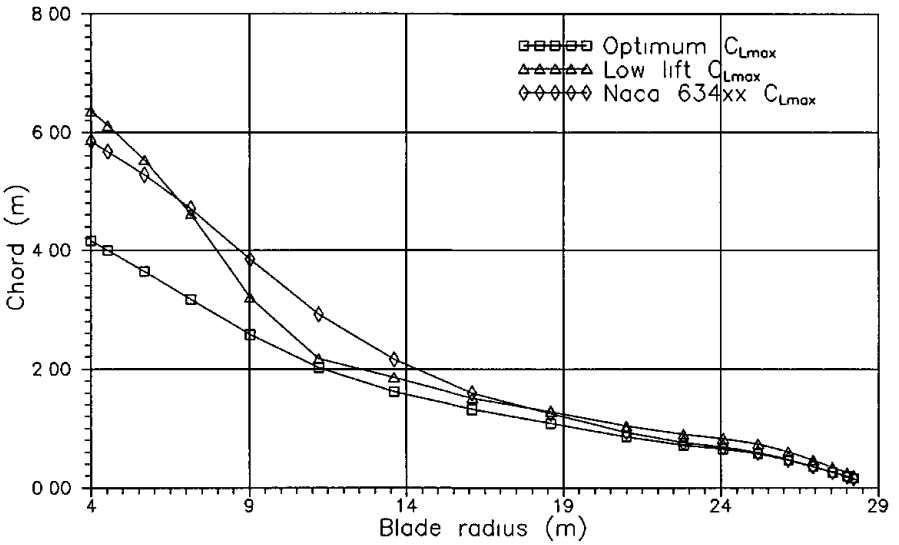

Figure G1 Chord distributions for the optimizations with different C_{Lmax} variations

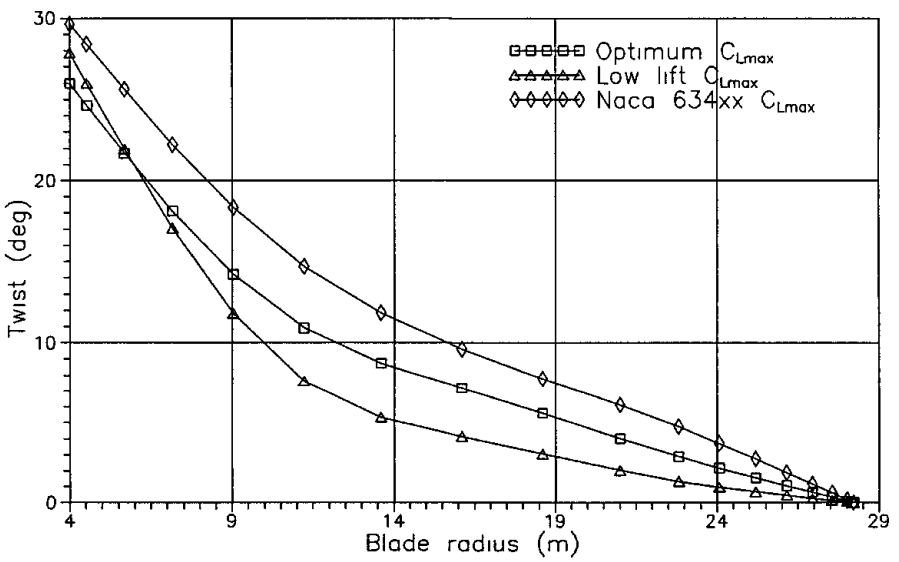

Figure G2 Twist distributions for the optimizations with different C_{Lmax} variations

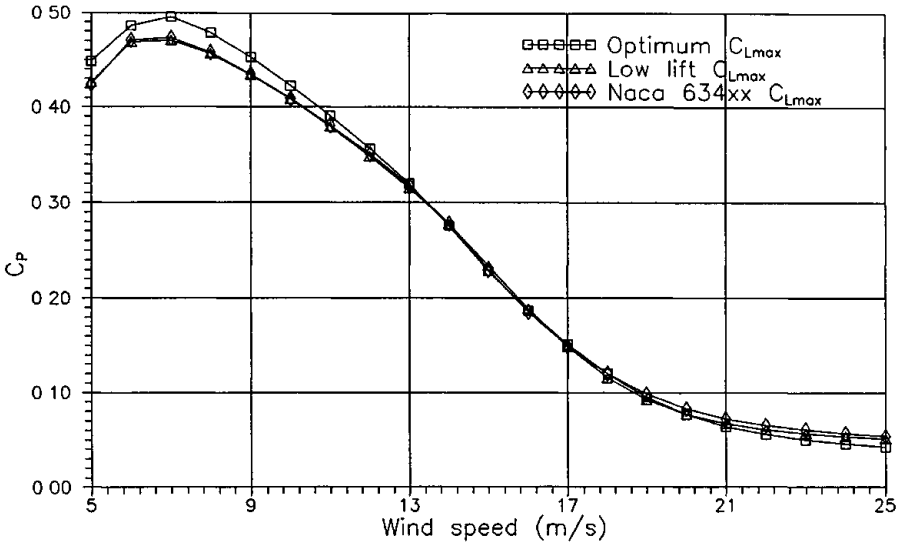

Figure G3 Power coefficient for the optimizations with different C_{Lmax} variations.

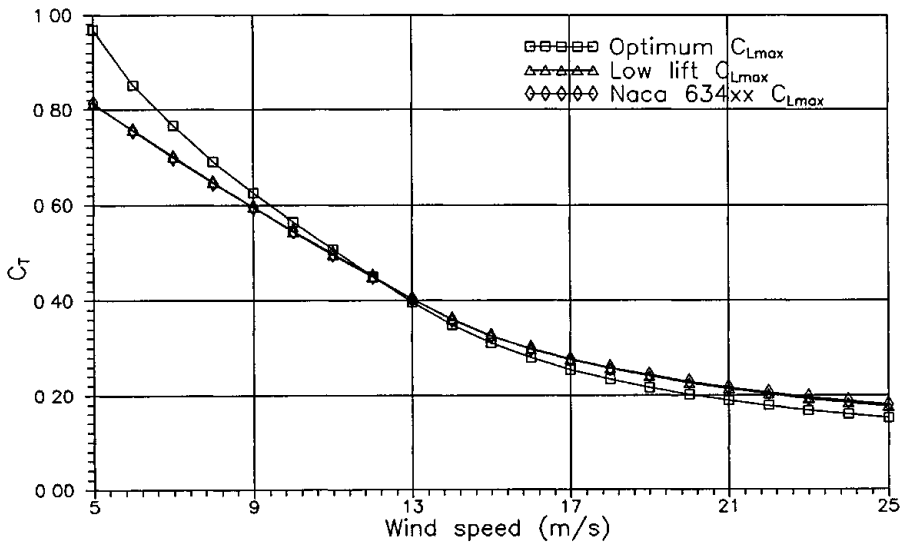

Figure G4 Thrust coefficient for the optimizations with different C_{Lmax} variations.

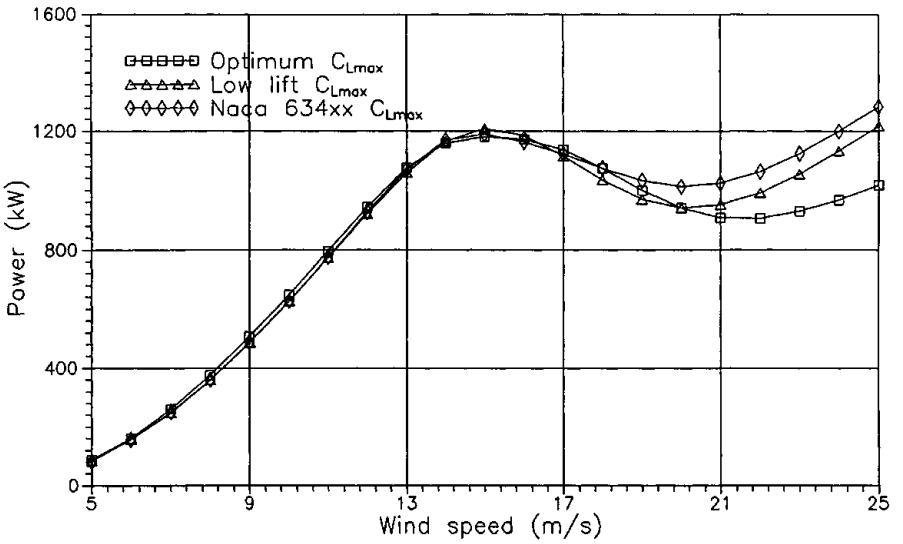

Figure G5 Power curve for the optimizations with different C_{Lmax} variations.

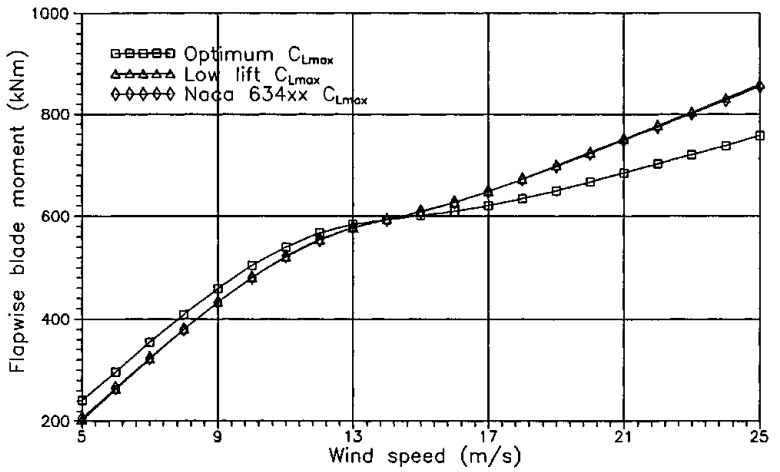

Figure G6 Blade root mean flapwise moment for the optimizations with different C_{Lmax} variations.

G.1 Optimum C_{Lmax} distribution

This Section contains figures concerning the rotor having optimum geometry and optimum C_{Lmax} distribution from Section 4.2 and Section 4.3.

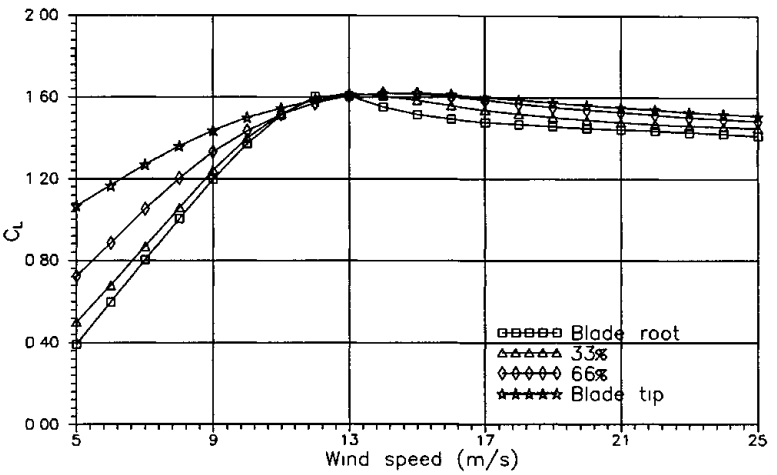

Figure G7 Variation in C_L versus wind speed at different blade positions.

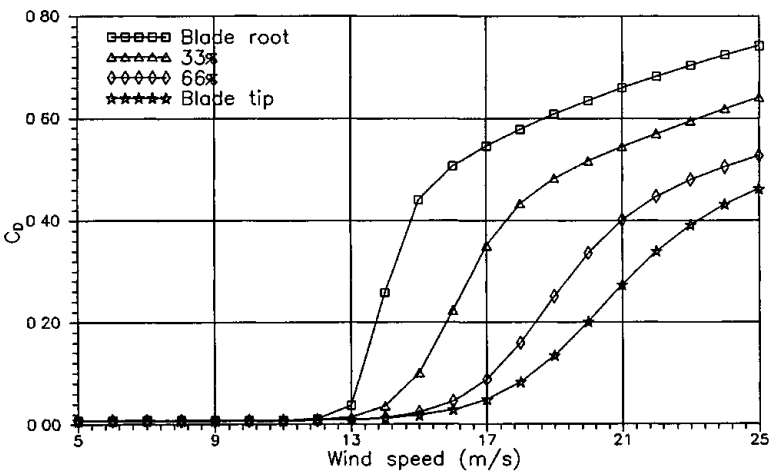

Figure G8 Variation in C_D versus wind speed at different blade positions.

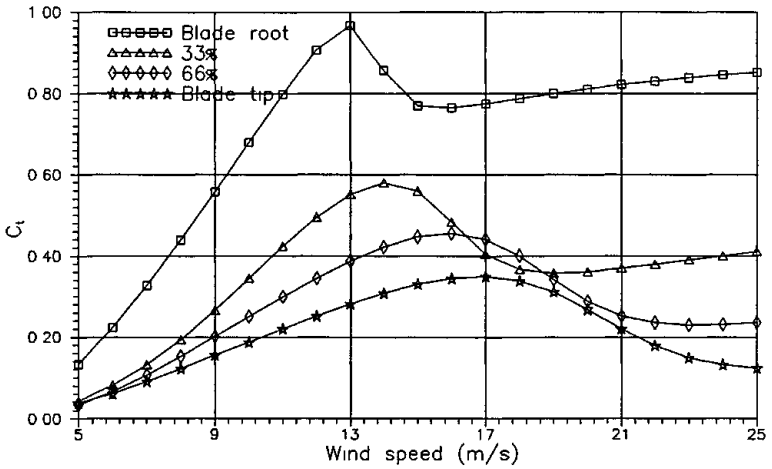

Figure G9 Variation in the tangential component of the aerodynamic forces, C_t, versus wind speed at different blade positions.

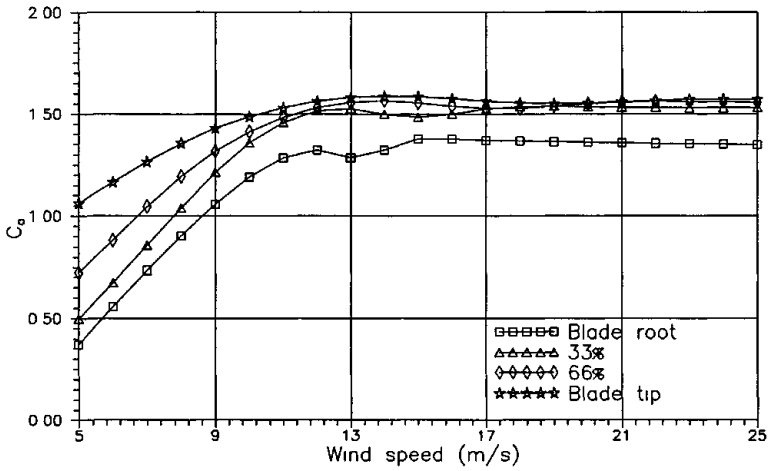

Figure G10 Variation in the axial component of the aerodynamic forces, C_a, versus wind speed at different blade positions.

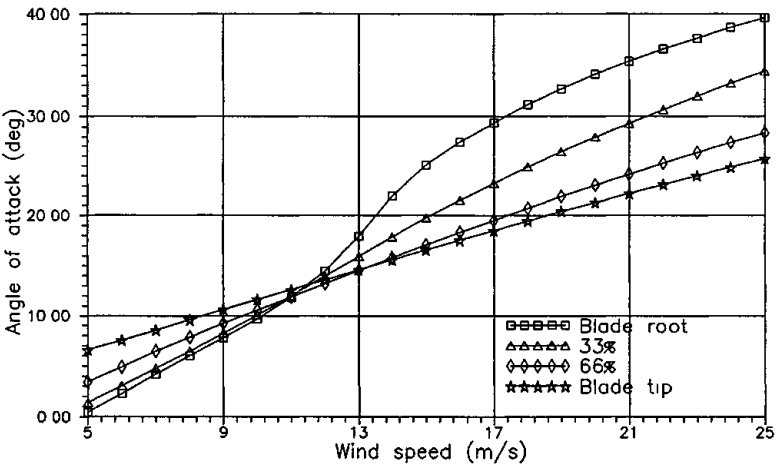

Figure G11 Variation in the airfoil angle of attack versus wind speed at different blade positions.

G.2 NACA C_{Lmax} distribution

This Section contains figures concerning the rotor having optimum geometry and a NACA 634xx C_{Lmax} distribution from Section 4.3.

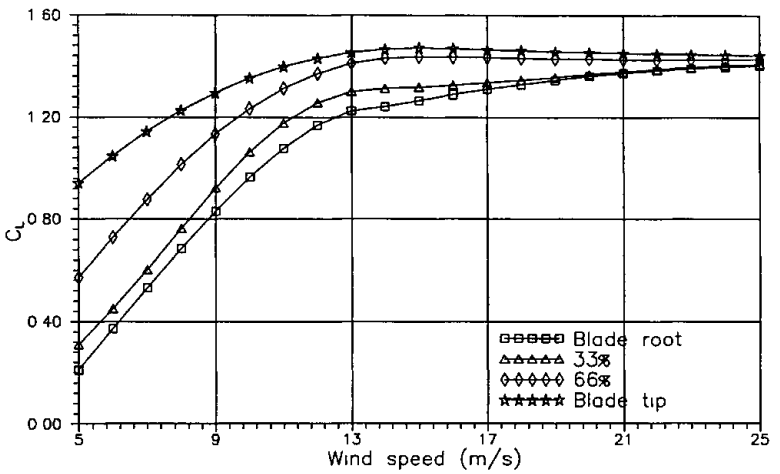

Figure G12 Variation in C_L versus wind speed at different blade positions.

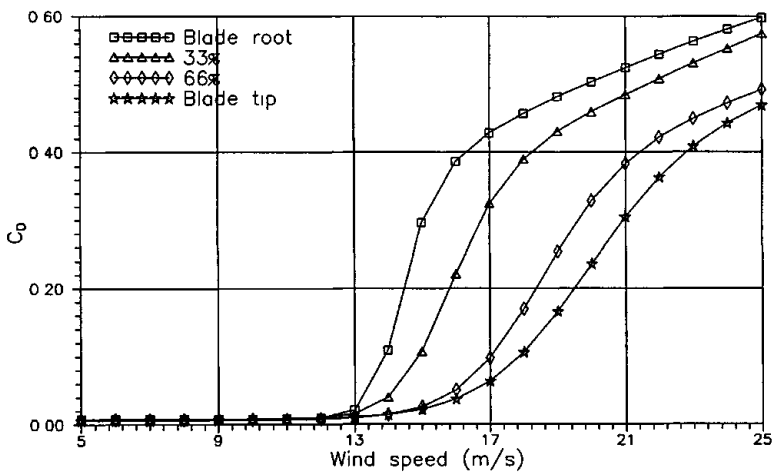

Figure G13 Variation in C_D versus wind speed at different blade positions.

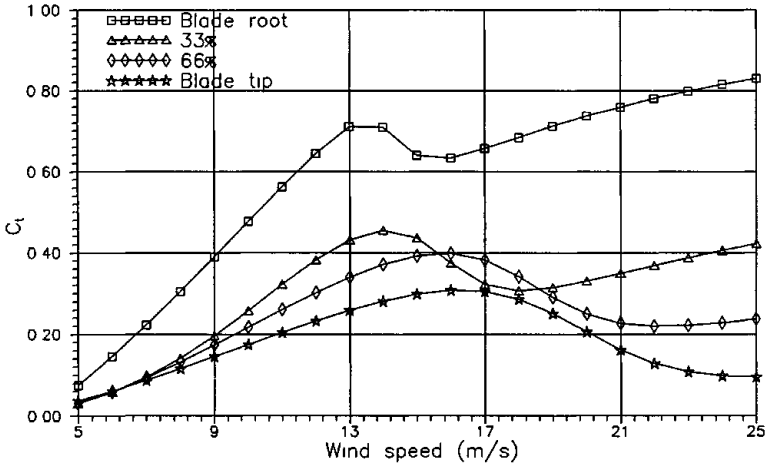

Figure G14 Variation in the tangential component of the aerodynamic forces, C_t, versus wind speed at different blade positions.

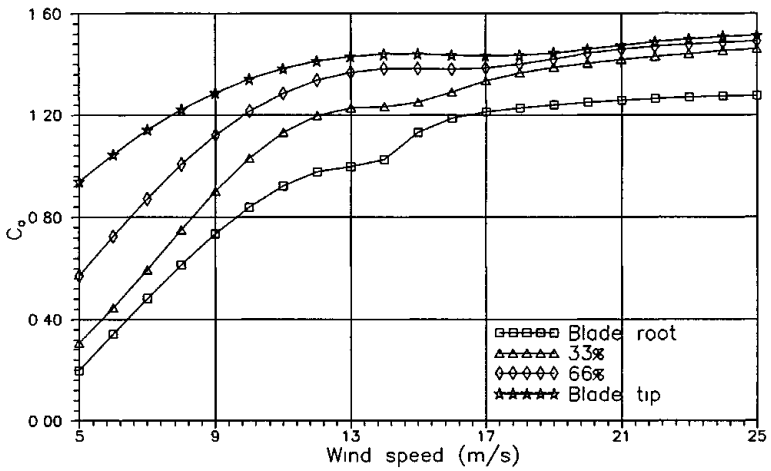

Figure G15 Variation in the axial component of the aerodynamic forces, C_a, versus wind speed at different blade positions.

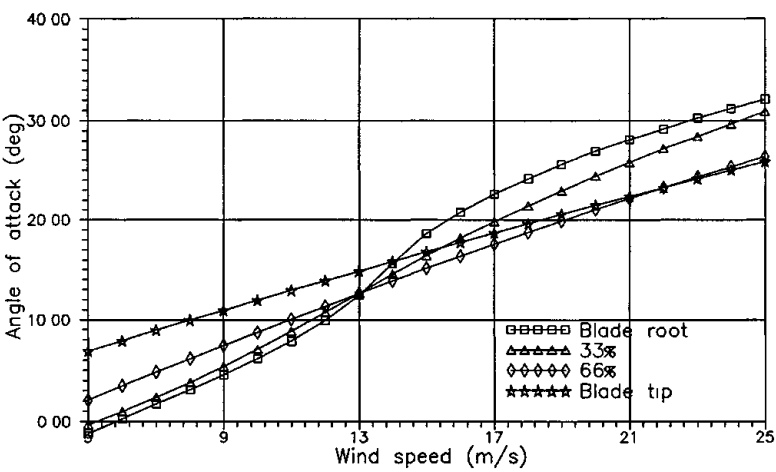

Figure G16 Variation in the airfoil angle of attack versus wind speed at different blade positions.

G.3 Low lift C_{Lmax} distribution

This Section contains figures concerning the rotor having optimum geometry and a low lift C_{Lmax} distribution towards the tip from Section 4.3.

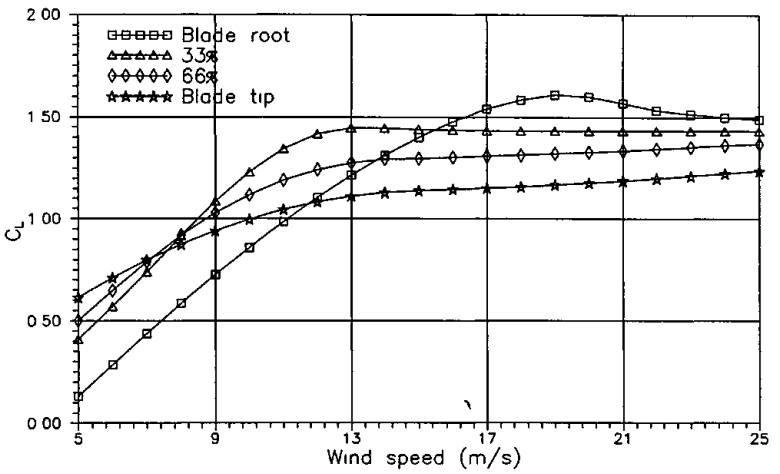

Figure G17 Variation in C_L versus wind speed at different blade positions.

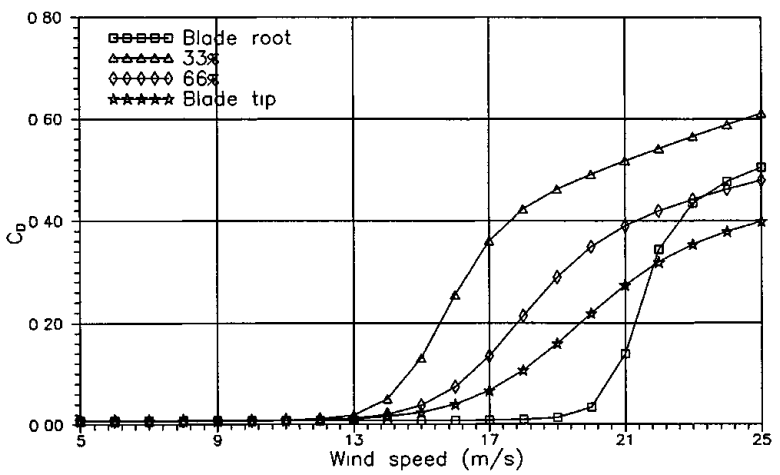

Figure G18 Variation in C_D versus wind speed at different blade positions.

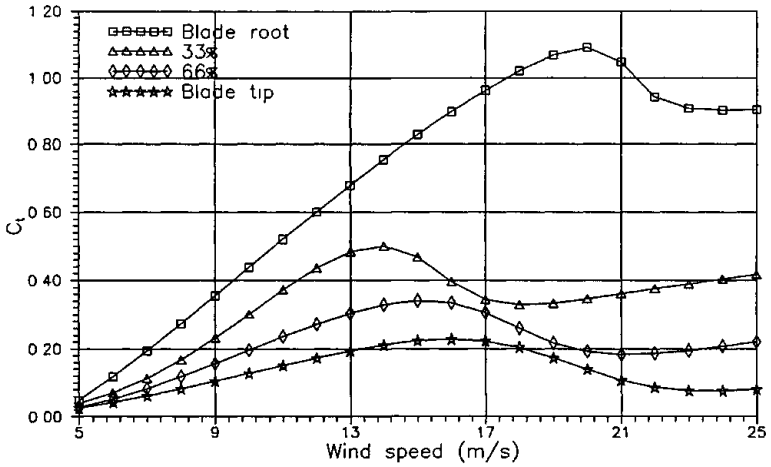

Figure G19 Variation in the tangential component of the aerodynamic forces, C_t, versus wind speed at different blade positions.

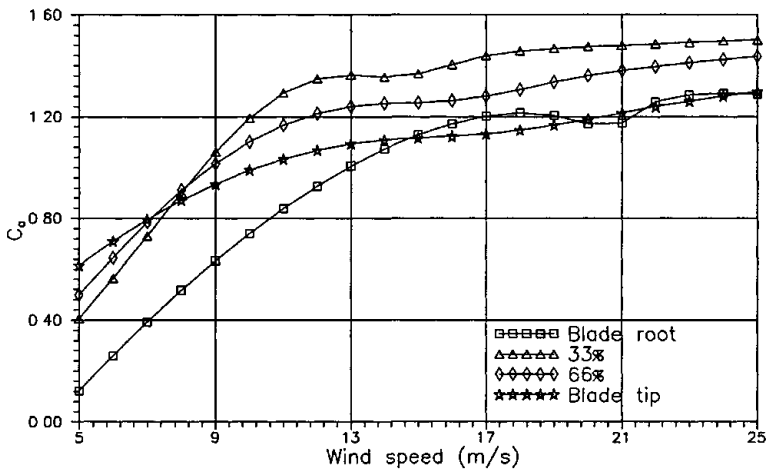

Figure G20 Variation in the axial component of the aerodynamic forces, C_a, versus wind speed at different blade positions.

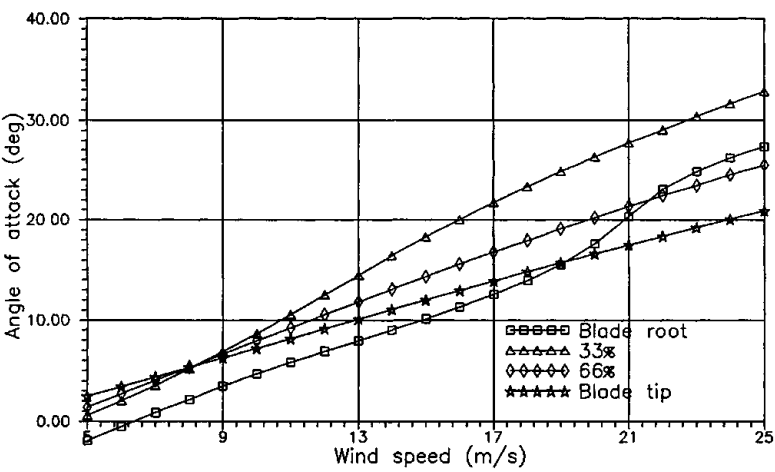

Figure G21 Variation in the airfoil angle of attack versus wind speed at different blade positions.

H Variation of tip pitch angle

Figures in this Appendix concern the optimization results from Section 4 4

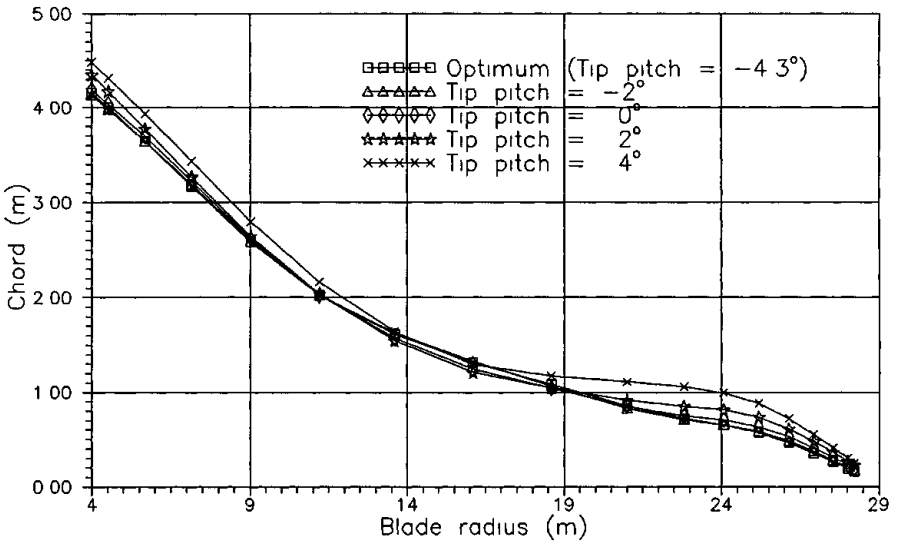

Figure H1 Chord distributions for the optimizations with different tip pitch angles.

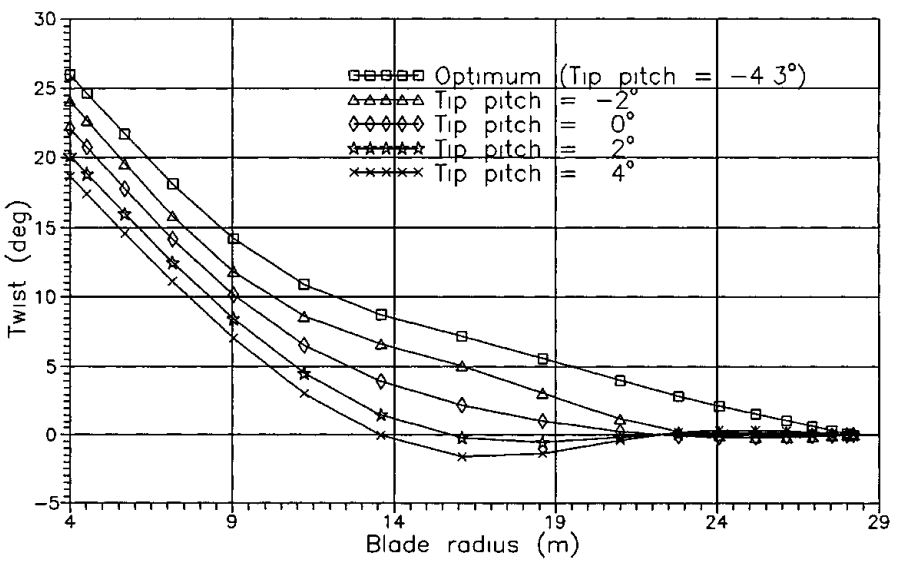

Figure H2 Twist distributions for the optimizations with different tip pitch angles.

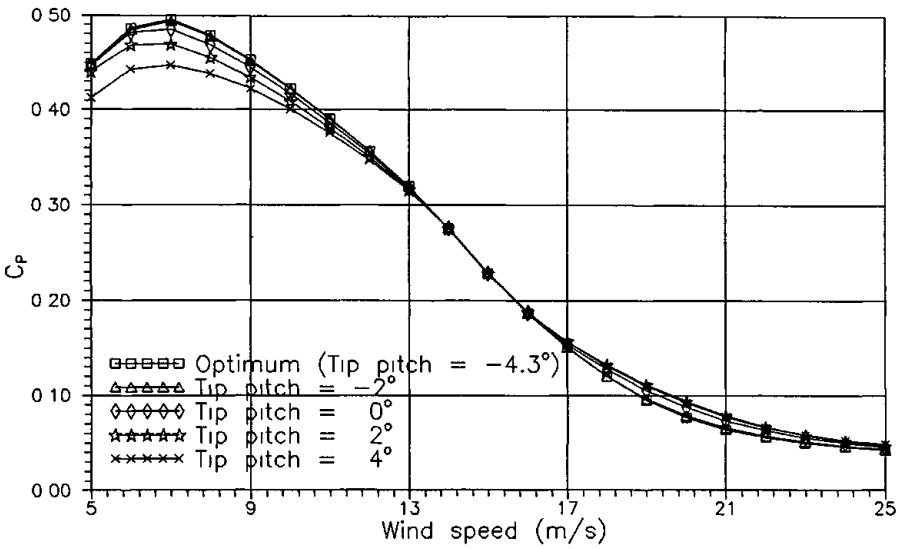

Figure H3 Power coefficient for the optimizations with different tip pitch angles.

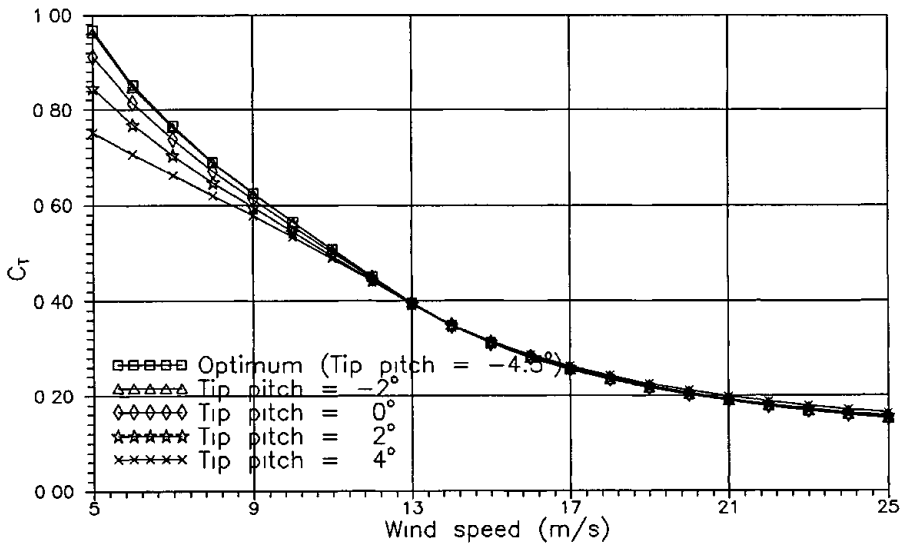

Figure H4 Thrust coefficient for the optimizations with different tip pitch angles.

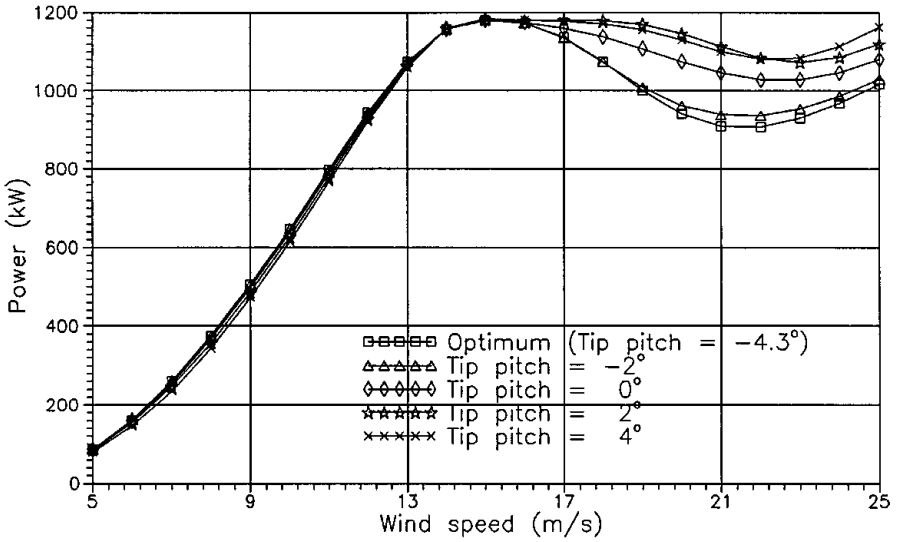

Figure H5 Power curve for the optimizations with different tip pitch angles.

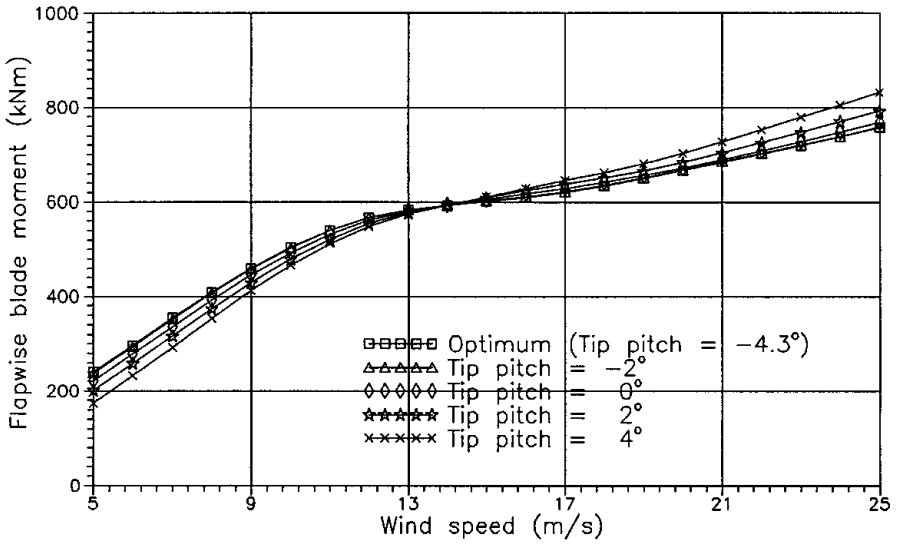

Figure H6 Blade root mean flapwise moment for the optimizations with different tip pitch angles.

Bibliographic Data Sheet **Risø-R-799(EN)**

Title and authors(s)

A DESIGN STUDY OF A 1 MW STALL REGULATED ROTOR

Peter L. Fuglsang, Helge Aa Madsen

ISBN	ISSN
87-550-2057-7	0106-2840

Dept or group	Date
The Test Station for Wind Turbines Dept. of Meteorology and Wind Energy	May 1995

Groups own reg number(s)	Project/contract no (s)
	ENS-1364/91-0009 ENS-1363/94-0001 ENS-1363/95-0001

Pages	Tables	Illustrations	References
105	14	121	25

Abstract (Max 2000 characters)

The main objective of the present work has been to design a 1 MW stall regulated rotor and investigate the potential improvements by using special tailored airfoils The target rotor should have an improved cost performance compared to existing rotors Cost performance is the annual production of energy seen relative to the material consumption A newly developed numerical optimization tool and an aeroelastic code have been used in the study

Design parameters have been the blade chord, twist, tip pitch angle, angular velocity and airfoil characteristics The objective function for the optimization has been the annual production of energy in the Danish roughness class 1 Constraints have been put on mean and extreme blade root flapwise moments, rated power, tip speed and blade geometry

By performing aeroelastic calculations on the optimized designs with different levels of constraints on the mean blade root flapwise moments, an almost linear correlation between the mean blade root flapwise moment and the equivalent fatigue loads appears The optimum ratio of rated power to swept area appears to be around 400 W/m^2 having the mean flapwise blade root moment constrained to 80%

The maximum annual production of energy has been obtained for the airfoil section maximum lift coefficient, C_{Lmax}, being high over the entire blade independent on constrained loads The direct improvement from the use of special tailored airfoils has been found to be around 4% on the annual energy production and 1 5% on the material consumption When the entire rotor geometry is included as optimization design variables, the choice of C_{Lmax} becomes less important since the design space is flat in the neighbourhood of the optimum Therefore other qualities like roughness insensitivity can be given more attention in the design process at the expense of a specific C_{Lmax}

The results indicate a potential improvement of the cost performance of about 11% of which 5 5% can be achieved with the use of traditional airfoils Whereas the proposed methodology have been very beneficial to constrain the fatigue loads, the extreme loads have not yet been entirely included

Descriptors INIS/EDB

AERODYNAMICS, COMPARATIVE EVALUATIONS, DESIGN, DYNAMIC LOADS, FATIGUE, HORIZONTAL AXIS TURBINES, OPTIMIZATION, PARAMETRIC ANALYSIS, POWER GENERATION, ROTORS, TURBINE BLADES WIND

Available on request from Information Service Department, Risø National Laboratory
(Afdelingen for Informationscervice, Forskningscenter Risø), P O Box 49,
DK-4000 Roskilde, Denmark
Telephone (+45) 46 77 46 77, ext 4004/4005
Telex 43 116 Telefax (+45) 46 75 56 27